MASTER OF SCIENCE BY RESEARCH

An investigation into scale open jet wind tunnel corrections through the use of CFD and wind tunnel testing

Jordan, Tom

Award date:
2015

Awarding institution:
Coventry University

Coventry University

Masters by Research Project

Author: Tom Jordan

Director of Studies: Remus Cirstea

Faculty of Engineering and Computing
Department of Automotive and Mechanical Engineering

Title: An Investigation into Scale Open Jet Wind Tunnel Corrections through the use of CFD and Wind Tunnel Testing

Submitted in partial fulfilment of the requirements for the degree of Master of Science

Year: 2014

Submission date of Thesis: 02/03/15

Contents

Table of Equations

Table of Figures

Table of Tables

Nomenclature

∇	Del Operator

$-(u_j\varepsilon_j)$	Transport of ε by diffusion
$\left(\frac{dC_p}{dx}\right)_{N,C}$	Static Pressure Gradient from the nozzle (N) or collector (C) in an empty test section over half of the model length
a	Coefficient/Constant for a Line
A*	Reduced Nozzle cross sectional area
A_o	Constant for Realizable k-ε
A_1	Area
A_C	Area of the Collector
A_M	Area of Model
A_N	Area of Nozzle
A_s	Model Parameter for Realizable k-ε
B	Nozzle Width
b	Coefficient/Constant for a Line
c	Coefficient/Constant for a Line
C_1	Constant for Realizable k-ε
C_2	Constant for Realizable k-ε
CAD	Computer Aided Engineering
C_D	Drag Coefficient
C_{Dcor}	Corrected Drag Coefficient
C_{Dm}	Measured Drag Coefficient
Count or Counts	A count of Drag is a C_D value of 0.001
$C_{\varepsilon 1}$	Constant for Standard k-ε
$C_{\varepsilon 2}$	Constant for Standard k-ε
C_μ	Model Coefficient for k-ε model
d	Coefficient/Constant for a Line
D_b	Distance from Balance
e	Exponential
f	Body Forces per unit Volume
G	Empty Tunnel Gradient
H	Height of the Nozzle
k	Turbulent Kinetic Energy
k-ε	K-epsilon turbulence Model
k-ω	K-omega turbulence Model
L_m	Model Length

LTS	Test Section Length
mmH20	Pressure Measurement Unit
p	Pressure
Pa	Pascal
q_∞	Free Stream Dynamic Pressure
q_{cor}	Corrected Dynamic Pressure
R_C	Radius of the Collector
R_N	Radius of the Nozzle
RNG	Re-normalised Group
RS	Reynolds Stress
S	Mean Strain Rate
SST	Shear Stress Transport
T	Total Stress Tensor
U*	Friction Velocity
UiUj	Reynolds Stress Tensor
Uiεi	Transport of ε by convection
v	Mean Velocity or Velocity
v'	Fluctuation Velocity
V_1	Velocity
V_M	Model Volume
W	Vector of Conservative Variables
X	Distance in x
X_M	Distance from Nozzle to Model Centre
X_{MC}	Distance from Collector to Model Centre for G calculation
X_{MN}	Distance from Nozzle to Model Centre for G calculation
X_S	Distance from Nozzle to Source Point
y+	Non-dimensional wall distance for wall bounded flow
Z	Distance in z
ΔC_{DHB}	Change in CD due to Horizontal Buoyancy
ε_C	Collector Blockage Correction Factor
ε_N	Nozzle Blockage Correction Factor
ε_{QN}	Nozzle Blockage Factor for Nozzle

	Method
ε_S	Jet Expansion Correction Factor
ε_t	Rate of change of ε
ε_W	Wake Blockage Correction Factor
η	Function of Time Scale ratio of the Turbulence to the Mean Strain
v_T	Eddy Viscosity
ρ	Density
σ	Boundary Layer Thickness
τ	Wind Tunnel Shape Factor
φ	Viscous Dissipation Rate
Ω	Rotational Rate

Abstract

Open jet wind tunnel corrections have been investigated for a number of years and the most comprehensive corrections that have been proposed were done so by Mercker and Wiedemann (1996). Their work presented the individual correction factors and the methods for implementing these corrections. Using these methods an investigation into the recently acquired wind tunnel at Coventry University was undertaken into the individual correction factors with the primary focus on finding the most influential factor.

Using an automotive model presented by Wong and Mair (1983) these corrections would be investigated within the wind tunnel. Alongside this a validation study is undertaken on all the wind tunnel tests and the wind tunnel itself through the use of CFD. Previous studies presented by authors have looked into direct comparison of wind tunnel and CFD simulations and noted good agreement between results, however, a number of set-up issues can arise. By investigating a number of the wind tunnel's properties a standardised model of the wind tunnel can be proposed for use within further CFD studies.

With a number set-ups available it is possible to test one model with a variety of supporting apparatus (sting). This being the case it is important to have support apparatus that is well constructed and that does not interfere with the flow structure of the model in a detrimental way. The University has one particular apparatus that was made in-house. Through a number of tests it was found that this sting could influence the measured results in a large way therefore a method to improve the sting has been proposed. By implementing already available ideas it was found that the stings influence could be reduced by 90 counts.

With the available data on the wind tunnel it was found that a CFD model could reproduce the investigated flow features to a level of reasonable accuracy. It is suggested, however, that for further validation, a more in-depth investigation of the wind tunnels flow properties such as span wise turbulence intensity and velocity profile is conducted.

Acknowledgements

I would like to thank all my tutors for their continued support and guidance throughout this project, especially my Director of Studies, Remus Cirstea. I would also like to thank the Universities' Wind Tunnel Technician for his assistance with all my wind tunnel tests as well as the various work shop technicians. A special thank you also goes to my girlfriend and my family for their constant encouragement and support.

1. Introduction

In the subject of automotive aerodynamics there are a number of ways to test a model or vehicle. Computational Fluid Dynamics (CFD) is one way of testing and is by far the cheapest form of testing as the tests are conducted virtually. A simulation within CFD can be very useful in showing a number of flow features that cannot be seen within a wind tunnel for example, this is another form of testing. Wind tunnel testing has been the main method of investigating the aerodynamic properties of objects for a number of years. A wind tunnel test is often complemented with a CFD study, with the wind tunnel used as a form of validation. The wind tunnel is the most practical way to test a model aerodynamically, other than CFD the alternative would be a road test. Road testing presents a number of variables that cannot be controlled such as, temperature, density, wind direction, rain and vehicle speed constancy to name a few. Wind tunnels allow a full vehicle or a scale model to be tested in a fixed position, where all the previously noted variables can be controlled. A scale model is often used instead of a full vehicle, as any features that may need to be changed on the vehicle, can be implemented. When a full vehicle is used it is very unlikely that any problems found can be rectified cheaply, if at all.

However, with all forms of testing there is an amount of error associated with the results. Aerodynamic test methods are no exceptions to this. The closed jet wind tunnel, which was once believed to be the only accurate way of testing, is susceptible to generating a large amount of error, meaning that there can be a large difference between the measured coefficients and the corrected ones. This feature is one of the downsides to the closed jet wind tunnels. This along with the added construction costs and temperature increase of continued running (if the tunnel is not temperature controlled) can result in the user seeking a different method of testing, such as an open jet wind tunnel. The previously closed test section is now open as the name implies.

There are many benefits to using open jet tunnels, such as the increased ease at which the model in the centre of the test section can be modified or replaced. Another benefit of the open jet tunnel is the reduced size in error (difference between measured and corrected). While the corrections are smaller in open jet wind tunnels, there are a number to be applied when compared to that of closed jets (Mercker and Wiedemann, 1996). These corrections have been proven to be more complex. The application of corrections are essential for all tests done in

open jet wind tunnels, as the tunnels themselves produce conditions that will not be replicated on the road. Both jet expansion and deflection will not occur on an open road, neither will nozzle or collector blockages as these too are wind tunnel specific effects (Mercker and Wiedemann, 1997).

Wind tunnel testing, whether open or closed, full scale or scaled, is expensive and this is why CFD is often used instead. However, CFD only provides a guide or an estimate of the features being measured. It is highly dependent on the choice of mesh density and turbulence model. Finding common ground between CFD and wind tunnel results can prove tricky even for experts in this field (Luca, 2013). The addition of corrected and uncorrected data can add to the confusion.

When conducting CFD simulations the test model is often in a very low blockage domain that often bears real resemblance to the wind tunnel test section. The added computational time of constructing a mesh around an actual wind tunnel test section and simulating all the flow features within the tunnel, is the main reason that this is not done as standard practice (Fischer et al, 2010). This along with a wind tunnel that was built in 2012, that has not had a correction study performed upon it, presents a possibility of four different sets of data; uncorrected, corrected, low blockage simulation and wind tunnel simulation. The level of agreement between them all is not known. This study aims to investigate and quantify the corrections for the new wind tunnel through the use of a simple model in this case the Wong Model (Wong and Mair, 1983). Then a comparative CFD study will be undertaken. From this a standard CFD model of the wind tunnel can be proposed for use in future university studies.

2. Literature Review

2.1. Wind Tunnel Testing & Model Choice

The wind tunnel used for this study is an open jet closed return tunnel which is also known as a Gottingen type wind tunnel (Barnard, 2009). A benefit of using an open jet tunnel is that the ambient conditions are constant. The test section temperature changes very little throughout the test, while in a closed section the temperature will continue to rise as the test continues due to friction (Katz, 2006). The wind tunnel that is used in this study is water cooled to ±2°C by a cooling coil. However, with respect to power usage, an open jet tunnel will use more compared to a closed jet of similar size in order to maintain the desired test

section speed (Katz, 2006). Katz explains that while there are advantages and disadvantages with all types of wind tunnels, the main factor that influences the wind tunnel design/construction is the cost.

With this in mind, open jet tunnels are cheaper to manufacture simply because they require fewer materials. Even with this fact, the total cost is generally a balance between the running costs and construction costs. Open test sections can accommodate blockage ratios twice the size of closed wind tunnels, this halves the air mass flow and thus decreases the power needed (Sims-Williams and Dominy, 2002). This could impact the corrections in a significant way as they are closely related to the model volume and this will be shown in more detail in a later section.

Another benefit of an open test section is the absence of the walls; this allows the user to easily mount and modify the model. While it is clear that the set-up is not like truly free flow (Barnard, 2009), the decreased effect of blockage is a great benefit. There is also another property present in open jets; that is the interaction between the jet and the still air (Barnard, 2009). This creates a shear layer that is not present in a closed tunnel. When conducting a CFD study it is important to model this effect in detail as it can have a large effect on the results generated (Fischer et al, 2007).

As the University wind tunnel is a closed return there are turning vanes, settling screens and honeycomb sections to manipulate the flow in both direction and quality respectively. Fischer demonstrated that it is possible to generate the hundreds of millions of cells when simulating a simple test section of a wind tunnel. Therefore, only the test section of the wind tunnel will be simulated, in this case, to avoid drastically increasing the number of cells and thus computational power needed to even run an empty tunnel.

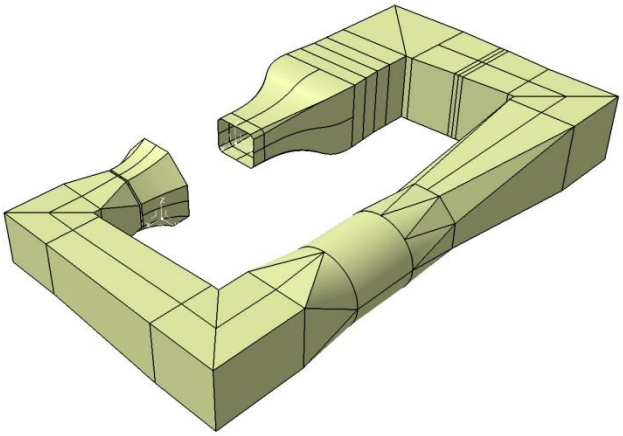

Figure 2.1-1 - Full Wind Tunnel CAD

In addition, Kulkarni et al (2010) investigated the effect of simulating honeycomb screens in a subsonic wind tunnel and found that the turbulence reduction produced by the honeycomb was insignificant, suggesting that the added complication of simulating the honeycomb will provide little or no benefit in this study. It was also found that the flow quality at the exit of the settling chamber was independent of the honeycomb cell size used. Considering the relatively small computational domain used by Kulkarni to simulate the honeycomb screens, 650,000 elements were needed to accurately map the honeycomb's effect on the flow (Kulkarni, 2010). This demonstrates that the increased demand on computational power will not provide an increase in result accuracy. The main components of the wind tunnel that will be referred to throughout this study are the nozzle and the collector. The nozzle is where the air flow is settled, accelerated and then exits into the test section. The area before the contraction is the settling chamber; in here there are honeycomb and settling screens that reduce the fluctuating components of the air.

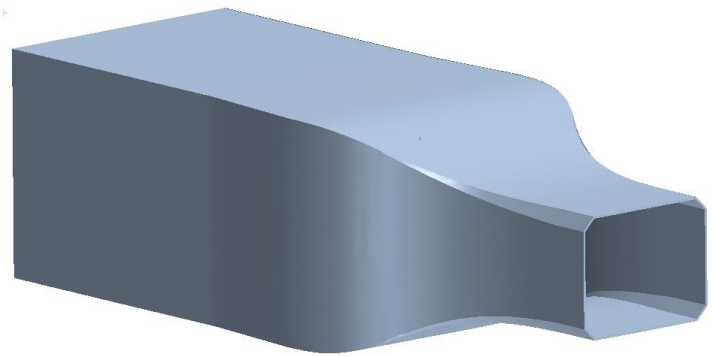

Figure 2.1-2 - The Nozzle

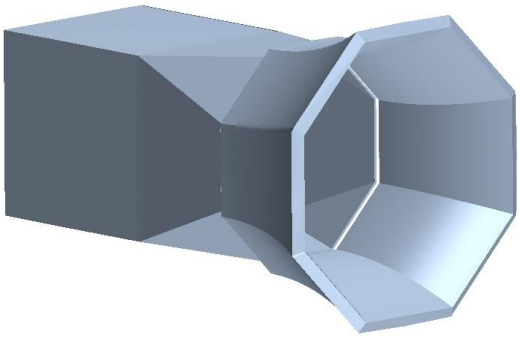

Figure 2.1-3 - The Collector

The collector is the other major component of the wind tunnel that has an effect on the corrections and this will become more evident in the following sections. Mallock and Finnis (2012) stated that the vent that is present after the collector has been placed there to reduce the effect of organ piping, which is an effect which results from a sine wave coming from the nozzle which causes fluctuations in the path of the air (Mallock and Finnis, 2012).

For this study, the model that will be used is the one presented by Wong and Mair (1983) which is a long 3D rectangular box with a rounded nose. There is also a selection of after bodies that can be attached to the model. Wong and Mair (1983) constructed these from wood and dowelled them together; they were truncated pyramids at both 70 and 80 degrees. It was found that there was a change in C_D of almost 120 counts when using seven of the 70° after bodies. A single count is a C_D value of 0.001; this is a more convenient way of comparing data as opposed to quoting full C_D values. From this point on the change in drag was minimal. The model that Wong and Mair created was suspended by wire in an overhead balance; this was done to reduce the effect of any support apparatus. This will not be replicated, due to the way in which the University wind tunnel is set-up. Instead a singular overhead balance will be used with different support apparatus (or stings). Wong and Mair noted that the C_D measured at the base of the model cannot exceed 0.15, also noting that the nose measures a value close to 0 (Wong and Mair, 1983). As the base cannot exceed 0.15, this also means that the change in C_D cannot exceed 150 counts. These values can be used as guidance values for all results gained from the tunnel and generated from CFD. It should be noted that all tests that Wong and Mair conducted were in a closed jet wind tunnel with a maximum speed of $42ms^{-1}$. At this speed Wong and Mair used a trip wire to energise the boundary layer; in this report a speed of $45ms^{-1}$ will be used. This is the maximum air velocity of the wind tunnel. The

additional velocity difference will remove the need for a trip wire as the increased velocity will energise the boundary an adequate amount. With the difference in wind tunnel and support method it would be reasonable to expect some small differences between the findings presented by Wong and Mair with the findings of this study.

Figure 2.1-4 - Wong Model with After Bodies 1, 2, 4, 6 & 8

2.2. Wind Tunnel Corrections

Due to the need for correlation between different wind tunnels, the need for corrections is clear. The issue with many open jet tunnels is they do not compare well to either open or closed tunnels (Mercker and Wiedemann, 1996). While closed wind tunnels show differences between each other the correction procedure is less complex and this being the case, a comprehensive correction method for open tunnels was needed. The classic corrections that were originally set out for closed jet tunnels are not appropriate due to the difference in tunnel and flow features. Mercker and Wiedemann set out the corrections stating that there are five, all of which must be considered for an accurate representation of the drag to be shown. The complexity of these corrections means that for mathematical ease they are assumed not to interfere with one another. Realistically this is not the case and Mercker and Wiedemann acknowledge this (Mercker and Wiedemann, 1996). There are five corrections; the first is the correction for the drag change in due to horizontal buoyancy (ΔC_{DHB}). Mercker and Wiedemann state that this effect arises due to the generation of a pressure gradient in the test section when a model is present (Mercker and Wiedemann, 1996). Essentially, this means that the presence of the model changes the static pressure gradient in the wind tunnel and this will modify the drag measured. The next correction factor is for jet expansion, this effect is present in open jet tunnels as flow is exiting the nozzle and interacting with the stagnant air which surrounds the test section. Depending on the pressure difference will depend on how much the jet expands or even collapse. Both the collector and the nozzle of the wind

tunnel also create blockage effects; these are dependent on the dimensions of the respective components as well as the model distance from each. Finally, there is the correction for the dynamic pressure correction for the nozzle. This correction depends on the method of pressure measurement which is either the nozzle or the plenum method. Both these methods are different ways to measure the pressure difference between the nozzle and the test section (Figure 3.8-1). All the corrections including the nozzle and the plenum method will be presented in Section 4.

Most studies that have looked into corrections have only covered drag; the correction of lift is still not fully understood and is more complex. With respect to this study this is not an issue and with the main area of interest in automotive sector being the reduction of drag, it is not a cause for major concern. Hoffman et al (2003) did briefly look into the corrections of lift and noted that there were some good trends, but also commented on the lack of data available for lift. It was found that the lift correction was limited by the level of uncertainty present in the actual force measurements themselves (Hoffman, 2003). The investigation concluded that the lift corrections did not work well and that they were limited by the amount of uncertainty present in the model, which in this case, was quite high (Hoffman, 2003).

The premise of the first paper by Mercker and Wiedemann (1996) was to set out and validate the corrections put forward, which was achieved even though data from some tunnels was missing due to complications. These ideas are expanded upon in the follow-up paper (Mercker et al, 1997), in which corrections are put forward for both the nozzle and the plenum-method (see Figure 3.8-1). Mercker et al (1997) commented on conflicting sources stating that “either the nozzle-method or the plenum-method is the only correct way to determine tunnel speed”, while these sources fail to state that both contain errors and therefore, both need correction. Yet both methods are in fact valid and the method chosen for each case must be justified. Mercker et al (1997) recommend using the plenum method for small wind tunnels that are used for automotive testing. Before selecting a method it is important to note the locations of any pressure taps; if the method that is selected results in these taps being contaminated with an adverse pressure gradient produced by the model, any form of correction becomes meaningless (Mercker et al, 1997). Mercker et al (1997) argue that both the nozzle and the plenum methods need a correction because when the model is in the test section the flow exiting the nozzle can be affected. The flow velocity

within the University can be controlled in a number of ways through the use of monitoring the dynamic pressure, the pressure or the velocity. For this study the velocity was used to constrain the test section velocity, rather than the other two methods, as this can also be done within CFD. Wickern and Schwartekopp (2004) found that by moving a model closer to the nozzle the drag will increase. Wickern (2001) states that if the model becomes closer than $2\sqrt{A_m}$ (where A_m is the frontal area of the model used) to the collector the coefficients become effected. This will be important to note when testing an increasing number of after bodies on the Wong model.

These corrections have been investigated on a number of tunnels by Meada et al (2005). Three open jet tunnels were investigated all of which were ¾ scale test section and all were slightly different from each other e.g. Nozzle area, test section length, tunnel shape factor and contraction ratio. Meada et al (2005) investigated four different models in each of these tunnels and presented his uncorrected and corrected findings. The nozzle method was used for two of the open jet wind tunnels and a pitot tube was used for the remaining. When looking at the individual corrections Meada et al (2005) found that the largest correction factor was the horizontal buoyancy in wind tunnel 2 (WT2), while the largest in the other tunnels (WT1 and WT3) was the nozzle blockage. It is worth noting that WT2 has a much longer test section and that WT1 & 3 have much larger nozzles.

2.3. Wind Tunnel Properties

It must be said that these corrections will not be valid if the tunnel in question has not been calibrated. For the purposes of this study it has been taken that the wind tunnel is in the same state as was recorded by Mallock and Finnis (2012) in the Tunnels Commissioning Report. All the measurements are made in the SCBTV (standard control box test volume) and the DPCP (dynamics pressure calibration point). The SCBTV is the size of a 20% scale F1 model and the DPCP is taken as the centre of this control volume. The entire pressure mapping within the commissioning report was conducted at $35ms^{-1}$. Mallock and Finnis state open jet tunnels exhibit low frequency pressure fluctuations and that these are not steady state effects, suggesting that for these to present in a CFD simulation, the case must be set as unsteady.

While it is acknowledged that there will be some minor discrepancies, the lack of both time and the necessary resources prevented the study being repeated. The commissioning report maps the turbulence intensity across a range on velocities;

by investigating this within the CFD simulations the set-up can be validated. The turbulence intensity (I) can be defined as a relationship between the mean velocity (**v**) and the fluctuation velocity (v'). To determine the fluctuation velocity the turbulence kinetic energy (k) is needed; this can be easily measured and plotted across the wind tunnel section in CFD.

$$v' = \sqrt{\frac{2}{3}k} \qquad (2.3\text{-}1)$$

$$I = \frac{v'}{\boldsymbol{v}}$$

Equation 2.3-1 - Turbulence Intensity (CD-adapco, 2014)

An investigation into the levels of turbulence intensity exiting a jet was conducted by Little and Wilbur (1951) where the level of the intensity was mapped from the centre of the pipe. It was found that the levels of turbulence peaked around the edges of the pipe. It is important to note any differences in Reynolds number when comparing data such as this. The study by Little and Wilbur took place at a lower Reynolds number than is present in the authors study, therefore, only general trends can be taken from this. As the turbulent intensity trend was similar for all the Reynolds numbers used by Little and Wilbur, it is sensible to predict that there will be some minor differences produced by the wind tunnel.

Sims-Williams and Dominy (2002) simulated an open return open jet looking into various nozzle contraction ratios and configurations, suggesting that a high contraction ratio is more desirable as this will aid toward the removal of non-uniformities in the flow. For reduced simulation time of this simple study, a symmetry plane was used through the centre of the tunnel (Sims-Williams and Dominy, 2002). This type of simulation is unlikely to show the effects of the shear layer very well. A coarse mesh of 200,000 cells was used; this is far too coarse to be applied to the author's study. In contrast, Fischer et al (2007) uses over 63 million voxels taking special care to ensure that the shear layer is accurately simulated. This demonstrates that it is important to have a fine mesh around the shear layer as this has a strong influence on the static pressure across the test section (Fischer et al, 2007). Even when simulating a number of flow features at once, Fischer et al (2007) concluded that it is possible to simulate the interference effects of wind tunnels using the k-ε turbulence model (see Section 2.4 for further details). Following on from this study Fischer et al (2010) go further with the mesh density to well over 200 million voxels. The run time for this mesh

is close to 24 hours, however, a high number of clusters were employed to achieve this yet the computational power employed was not stated. Even with this fine mesh a difference of 10 counts in C_D is still present between CFD and wind tunnel results. This would suggest that the density of the mesh for each tunnel varies greatly from hundreds of thousands, to hundreds of millions, proving the importance of a mesh study. Figure 2.3-1 shows Fischer et al (2007) findings for their first configuration, showing that the coefficient with the smallest deviation from experimental values is the C_D. However, there is still a notable difference.

This image has been removed

Figure 2.3-1 – Comparison of Experimental and Numerical Drag and Lift Values (Fischer et al, 2007)

ERCOFTAC (2000) provides a detailed account of guidelines that should be followed when conducting any CFD study. The aspects of grids and grid design (mesh) are highlighted in detail. The guide states various configurations that should be avoided such as tetrahedral cells in boundary layers, highly skewed cells and highly warped cells (ERCOFTAC, 2000). ERCOFTAC recommends the use of prism or polyhedral cells in boundary layers as this will provide regular shaped cells in an extremely important part of the study. This also allows for the cells to be easily adjusted for achieving y+ values that are not in the buffer layer. ERCOFTAC highlights the importance of the resolution of the boundary layer and that adequate boundary layer resolution requires at least 8-10 points in this layer (ERCOFTAC, 2000). For the specific values of y+ that should be implemented, these guidelines state that the user should consult the code being used.

The CFD software chosen for this study is STAR-CCM+ due to the author's familiarity with the software, the availability and the commercial validity of the CFD code. STAR-CCM+ is also very diverse in the number of problems that it can be applied to such as automotive, defence, aerospace and even medical

(CD-adapco, 2013). This software also has graphical user interface that allows the user to easily see the model configuration as well as any model problems. Within STAR-CCM+ there are a number of wall treatments that can be selected. The Two Layer All y+ Wall Treatment is a hybrid of the two other treatments available (high and low y+). This model is used to provide good results for low y+ (0-5) and high y+ (>30). The region in-between these two is called the buffer layer. When cells enter this layer the results that are predicted become very poor. This wall treatment does state that the results generated in this buffer layer are reasonable, however, with this in mind the region will still be avoided where possible (CD-adapco, 2014).

2.4. Turbulence Model

Firstly the equation which the CFD code will be solving is the Navier Stokes Equation, which in its general form is as follows:

$$\rho\left(\frac{\partial v}{\partial t} + v \cdot \nabla v\right) = -\nabla p + \mu \nabla^2 v + f \qquad (2.4\text{-}1)$$

Equation 2.4-1 - Navier Stokes Equation

This equation shows the conservation of momentum in a fluid. Its complex nature (especially when written out in full) means that it would take an extremely long time to determine the flow features for just one cell or point. This is why turbulence models are used to conduct all the calculations.

Due to the complexity of the geometry it is recognised that a turbulence model such as Spalart Allmaras should not be selected. Spalart Allmaras performs well for simple geometries, such as aerofoils, and will converge quickly under steady state conditions (Blazek, 2005). However, as the properties of the wind tunnel are unsteady (properties change over time), convergence with this model is unlikely to be quick. The unsteady nature of the flow which contains varying boundary layers, recirculation (with models), shear layers as well as internal and external flow, further suggests that this model would be an inappropriate choice. Due to the number of features in the flow, the amount of simulations that are to be run and the complex geometry, it is logical to use a more appropriate model. A two equation model such as k-ε or k-ω would be more suitable. Both of these models are available for use in a number of CFD codes.

Within STAR-CCM+ there are number of variants of these models. As standard the k-ω model that is implemented when selecting this model in STAR-CCM+ is

the SST model. This was first presented by Menter (1992). It is initially noted that the widely used k-ε model over predicted the shear stress and often delays separation (Menter, 1992). Menter states that this model treats the shear stress as being proportional to the turbulent kinetic energy.

$$\tau_1 = \rho a_1 k \ , \qquad (2.4\text{-}2)$$

Where $a_1 = 0.3$

Equation 2.4-2 - Shear Stress

For this equation to be satisfied the eddy viscosity model was redefined by Menter (1992):

$$\nu_t = \frac{a_1 k}{\Omega} \qquad (2.4\text{-}3)$$

Equation 2.4-3 - Eddy Viscosity Model

In areas of adverse pressure gradient the denominator becomes $\max(a_1\omega; \Omega)$. Once this model was created a number of tests were performed upon it. It was found that this model showed identical results to that of the k-ε in the prediction of free shear flows and a 13% difference was found when looking into reattachment length on a backward facing step (Menter, 1992). Predictions were found to be highly accurate when measuring the velocity profiles of an aerofoil, noting that the data compared excellently with experimental findings (Menter, 1992). While this is a beneficial trait, the margin of error that was found when looking into the backward facing step (which could be thought of as the Wong Model with no after bodies) and the identical way in which free shear layers are shown (against the k-ε model), this model will not be chosen. The default k-ε model is the Realizable k-ε model. This model is an improvement on the standard k-ε model, whose weaknesses are well documented. A couple of these weaknesses are as follows; highly swirling flows are predicted poorly due to the complex strain fields, poor prediction of flow separation in adverse pressure gradients and far field spreading rates of round jets is also poorly predicted (ERCOFTAC, 2000). While the weaknesses of the standard model are known, it is still widely used in industry and academia. This is because the model can be used on a variety of different geometries, both simple and complex, providing reasonably robust results. Realizable k-ε provides a relatively stable solution with a good level of convergence, also being less computationally demanding than k-ω. The Realizable model which was proposed by Shih et al (1995) aimed to improve upon some of these issues.

Shih et al (1995) found that by removing the Reynolds stresses from the source terms (from the dissipation rate equation) the model becomes more robust.

Standard epsilon (turbulent dissipation rate):

$$\varepsilon_t + U_i\varepsilon_i = \nu\varepsilon_{ii} - \overline{(\varepsilon' u_\iota)}_i - C_{\varepsilon 1}\frac{\varepsilon}{k}\overline{u_\iota u_J}U_{i,j} - C_{\varepsilon 2}\frac{\varepsilon^2}{k} \quad (2.4\text{-}4)$$

Equation 2.4-4 - Standard Turbulent Dissipation Rate

Realizable epsilon with the removal of the Reynolds stresses:

$$\varepsilon_t + U_j\varepsilon_j = -\overline{(\varepsilon' u_j)}_j - C_1 S\varepsilon - C_2\frac{\varepsilon^2}{k+\sqrt{\nu\varepsilon}} \quad (2.4\text{-}5)$$

Equation 2.4-5 - Realizable Turbulent Dissipation Rate

These changes aid simulations that have poor initial conditions (Shih et al, 1995). Shih et al (1995) also showed that the Realizable model performs reasonably well in regions where there are large amounts of separation. Realizability is met by changing the variable, C_μ, to a function of the mean strain and rotation rates (Lateb et al, 2013), where the original k-ε assumed that it was constant. By changing the way in which this variable is determined, the value more closely matches experimental observations of boundary layers (CD-adapco, 2014). Shih et al (1995) further emphasis that both experiments and DNS simulations have been conducted on boundary layers and show that this value is not constant. As C_μ is not constant, an equation was needed to determine its value.

$$C_\mu = \frac{1}{A_0 + A_s U^*\frac{k}{\varepsilon}} \quad (2.4\text{-}6)$$

Equation 2.4-6 - Realizable k-ε Model Constant

Where,

$$U^* = \sqrt{S_{ij}S_{ij} + \widetilde{\Omega}_{ij}\widetilde{\Omega}_{ij}} \qquad \widetilde{\Omega}_{ij} = \Omega_{ij} - 2\varepsilon_{ijk}\omega_k$$

$$\Omega_{ij} = \overline{\Omega_{\iota J}} - \varepsilon_{ijk}\omega_k \quad (2.4\text{-}7)$$

Equation 2.4-7 – Rotational Rate

Where $\overline{\Omega_{\iota j}}$ is the mean rotation rate and ω_k is the angular velocity. The two 'A' terms which are the model constants are defined in the following way:

$$A_s = \sqrt{6}\cos\phi \qquad \phi = \frac{1}{3}\cos^{-1}\left(\sqrt{6}W\right) \qquad W = \frac{S_{ij}S_{jk}S_{ki}}{\tilde{S}^3} \qquad \tilde{S} = \sqrt{S_{ij}S_{ij}} \quad (2.4\text{-}8)$$

Equation 2.4-8 – Various Realizable k-ε Parameters

There are a number of constants and below they are summarised, but it is suggested that for a further in depth description on how these are derived the reader refers to the original paper by Shih et al (1995).

$$C_1 = max\left\{0.43, \frac{\eta}{5+\eta}\right\} \quad (2.4\text{-}9)$$

Equation 2.4-9 - Model Constant, C1

$$\eta = \frac{Sk}{\varepsilon} \quad S = \sqrt{2S_{ij}S_{ij}} \quad (2.4\text{-}10)$$

Equation 2.4-10 - Mean Strain Rate

σ_k	σ_ε	C_2	A_0
1.0	1.2	1.9	4.0

Table 2.4-1 - Model Coefficients for Realizable k-ε

Lateb et al (2013) investigated pollutant dispersion over a range of different sized roof stacks, using three different k-ε models. It was found that the Realizable model was the only model that was able to provide the best trend with wind tunnel values, also noting that the standard model was inadequate (Lateb et al, 2013). Whilst investigating the aerodynamic properties of a spinnaker, Lasher and Sonnenmeier (2008) used a selection of turbulence models to determine which model provided the best agreement to wind tunnel results. Along with the Realizable model, the standard k-ε, RNG k-ε, standard k-ω, SST k- ω and RS models were tested (for the full names of these turbulence models, refer to the Nomenclature section). These turbulence models were used for all the spinnaker configurations that Lasher presented. When compared to that of the standard k-ω and SST k-ω, the Realizable model provided a smaller percentage in error. The RNG k-ε model actually produced the lowest level of percentage error; however the solution was not the most robust (Lasher and Sonnenmeier, 2008). The findings suggested that the Realizable model performed the best for both accuracy and robustness with the measured force coefficients. Lasher and Sonnenmeier did note that while all the results were valid, all the turbulence models used struggled to predict the effect of the sail camber (Lasher and Sonnenmeier, 2008).

It is acknowledged that there are short comings in all turbulence models; it is therefore a difficult decision when it comes to selection. This is especially true in this case where there is a number of flow features all being simulated at once. The choice of model has, therefore, been a balance between how well the model will predict the characteristics of the flow in the wind tunnel, as well as, modelling the flow accurately around the test model.

2.5. Jet Properties

The Mercedes AMG PETRONAS wind tunnel has a nozzle with a square exit, due to its similarity with a square free jet; a validation study can treat it as such. Xu et al looked into the effect of Reynolds number on properties a jet exiting a square nozzle. For turbulence intensity, it was found that as the Reynolds number increased, the intensity decreased overall and over the same distance while the shape of the trend generally remained the same (Xu, 2013). Quinn and Militzer (1988) investigated the properties of square jet both numerically and experimentally, plotting the velocity profile and turbulence intensity. Again, this study had a lower Reynolds number than is used in this study, however, the trends that Quinn and Militzer found in turbulence intensity as you move away from the jet will be useful to ensure that the jet is presenting the correct properties. As the tunnel can be treated as a non-circular jet, its properties can also be compared to a study which was conducted by Miller et al (1995). The turbulence intensity as well as the velocity profile is investigated on square jets. The findings suggest that for turbulence intensity there should be peaks at the edges of the jet (Figure 2.5-2). These peaks gradually move further away from the centre of the jet with an increase in distance from the jet exit (Miller et al, 1995). Miller et al (1995) uses only numerical methods to investigate the properties of these jets and notes that the literature on the numerical analysis of 3D jet flow is very limited. When comparing results of different Reynolds numbers it is important to note that a direct comparison can’t be made, only very general comparison can be made.

Figure 2.5-1 - Velocity profile of Square Jet (Miller et al, 1995)

These images have been removed

Figure 2.5-2 - Turbulence Intensity of Square Jet (Miller et al, 1995)[1]

3. Methodology

3.1. Project Objectives

This project has the following overall aim:

- Investigate and quantify the corrections that need to be applied on C_D in the Mercedes Open Jet Wind Tunnel through the use of the Wong model

With the following objectives:

- Run comparative simulations on all wind tunnel tests and investigate the differences
- Create a standard wind tunnel model for future CFD use

[1] Where x*, y* and z* are the position in x, y and z respectively, over the nozzle radius.

- Run simulations at various speeds (increasing in steady increments)
- Investigate the turbulence intensity levels throughout the test section in both the CFD model and the Wind tunnel
- Improve the support apparatus for various models in the wind tunnel, simulate the improvements in CFD and then manufacture

3.2. Project Outline

This study is dominated by the CFD aspect; this is purely down to the amount of time that is needed to conduct a simulation. All the geometry used has been provided by Mercedes AMG PETRONAS Formula One Team when The Commissioning Report was compiled, unless stated otherwise. Where necessary the geometry has been modified so that it can be used in CFD, such as making all surfaces 'water tight', simplistic (removal of fixings such as screws, holes for fixings and overlapping layers) and made hollow. This was done so that meshing can take place. It is acknowledged that this will make the wind tunnel model and the CFD model have minor differences but, to remain computationally efficient there is no need to simulate in such a fine detail outside of the area of interest, which is the Wong Model.

The Mercedes AMG PETRONAS wind tunnel was used to gather all the wind tunnel data; it is a $1/5^{th}$ scale open jet wind tunnel with a top speed of $45ms^{-1}$. The model that has been chosen for testing is the Wong model (see Figure 2.1-4), two different versions of this model were used for comparison, with the second being a more accurate and sleek model than the first. The main difference between the two models is the way in which the model mounts to the balance, with the first being fixed to the top of the model with all the fixing exposed to the airflow.

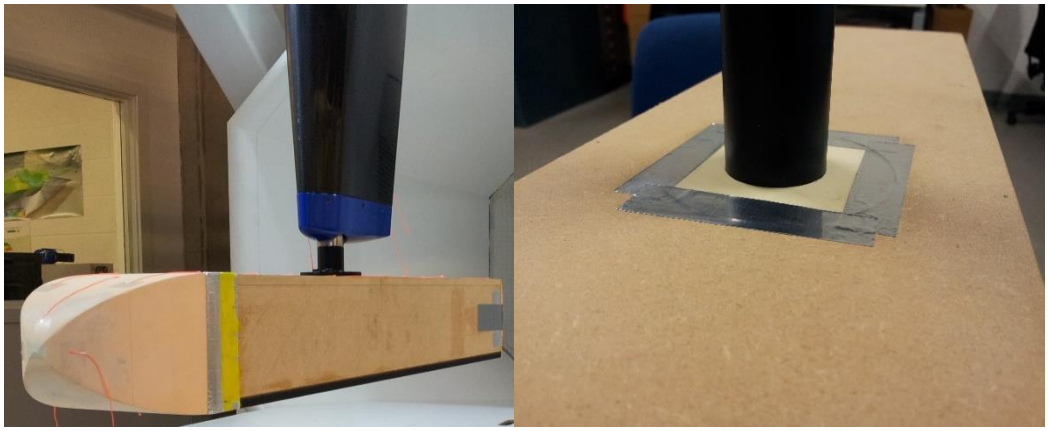

Figure 3.2-1 - Old Wong Model (left) & New Wong Model (right)

The second having a hole in the top which allows for the sting to be inserted into the Wong Model, with the fixings out of the airflow, the hole is also sealed with a foam disc. Both models have been tested with the Shroud (Left of Figure 3.2-1), Carbon Sting (Figure 5.2-2) and the Short Sting (Figure 5.3-1). Also with and without the ground board and at a variety of speeds which will be discussed in greater detail in the results section of the report. Both models were also tested with a variety of after bodies; this is also true for CFD. However, the CFD cases would only simulate one version of the Wong Model. The minor differences between the old and the new model would be too computationally demanding to accurately simulate. The after bodies used by Wong and Mair are 0.8 of the model width (153mm), however in this study the after bodies are twice this.

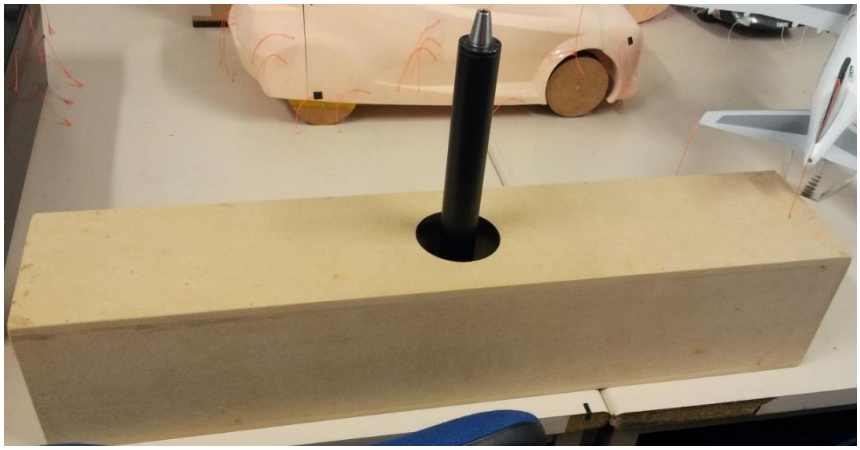

Figure 3.2-2 - New Wong Model with Internal Fixings and without Nose and After Bodies

With the maximum speed of tunnel being 45ms^{-1} this was the speed in which all the CFD simulations were set-up to run at. However, as the CFD schematic in Figure 3.5-3 and Figure 3.5-4 show the inlet of the flow is not the nozzle exit. This meant the entry velocity had to be calculated using continuity.

3.3. CFD Assumptions

As the majority of the work is being conducted on CFD there are some assumptions that have to be made. The reason for these assumptions is so that the complexity of the simulations can be kept to a minimum, thereby reducing the computational power necessary and thus simulation time. It also isn't always necessary to include extremely fine detail such honeycomb screens, collection nets and balance fixing as these will not affects the results in a noticeable way. With this in mind the following assumptions have been made:

- All the wind tunnel geometry is accurate to the physical wind tunnel

- The inner and outer walls, balance, Wong Model, mountings, table and aluminium board are smooth
- The various mountings are completely sealed with the balance and the Wong Model
- The settling screens do not affect a flow so much to warrant their inclusion in the simulations (Kulkarni, 2010)
- The table and aluminium board are horizontal in the test section
- All fixings are inside the Wong Model leaving the upper surface sealed and horizontal
- All the assumptions that come with the Open Jet Wind Tunnel Corrections as stated in 'On the Correction of Interference Effects in Open Jet Wind Tunnels' (Mercker and Wiedemann, 1996)
- Convergence of the simulation is met once the residuals have levelled off in the region of 0.001 for 3 time steps
- Convergence of the Coefficients was determined by a change of less than a couple of counts between each time step
- Model Coefficient, C_{μ}, is not constant and is determined by 2.4-6

3.4. Simulation Set-up

Once it was established that the tunnel did indeed show transient properties and the flow was unsteady (see Figure 3.4-1), all the simulations that proceeded were set-up to run Implicit Unsteady physics parameters, with the same model (Realizable k-ε). Each simulation also had the same number or inner iterations and time steps e.g. 100 inner iterations with 0.5s long time step. They all ran to the maximum amount of time that was pre-selected, unless it was found that the simulation did not converge, it was then run until convergence. In a case such as this, the force coefficients were used as monitors to determine the level of convergence. The size of the wind tunnel room (outer box that contained the tunnel) was maintained and was simulated as symmetry planes, so that their influence on the flow could be kept to a minimum.

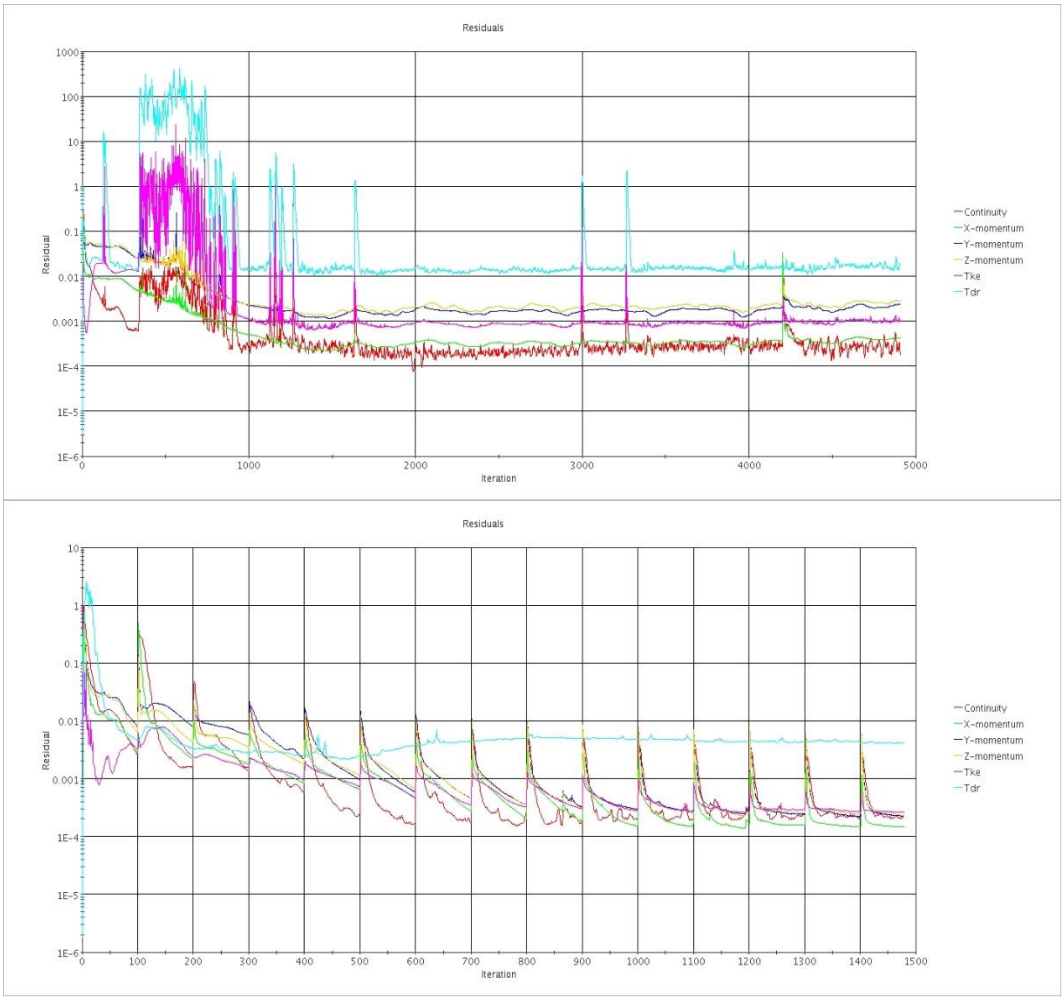

Figure 3.4-1 - Residuals of Steady (top) & Unsteady (bottom) Physics Parameters

All meshing values were also kept constant for each simulation so that the results could be compared with greater accuracy. Where mesh values were changed they were done so that the surface of the model was within the desired y+ region. The main area of interest for all the simulations is to get as close as possible to actual wind tunnel conditions. It was, therefore, very important to simulate the near wall components of the flow accurately. As was previously mentioned, this was done for the inner surface of the nozzle by calculating the Reynolds number for the whole nozzle length to determine the boundary layer thickness and then apply this value to the prism layer thickness. It was then found that separation did not occur until near the nozzle exit, this length was then used to determine the necessary prism layer thickness. Using this calculation is was found that the boundary layer thickness was 23mm. However, in an effort to reduce the computational demand and produce a mesh that will generate high Y+, the prism layer thickness was reduced to a thickness of 13mm. As previously stated in the literature review, it is important to balance the level of accuracy with the

computational power, this will also become clearer in Section 3.5. Also with the exit velocity and nozzle pressure showing good agreement with the experimental data, the added computational power is likely to produce little benefit. Monitoring the growth of the boundary layer on the inner nozzle surface with the use of a scalar scene (using Velocity Magnitude), it was clear to see that this was predicting the boundary layer adequately. All the components of the Wong Model were meshed so that they would be in the high y+ range.

$$\frac{\delta}{x} = \frac{0.16}{Re^{\frac{1}{7}}} \tag{3.4-1}$$

Equation 3.4-1 - Boundary Layer Thickness (White, 2009)

With the addition of the ground board, all the mesh and physics values remained constant. Some areas of the ground did need some modification, for example, all components of the ground board that were not in direct contact with the test section flow had all their prism layers removed. Also, due to the complexity of the CAD model, the legs of both the aluminium board in the centre were removed as were the table legs. In Figure 3.4-2, the New Wong Model is being used and it can be seen that the aluminium board (board between the table and the Wong Model) is not in close proximity to the model.

The original plan was to test and simulate the Wong Model in ground effect, however, as the sting had to be inserted into the model the height of the Wong Model was increased, preventing the board from getting in close proximity.

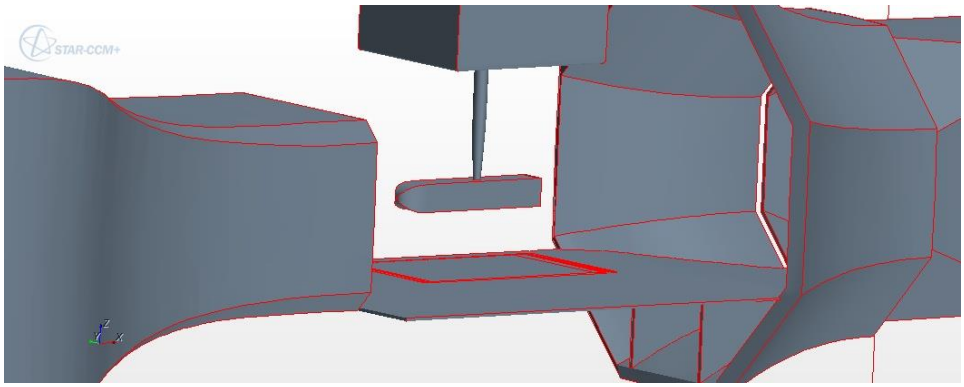

Figure 3.4-2 – Carbon Sting with Wong Model and Ground Set-up

3.5. Mesh Independency Study

The initial simulation in this project was set as a steady state case with the Realizable k-ε turbulence model to see how the flow and the residuals would behave. It was expected that the flow would indeed be transient and the results

from this simulation showed that this was indeed the case, with the residuals showing clear transient properties. Yet with there being clear transient properties, the results on an empty tunnel case presented little difference when it was run at either steady or unsteady. This simulation set a bench mark for the rest of the simulations e.g. investigating the parameters that were needed to generate a good quality mesh. So for this simulation to set the ground work, all the parts of the wind tunnel were meshed with a base size of 0.2m and with prism layers on all the internal surfaces. It is not necessary to have prism layers on the outer surfaces of the wind tunnel due to the obvious absence of flow. Once the simulation converged, an iso-surface was generated showing the zero total pressure. This was done so that the point at which the flow begins to separate from the inner walls of the nozzle could be determined and once this was known and measured, a more accurate value could be used for calculating the thickness of the prism layer in the rest of the simulations.

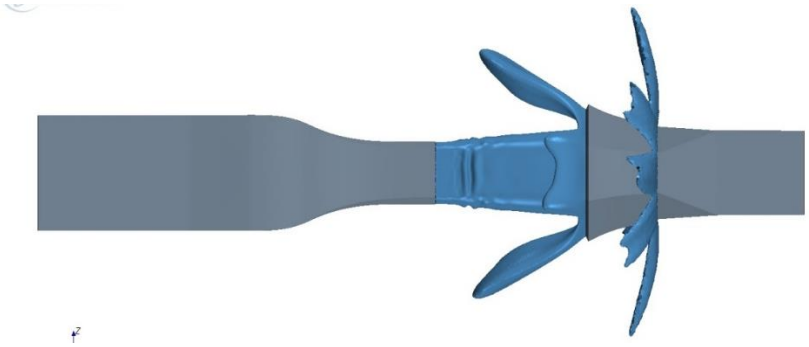

Figure 3.5-1 – Iso-surface of Empty Tunnel

The inlet velocity was determined through the use of continuity:

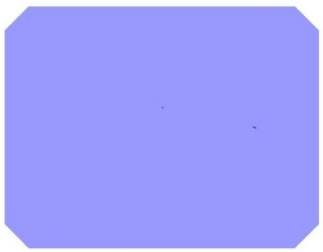

Figure 3.5-2 - Frontal Area of Nozzle Exit A_1

$$A_1 v_1 = A_2 v_2 = A_3 v_3 \tag{3.5-1}$$

$$\rho \; not \; present \; as \; density \; is \; constant$$

$$A_1 = (1 \times 1.3) - 4(0.5 \times 0.1 \times 0.1) = 1.28 m^2$$

$$A_2 = 1.89 \times 2.46 = 4.649 m^2$$

$$A_3 = 1.89 \times 2.286 = 4.325m^2$$

$$v_1 = 45ms^{-1} \quad \therefore \quad \frac{1.28 \times 45}{4.325} = v_3 = 13.316ms^{-1}$$

Equation 3.5-1 - Continuity Calculation

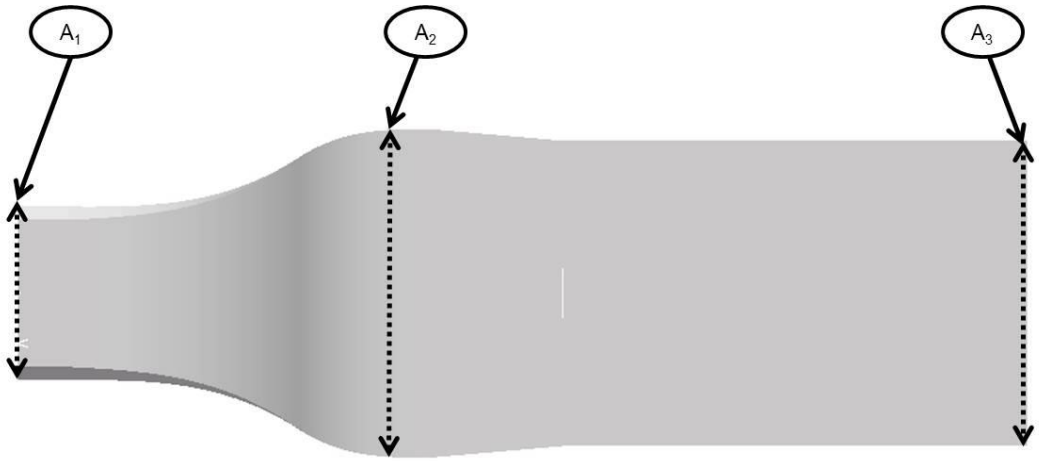

Figure 3.5-3 - Nozzle Diagram for Continuity Equation

From this calculation every simulation was set-up to have an initial velocity of 13.3ms^{-1}. In order to determine whether this value obtained from Equation 3.5-1 would be close to the simulated wind speed it was necessary to monitor the nozzle exit velocity and this was done by creating a plane on the exit to monitor the mass flow average. From Table 3.5-1 it is clear that the calculation is valid, with the difference in velocity being very small. The CFD exit velocity was determined through the use of a constrained plane on the exit of the nozzle, monitoring the averaged mass flow and selecting velocity magnitude as the scalar field function.

Inlet Velocity	Calculated Exit Velocity	CFD Exit Velocity
4.44	15	15.04
7.40	25	25.05
10.36	35	35.05
13.31	45	44.98

Table 3.5-1 - Exit Velocities

As well as the above (Table 3.5-1), it was found that there was a velocity gradient in the test section (Section 3.6). This was also investigated and the results of which can be seen in the next section. This aspect of the study was only conducted within the CFD simulations.

The importance on the mesh in any CFD simulation has already been highlighted in the literature review as it is one of the main areas which errors can be made (ERCOFTAC, 2000). As the geometry is slightly different for each individual set-up e.g. after bodies and wind tunnel ground board, an empty wind tunnel set-up was used to conduct the initial mesh study as this was the simplest case. In Figure 3.5-4 is the domain that was used for all the simulations.

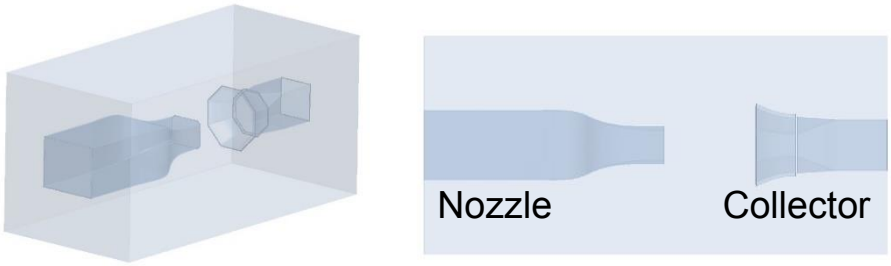

Figure 3.5-4 - Wind Tunnel Geometry

There are a number of ways in which the mesh can be altered; each surface can have a specified minimum and target size as well as customising the prism layers on each surface. As there are a large number of variables that can be changed, it was decided that only base size would be changed in each individual simulation. All the meshing parameters, excluding the prims layers (whose dimensions are determined with Equation 3.4-1) were set to a percentage of the set Base Size e.g. the Nozzle Volumetric Control (Figure 3.5-5 and Figure 3.5-6) was set to 20% of the Base Size. By starting with a coarse mesh, the base size can then be reduced in size to determine the optimum mesh size. This approach reduces the amount of time spent on this portion of the study. For all the base size reduction a speed of 13.3ms^{-1} was used at the inlet (45ms^{-1} in the test section), this was because the investigations on the Wong Model will be done at this speed.

There are a number of volumetric controls (VC's) within the simulation set-up, whose minimum and target size were kept at the same percentage of base size for all simulations. A volumetric control is a volume of cells that are kept at a constant size/volume. The largest of these VC's is in the nozzle and this can be seen in Figure 3.5-5 and Figure 3.5-6 as green and orange respectively. The Nozzle VC is there to ensure that there is an even distribution of cells across the flow inlet. The two remaining VC's are for the test section flow and the shear layer. For this shear layer to be measured and shown accurately, volumetric controls were needed. Initially, the size of the volumetric controls was estimated as the exact location of the shear layer was not known. They were constructed in

CAD from two truncated pyramids, one within the other. This meant that whilst creating an area where the mesh can be fine-tuned to measure the shear layer, the test section mesh quality can be maintained. As can be seen, these VC's were changed to cover the entire test section and the shear layer. The shear layer was also investigated in more detail in Section 3.5.1 (see Figure 3.5-8). In Figure 3.5-6 for the simulations with no Ground Board the VC's are as follows; Nozzle VC (A), Shear Layer VC (B), Test Section VC (C) and The Wong Model VC (D). The different VC's for the simulations with the Ground Board can be seen in Figure 3.5-10.

Figure 3.5-5 - Previous Volumetric Controls

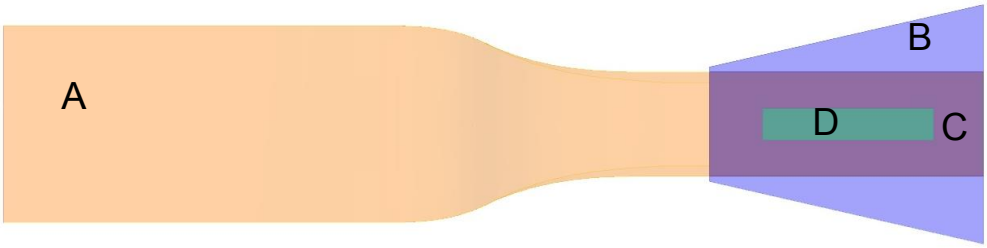

Figure 3.5-6 - Recent Volumetric Controls for No Ground Set-up

The Test Section VC (C) is positioned around the entire test section of the wind tunnel to ensure that all the cells are a uniform size. These cells lead up to and around The Wong Model VC (D). This is positioned around the Wong Model to ensure that the wake is modelled in high detail. Failing to do so will results in the software generating a less accurate value of drag.

Another measurement that was made within CFD is the pressure difference within the nozzle (between A_1 and A_3 in Figure 3.5-3). This was recorded for $45ms^{-1}$ as $125mmH_2O$ with a digital manometer, which is 1225Pa. This value is the same with and without the table inserted into the test section. The wind tunnel also has a nozzle exit pressure that is atmospheric, so for this to be true within the simulations the outlet pressure has to be modified to increase the pressure at the nozzle exit. This was monitored in the same way as the nozzle exit velocity, through the use of a constrained plane on the nozzle exit.

Base Size (m)	ΔP in Nozzle (Pa)	ΔP from atmospheric at Nozzle Exit (Pa)
0.50	1132	+4
0.40	1121	-8
0.25	1134	+5
0.20	1153	+9
0.15	1126	-1

Table 3.5-2 - Base Size Pressure Difference

Table 3.5-2 shows that as the base size decreases there is a slight increase in the pressure predictions, however, the differences are only small. Also note that in Table 3.5-3 the velocity at the exit of the nozzle changes very little. These two sets of results would suggest that even with a course mesh some of the tunnels features are still simulated with a good degree of accuracy.

Base Size (m)	Nozzle Exit Velocity (ms^{-1})
0.5	45.08
0.4	45.00
0.25	44.99
0.2	44.98
0.15	45.03

Table 3.5-3 – CFD Results of Base Size Exit Velocities

3.5.1. Shear Layer Investigation

As was previously stated, the shear layer is an important feature of the wind tunnel as it can affect the flow in a number of ways. Depending on the shear layers characteristics, it can increase or decrease the jet velocity which can also cause the jet to undulate. Any changes in the jet characteristics, will affect the flow around the model and thus any force measurements. The shear layer can be investigated by looking at the changes in velocity in the ‘z’ direction. Using a pitot tube which is attached to the front of the balance in the wind tunnel, it is possible to determine a thickness of this shear layer. Due to the pitot tubes positioning it was only possible to take the first reading at 30mm into the jet (30mm down from the balance); ideally the first measurement would occur where the flow is stationary.

Figure 3.5-7 - Tube Positioning (left) & Pitot Tube Starting Position (right)

As the purpose of this measurement is to ensure that the simulations are in fact accurately simulating the wind tunnel features, this is more than adequate. The measurement was made in the centre of the jet at a distance of $0.7R_N$ in the 'x' direction. Figure 3.5-8 shows the results from the wind tunnel and the various mesh base sizes (0.5, 0.4, 0.25, 0.2 and 0.15), where z/D_b, is the distance the Pitot tube has moved in the 'z' direction over the distance between the balance and the nozzle edge. It is again interesting to see that all the mesh variants perform similarly. With all the base sizes under predicting the initial velocity, then producing good agreement with the wind tunnel results, as the Pitot tube gets closer to the test section. This follows what Shih et al (1995) found, that the Realizable model performs reasonably well in this region of high separation. Once the finest mesh showed that there was still little difference a comparative investigation was conducted into the use of difference turbulence model, SST k-omega in this case. The results of which can be seen in Figure 3.5-9. The figures showing the Shear Layer investigation show the previously mentioned base sizes in comparison to the wind tunnel findings.

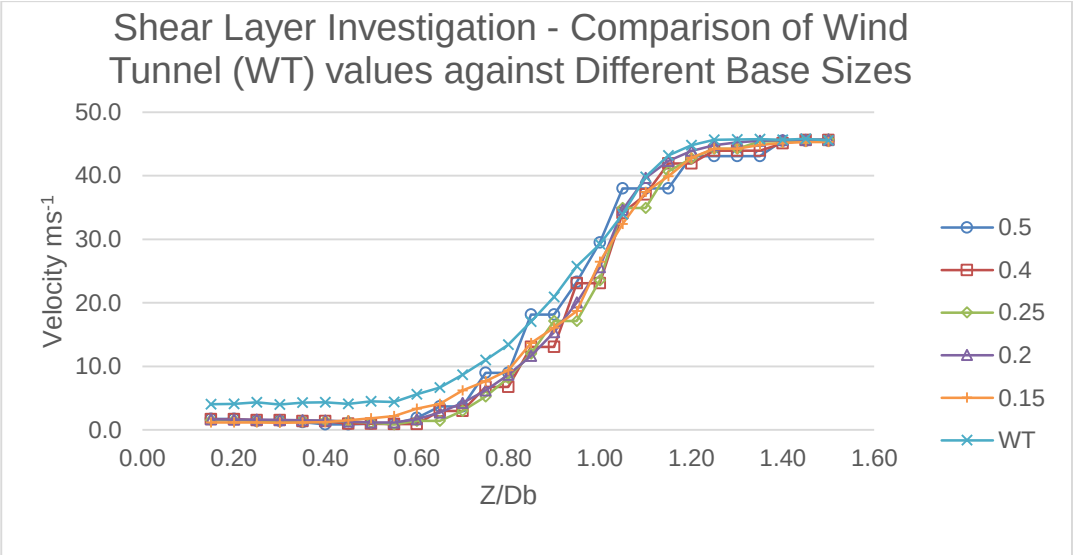

Figure 3.5-8 - Shear Layer Investigation with Realizable k-ε (above)

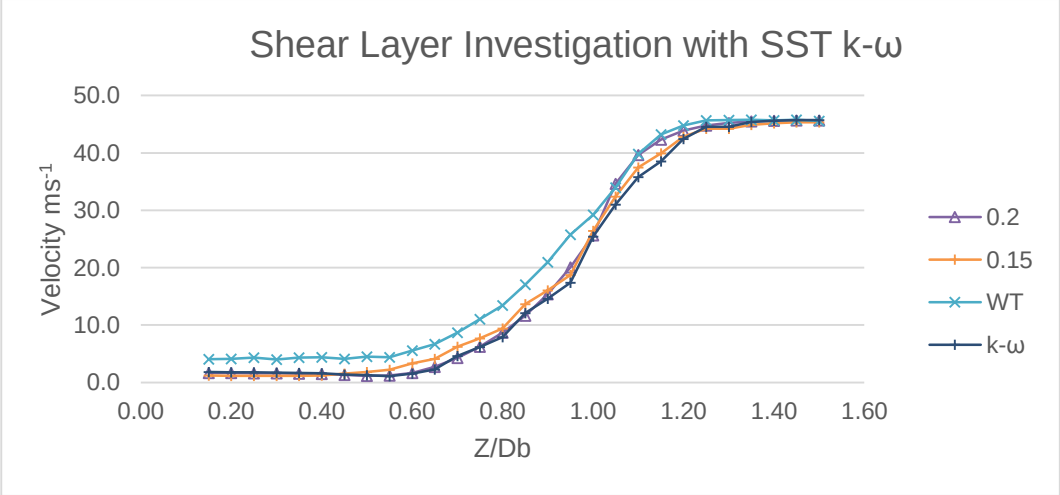

Figure 3.5-9 - Shear Layer Investigation with SST k-ω (above)

Using the SST k-ω turbulence model (with a base size of 0.15) generates similar results to the previously shown data, with very few differences to that of the coarser mesh with a 0.2 base size or the finer. The mesh study on the empty tunnel has shown that the most of the tunnel features are simulated well by all the mesh sizes. This does not mean, however, that the coarsest mesh is appropriate when a model is inserted into the test section.

3.5.2. Wong Model Mesh Independency

Once a model is inserted with or without its respective support apparatus, the already complex flow features become more complex. There is the addition of more boundary layers of different properties, flow separation, flow recirculation and possible vortex shredding. Therefore, the addition of the Wong Model

requires further mesh refinement around the model in question. The procedure for this mesh study is the same as with an empty test section. It may be necessary in some cases to add addition VC's and as was mentioned previously, one was inserted around the Wong model. The VC labels are the same as those in Figure 3.5-6.

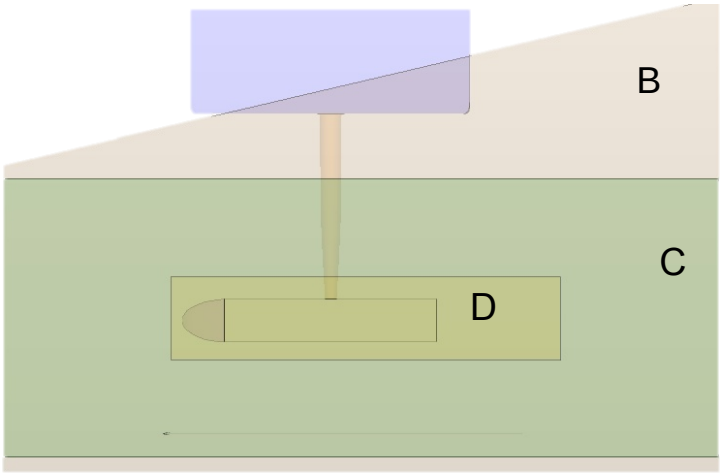

Figure 3.5-10 - All VC's with Wong Model with Ground Set-up

As there are different model set-ups in this study the mesh investigation was conducted on the Wong Model with '0' after bodies and without the addition of the ground board. This particular set-up is the easiest of the configurations to implement. The addition of the ground board complicated the surface separation and integration in the initial stages of set-up. Even with the geometry being drastically simplified, with the removal of all nonessential components the simulations with the ground board required significantly more time to initialise.

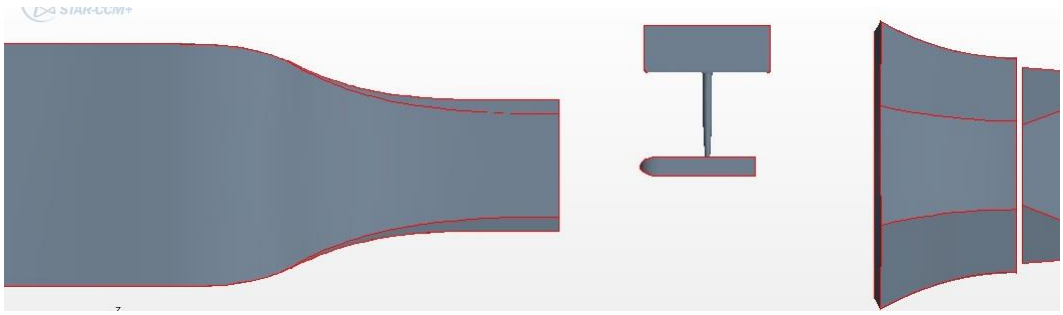

Figure 3.5-11 – Wong Model Set-up

As the base size was decreased the number of cells increased, thus the run time of the simulation increased, ranging from a few hours to 72 hours for full convergence. The CFD predictions are compared to that of the wind tunnel (WT) measurements to ensure the accuracy of the mesh.

Mesh	Base Size (m)
1	0.5
2	0.4
3	0.25
4	0.2
5	0.15
6	0.14

Table 3.5-4 - Mesh Number with Corresponding Base Size

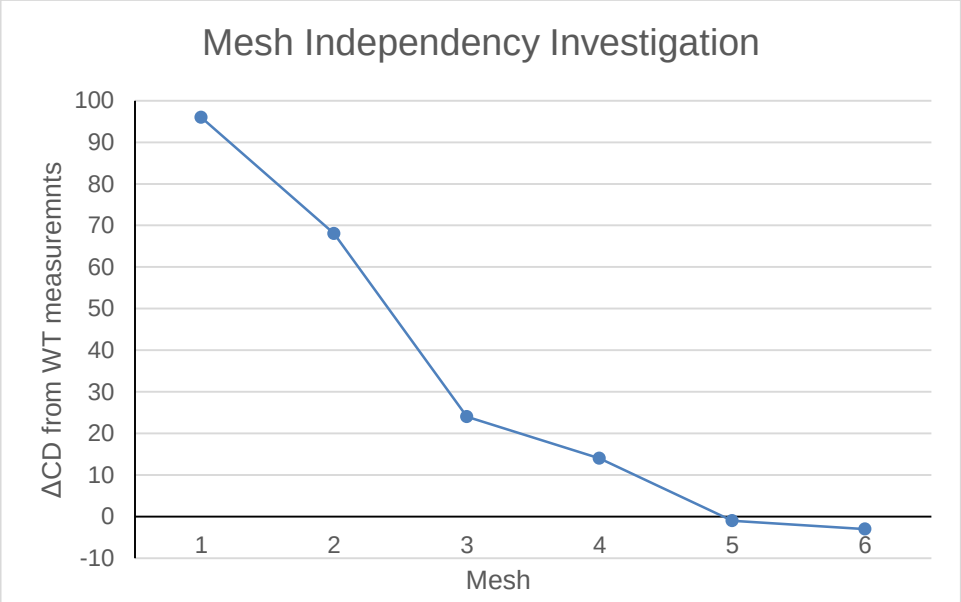

Figure 3.5-12 - Mesh Independency Investigation

It is now much clearer to see that the difference in base size has a large difference in the C_D values of the Wong Model. With a difference of almost 100 counts the coarsest mesh clearly isn't appropriate. Also note that the reason that the base size does not decrease in constant increments from 0.5 to 0.1, is due to the amount of time it took for the smallest base size to mesh. Base sizes of 0.1 often lead to a meshing processes aborting due to a limit in computational memory. It's clear from the results of the different meshes that reducing the base size further would not produce any benefit. This mesh independency study will be referred to later as recommendations are made on which mesh should be used for future studies. For the remaining simulations, a base size of 0.15 was chosen as this was the closest to the wind tunnel values while not being too computationally demanding. This is also the point where the values of C_D converged and decreasing the base size further shows no great benefit.

3.6. Turbulence Intensity and Velocity Profile Investigation Realizable k-ε

The nozzle can essentially be modelled as a square pipe with a contraction from which a free square jet exits. While the nozzle exit does have chamfered corners and the Reynolds numbers of the various tests conducted in the wind tunnel are higher than that which are presented by Quinn and Militzer (1988), the trends from both data sets can be compared. The general trends of turbulence intensity in a stream wise direction, measured across the span of the jet do show similarities when comparing Figure 3.6-1 and Figure 3.6-2. The intensity within these peaks is also expected to increase with distance. For this comparative investigation, it is important to note that is was not possible to do this within the wind tunnel as the necessary equipment was not available to undertake a comparative study. It is acknowledged that this would be an advantageous investigation to further back up the CFD set-up and this is why it will be suggested as a possible route for future work. At the time of this study the necessary equipment was not available. As was previously done in the Shear Layer Investigation, two turbulence models will be compared within this section.

Figure 3.6-1 - Turbulence Intensity (Quinn and Militzer, 1988)[2]

[2] $Y/Y_{1/2}$ is the position in y over the velocity half width. $\sqrt{\overline{u^2}}/u_{c1}$ is the turbulence intensity

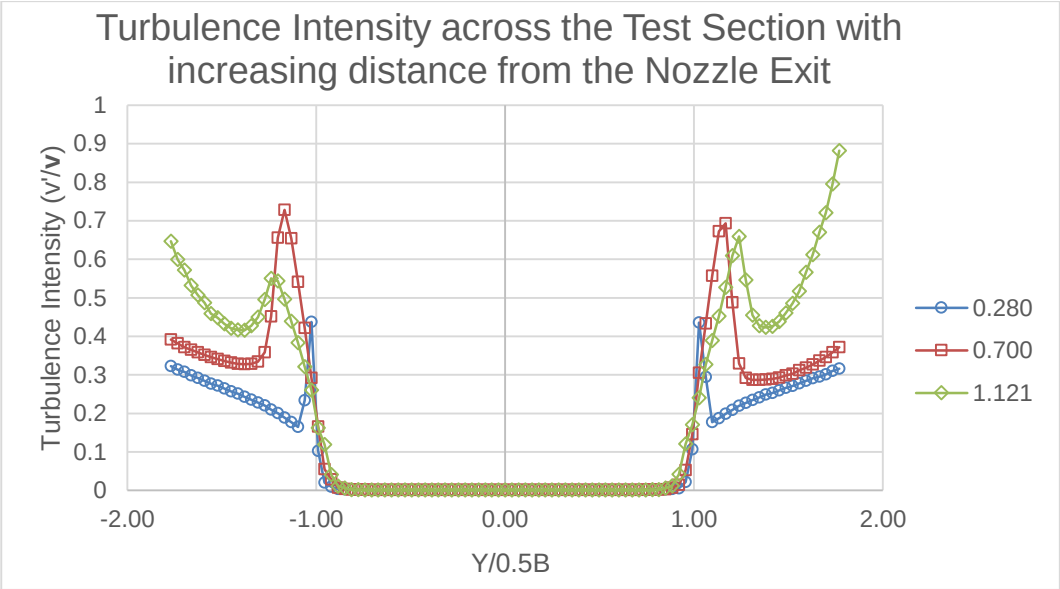

Figure 3.6-2 - Turbulence Intensity 1a

Here, $Y/0.5B$ is the distance in 'y' over half the nozzle width. The estimated values are taken on a line probe that passes through the test section perpendicularly to the flow direction at a constant value of 'z', which is the centre of the nozzle. The values for the different 'x' positions (0.280, 0.700, 1.121, 1.504, 2.035 and 2.212) have been non-dimensionalised by dividing the distance moved in 'x' by the equivalent nozzle diameter to match the positions presented by Quinn and Militzer (1988). All the readings that have been taken on the levels of turbulence intensity and velocity gradient have been made in the same positions. Due to the test section length it was also not possible to do a comparative measurement of the last measurement in the initial region presented by Quinn and Militzer (1988), therefore a reading was taken in-between Quinn and Militzer's first two measurements. When comparing these results it is clear to that the trends produced in both cases are of a similar nature (Figure 3.6-1). The major difference is in the levels of turbulence are in the two extremities of the plot. This is to be expected as this shows the position of the shear layer, where levels of turbulence intensity are at their highest and this case has much higher Reynolds number. However, the estimated values taken at 0.700 and 1.121 show little difference in the peak intensity; this is likely due to the transient feature of the shear layer which can be seen in Figure 3.5-1, where there is a ripple in the shear layer that travels across the test section.

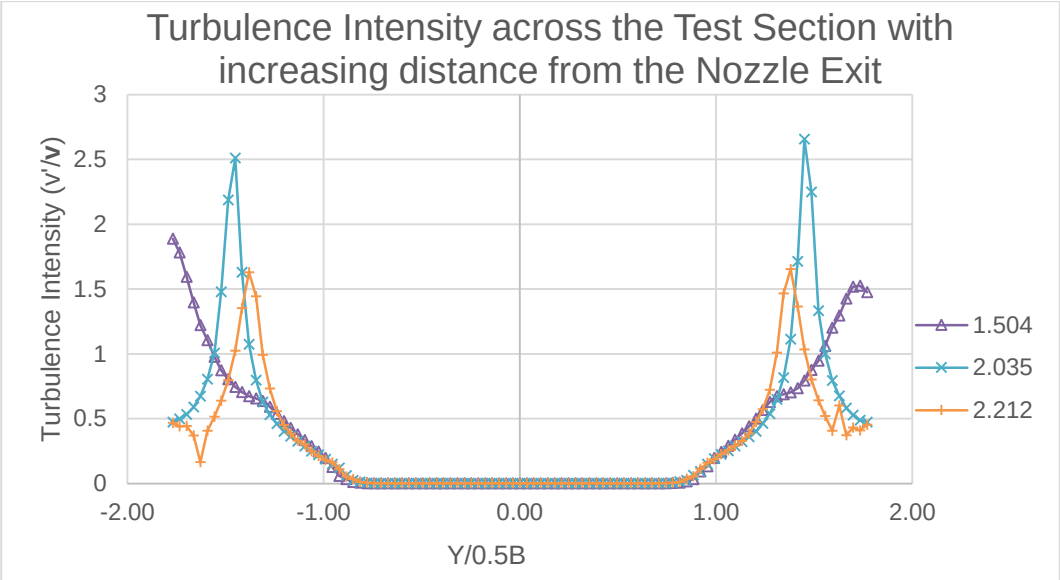

Figure 3.6-3 - Turbulence Intensity 1b

The measurement taken at 2.212 is at the face of the collector, it is interesting to note that the highest peak in intensity is before the collector. It is likely that this is down to the high turbulent viscosity of the flow, which then decreases upon meeting the collector. Quinn and Militzer found that there is a decrease in intensity after the peak that continues to decrease; where as in this case, it is found that the intensity increases again in some case, highlighting the complex nature of the test section flow (Figure 3.6-1). Little and Wilbur (1951) found trends of a similar nature with the highest Reynolds number that was investigated. While this Reynolds number was still below that of this investigation, the closely related trends are encouraging (Little and Wilbur, 1951). Looking at Figure 3.6-2 it would seem to show that the level of turbulent intensity is constant for all distances; however, by looking closely at the lower values this is not the case. There is now a much clearer difference in the levels of turbulence intensity as the flow moves further away from the nozzle, for example the level of intensity decreases within the test section with increasing distance away from the nozzle.

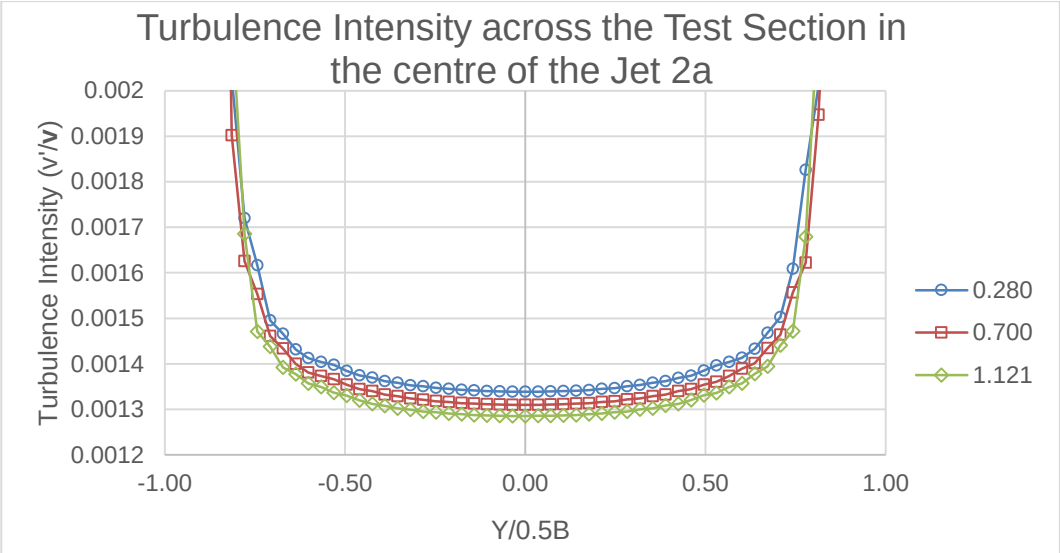

Figure 3.6-4 - Turbulence Intensity 2a

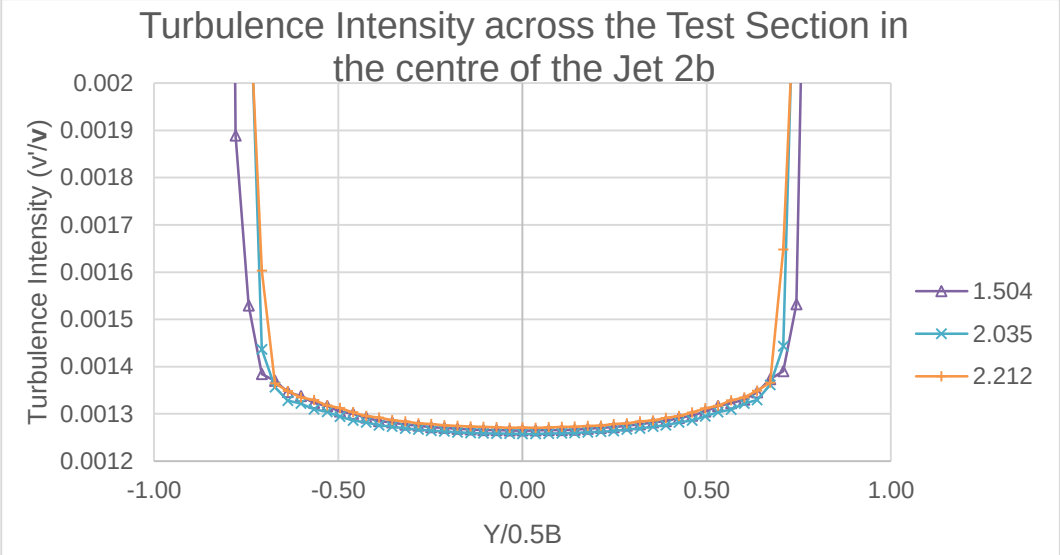

Figure 3.6-5 - Turbulence Intensity 2b

The velocity profile also exhibits traits that look like that which were found by Miller et al (1995) and Quinn and Militzer (1988), where the profile gradually dissipates outwards as the distance from the jet increases. This suggests that the tunnel is behaving like that of a simple jet. It is again important to mention that the velocity across the nozzle width is not constant. This is a crucial feature to be aware of especially in open jet wind tunnels. This velocity gradient throughout the test section (especially around the model position) needs to be known as this will affect the coefficient readings if the velocity is not constant. In essence this profile highlights the importance of knowing the model position and also being aware that the model is not sitting within one of these gradients. Another feature of the

flow that can be seen by comparing Figure 3.6-2 and Figure 3.6-7 is the region between 1 and 2 Y/R_N.

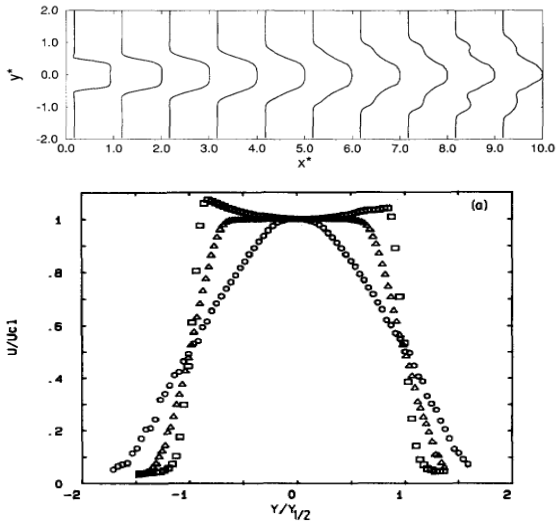

Figure 3.6-6 - Velocity Profile found by Miller (1995) and Quinn (1988) respectively[3]

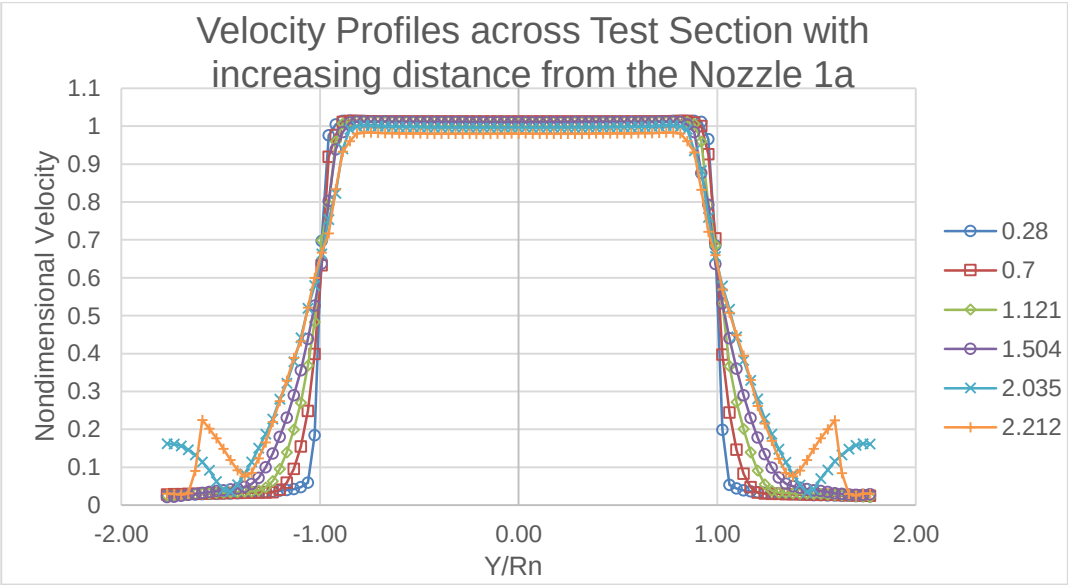

Figure 3.6-7 - Velocity Profile 1a

A different perspective shows the previously unseen peaks in velocity in Figure 3.6-9. These velocity peaks also correspond with shape of the wind tunnel, where the flow is accelerated around the edges of the outlet due to the contraction in

[3] Where y* and x* are the position in y and x respectively, over the nozzle radius. $Y/Y_{1/2}$ is the position in y over the velocity half width. $U/U_{cl} = K_d (X/D_e + C_k)$, where K_d is the decay rate of the jet and C_k is the kinematic virtual origin. For more details please refer to Quinn and Militzer (1988).

the nozzle, creating a concave jet. A favourable property is also highlighted in Figure 3.6-9, the velocity gradient in less prominent in the centre of the test section, where the model is positioned. It is shown that the model is in a good position for force measurements to be made within the wind tunnel, as there is minimal velocity change across the width of the test section. If a more prominent velocity gradient was present in the centre of the test section, the velocity that is used to calculate the forces would be in correct (Mercker, 1997).

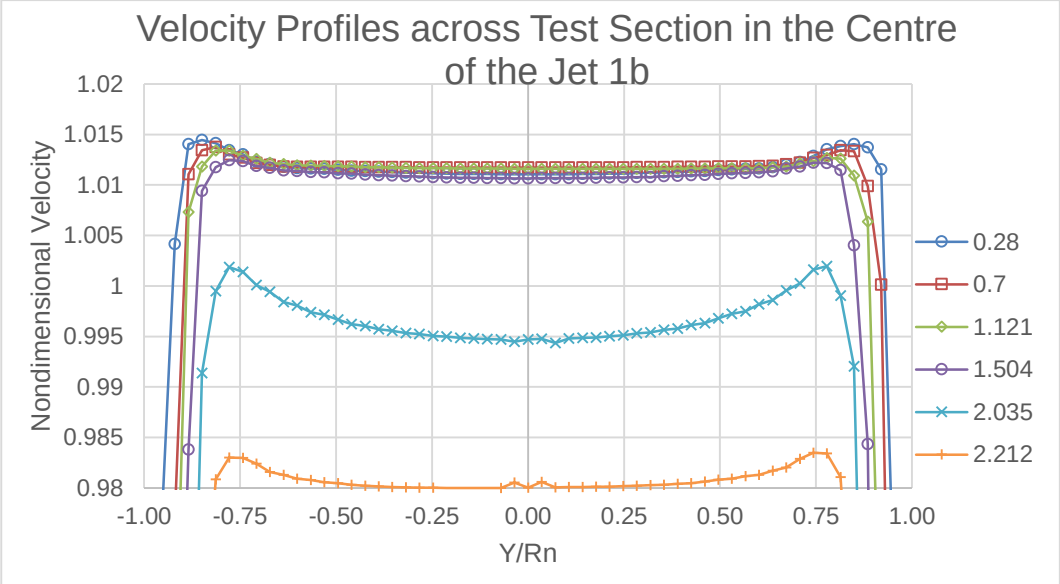

Figure 3.6-8 - Velocity Profile 1b

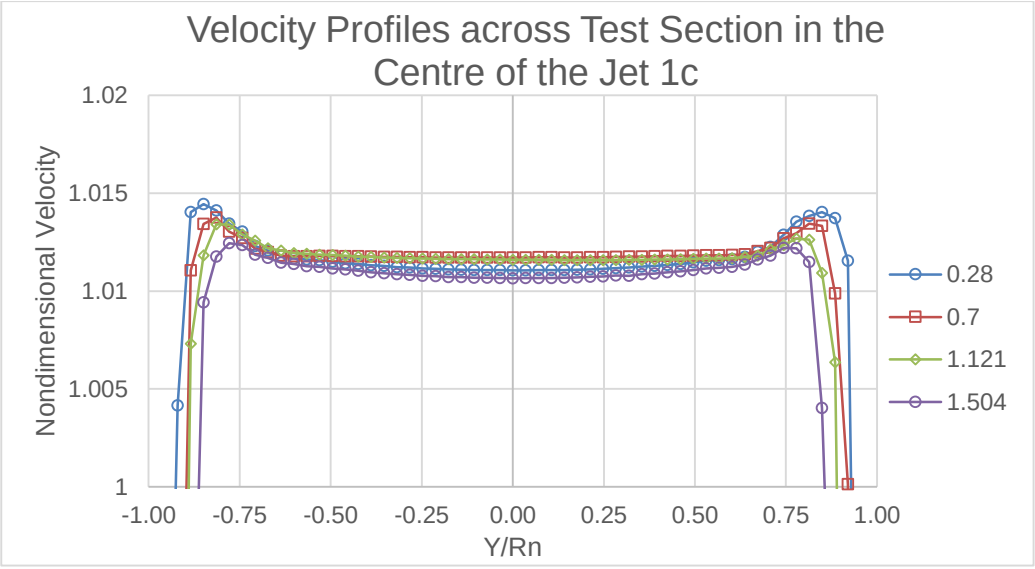

Figure 3.6-9 - Velocity Profile 1c

3.7. Turbulence Intensity and Velocity Profile Investigation SST k-ω

The Realizable k-ε showed that it was predicting the presence of a shear layer well and that the velocity profile was shown to be similar to that found by Quinn and Militzer (1988). In this section the SST k-ω is used for comparative purposes. The positions in which the estimated values are taken is identical to that of the previously shown Realizable k-ε results in the previous section (Section 3.6)

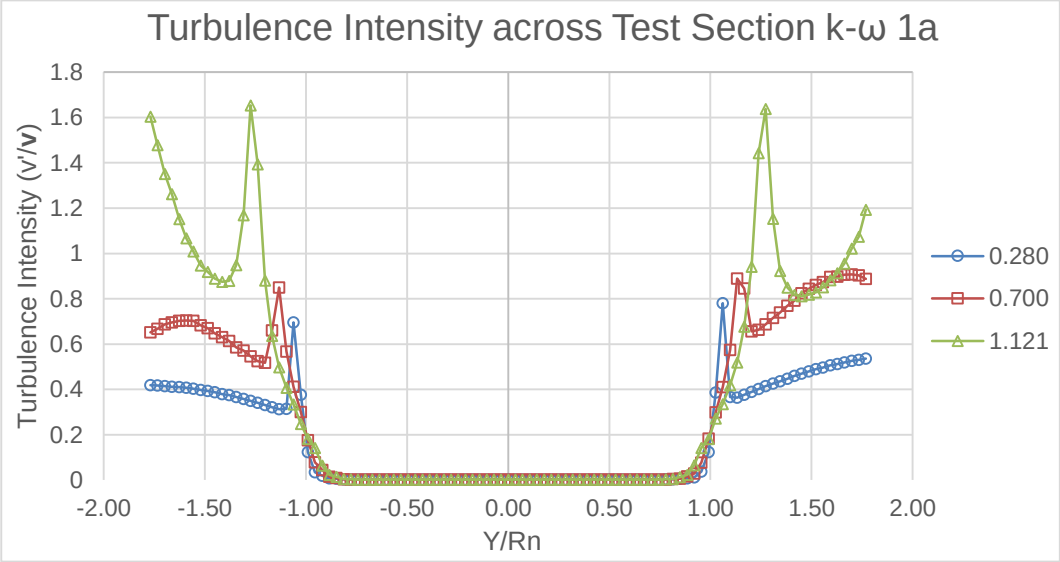

Figure 3.7-1 - Turbulence Intensity k-ω 1a

Examining Figure 3.7-1 and Figure 3.6-2 it can be seen that the k-ω predicts higher levels of turbulence than that of the Realizable k-ε model. This remains true throughout the test section. The peaks in intensity have also moved further away from the centre of the nozzle as well as increasing in value.

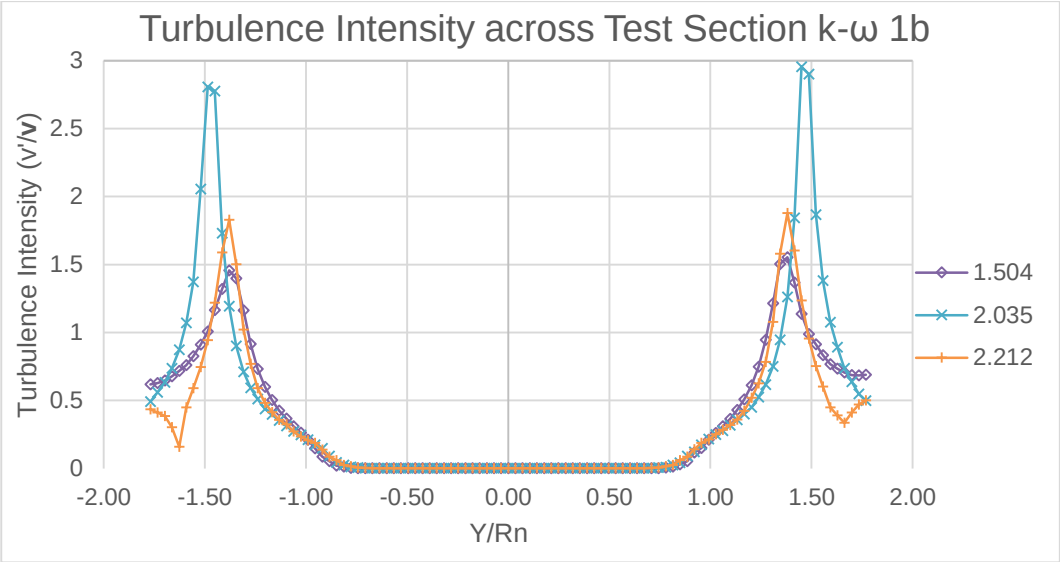

Figure 3.7-2 - Turbulence Intensity k-ω 1b

Again looking at the low levels of turbulence in the centre of the test section it can be seen that the intensity drops the flow continues along the test section.

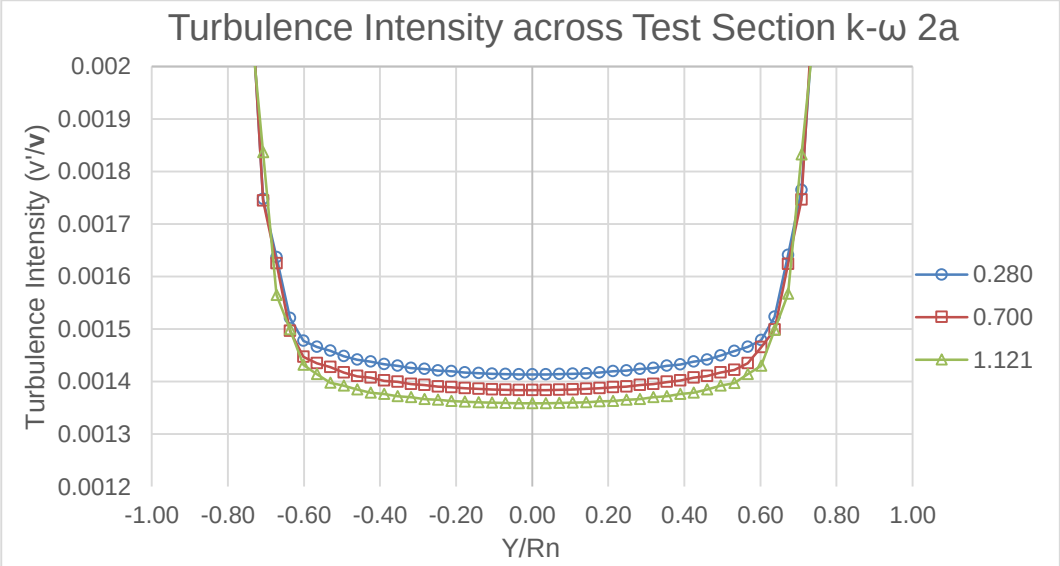

Figure 3.7-3 - Turbulence Intensity k-ω 2a

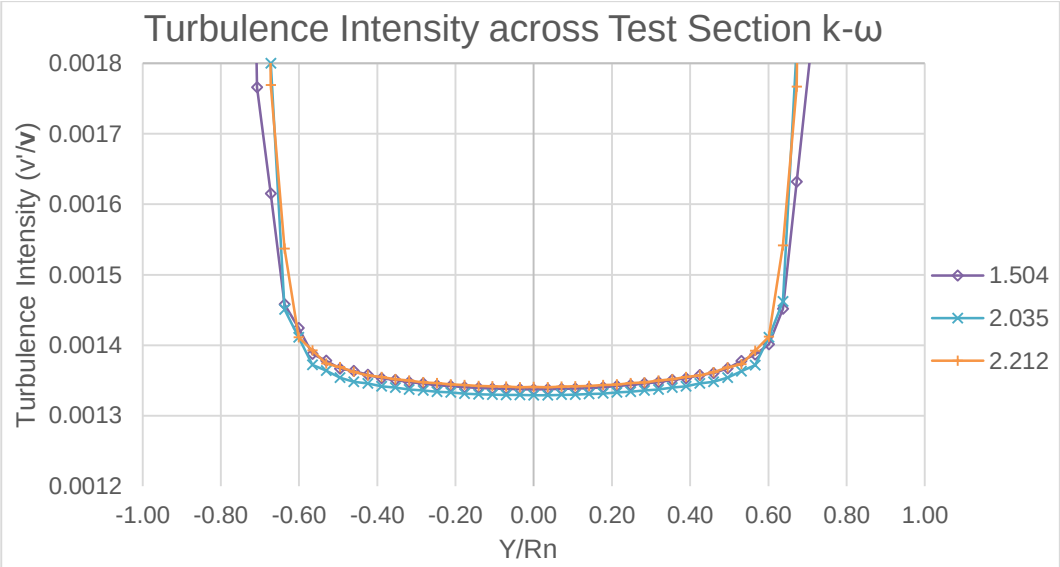

Figure 3.7-4 - Turbulence Intensity k-ω 2b

When comparing the two turbulence models, with respect to velocity profile yields very few differences looking at the initial graphs (Figure 3.6-7 and Figure 3.7-1). Both show the trends that were found by Quinn and Militzer (1988). The differences between the two models do become more apparent with closer inspection at the velocity peaks in the test section. All the graphs so far showing the Turbulence Intensity across the test section show that the model can be positioned between -0.5 and 0.5 Y/Rn.

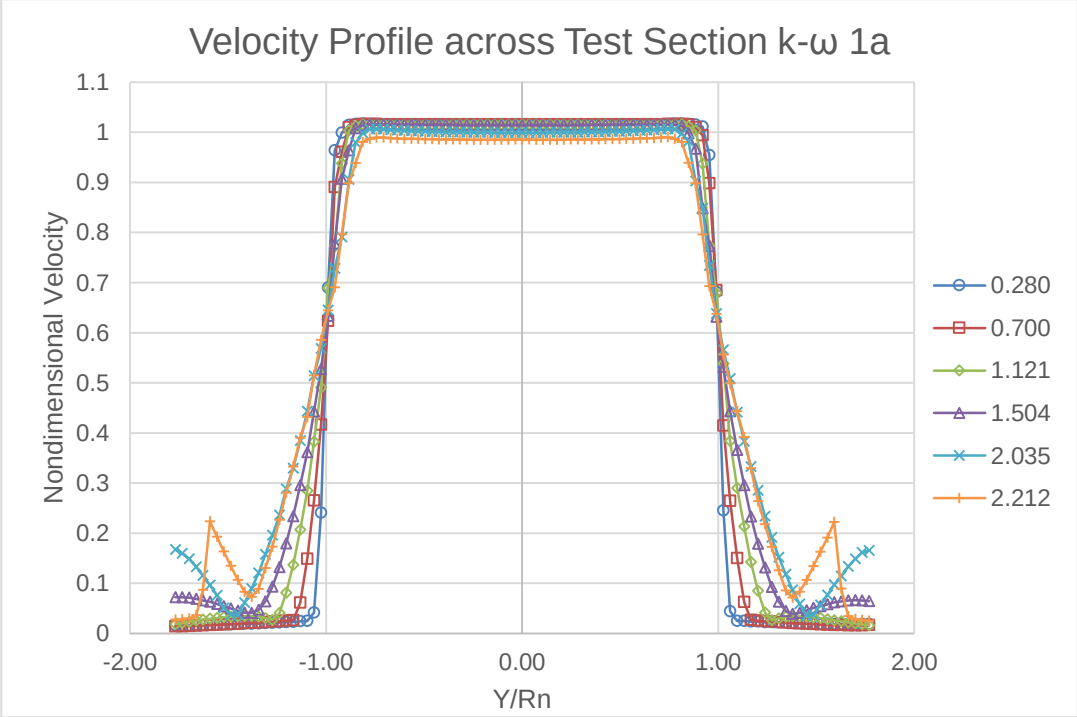

Figure 3.7-5 - Velocity Profile k-ω 1a

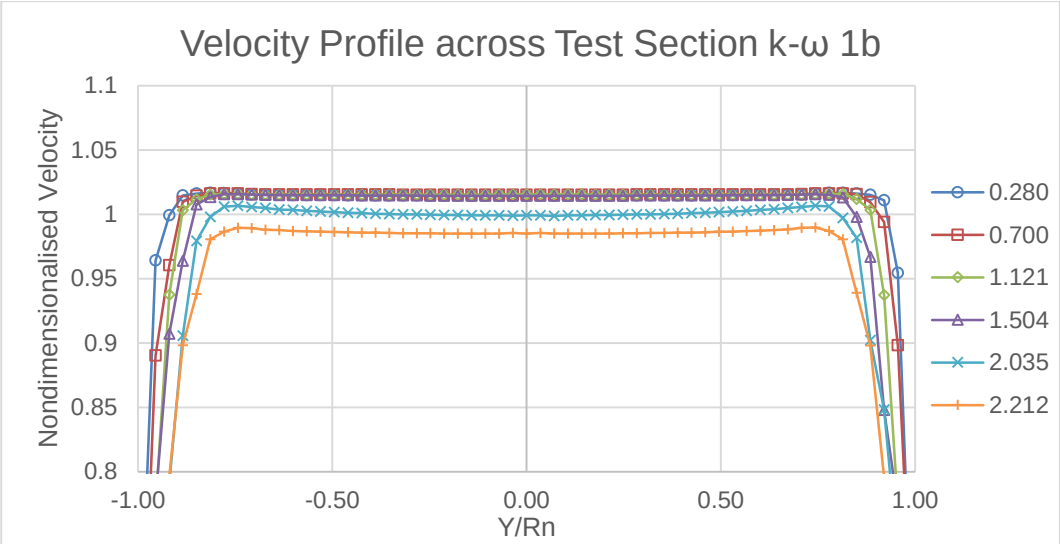

Figure 3.7-6 - Velocity Profile k-ω 1b

The SST k-ω model predicts that the velocity profile within the test section is slightly larger than that predicted by the Realizable k-ε model. The final graph showing the velocity profile (Figure 3.7-7) shows that the velocity gradient measured at 0.280 and 1.50 are near identical; this is not the case with the previous turbulence model. It also emphasises the miniscule the velocity gradient within the test section is, suggesting that the model could be placed between value of Y/R_n of -0.5 and 0.5. Already has it been mentioned, that this study could not be repeated experimentally due to the necessary equipment being unavailable. This investigation suggests that repeating this process in the wind tunnel would be beneficial as it would provide clarity as to which model predicts the characteristics of the flow more accurately.

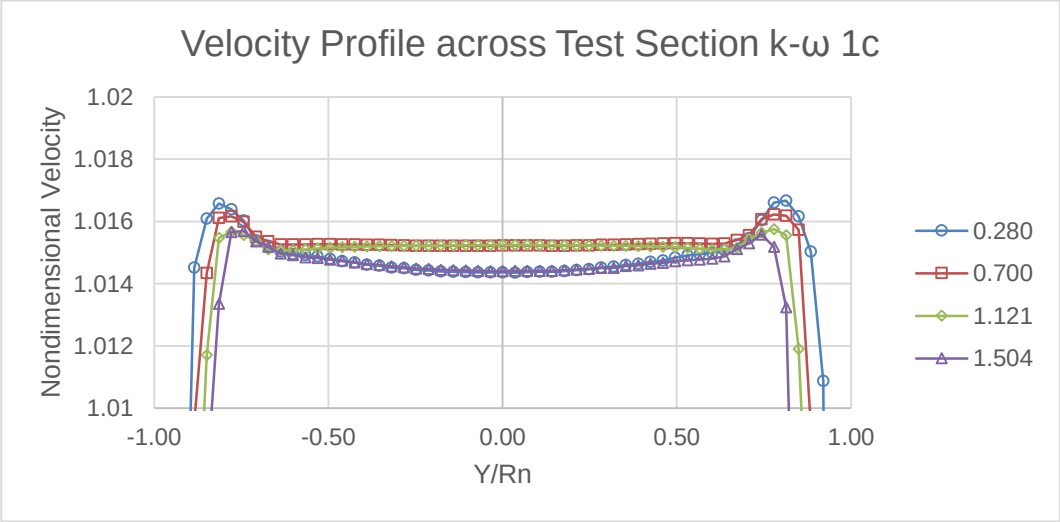

Figure 3.7-7 - Velocity Profile k-ω 1c

3.8. Sensitivity Study

The investigation into turbulence intensity in Section 3.6 and 3.7 focused on the intensity level perpendicular to the direction of the flow. Within this section an investigation into the turbulence intensity in the stream wise direction will be presented.

This investigation was undertaken so that the turbulence decay and the level of intensity could be predicted mathematically at a certain point. Previously the level of decay was unknown, so it was not possible to set an inlet value of intensity, to get a desired value of intensity at a certain point. However, this study aims to provide a way to fix this. Meaning that for a specific case where certain prerequisites are known e.g. β, **v** and x, the turbulence intensity can be estimated.

The domain in this case is the same as the one shown in Figure 3.5-4 but, the wind tunnel geometry has been removed. This gave a domain just over 12m in length with a mesh density of 200,000 cells. The low mesh density allowed for a quick run time. Once this simple mesh was constructed a line probe was created through the centre of the domain in the stream wise direction to monitor the turbulent kinetic energy (k). From this the turbulence intensity could be calculated using Equation 2.3-1. Then one set-up parameter such as the viscosity ratio (β) was chosen to be monitored. The parameters effect on turbulence decay would be monitored against different velocities. For example, the initial investigation looked in to values of '**v**' ranging from 5, 10, 15, 25, 35 and 45ms^{-1} at a constant β. All other parameters effecting turbulence intensity such as k, ε, Inlet Turbulence Intensity and Length scale remained constant unless they were being investigated (at values of 0.001Jkg^{-1}, 0.1m^2s^{-3}, 1% and 0.01m respectively).

There are areas on the graph where it appears that the intensity levels off briefly, this is because a number of points on the line probe are taken within the same cell. Hence the same value being generated.

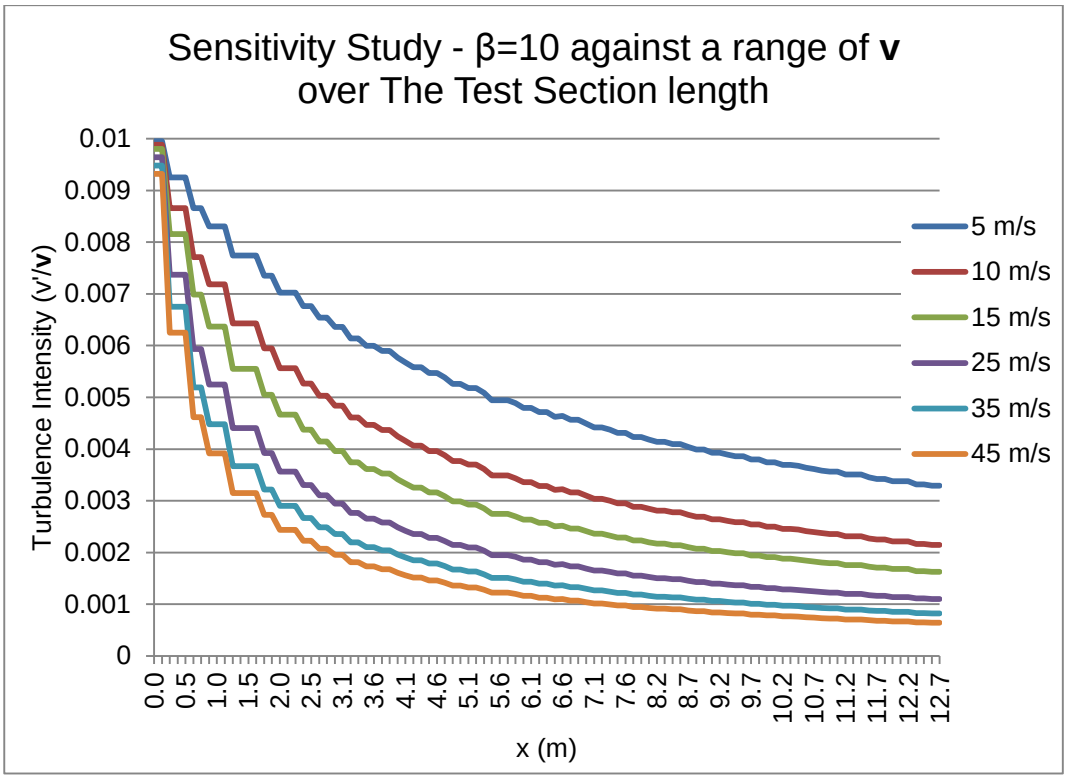

Figure 3.8-1 - Constant value of β=10 across a range of v

Once this data was obtained it was transferred to MATLAB. Where the curve fitting tool could be used to find an equation that would predict the value of the turbulence intensity for a given position of 'x', at a given velocity for a particular input value e.g. β. Figure 3.8-1 shows that the decay produced is clearly exponential. This exponential decay can be put into the form of an equation such as:

$$I = ae^{-bx} + ce^{-dx} \tag{3.8-1}$$

Equation 3.8-1 -Sensitivity Study Equation for Turbulence Intensity at a given value of 'x'

Where 'I' is the turbulence intensity and the coefficients 'a', 'b', 'c' and 'd' for each line in Figure 3.8-1 can be determined. The equation for each individual line can then be plotted through the use of the MATLAB curve fitting tool. Then the trend between the coefficients of each line can be plotted against the variable range ('**v**' in this case). From Figure 3.8-2 to Figure 3.8-5 it can be seen that in this case all the coefficients (a, b, c and d) show a clear exponential relationship against velocity.

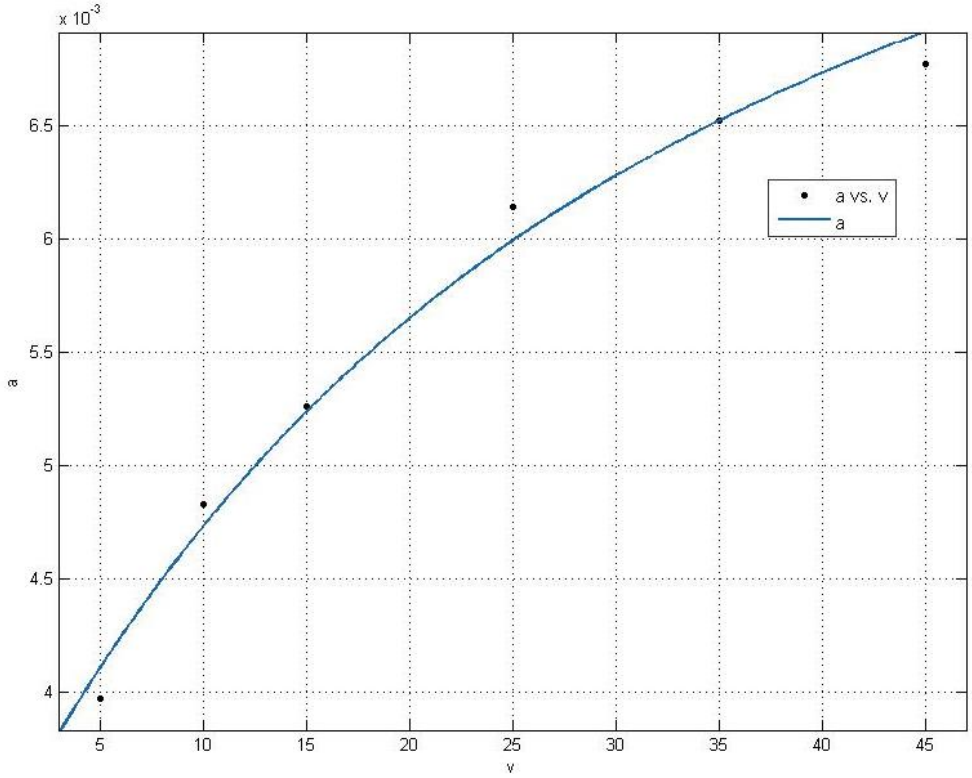

Figure 3.8-2 - β=10 Coefficient 'a' against Velocity

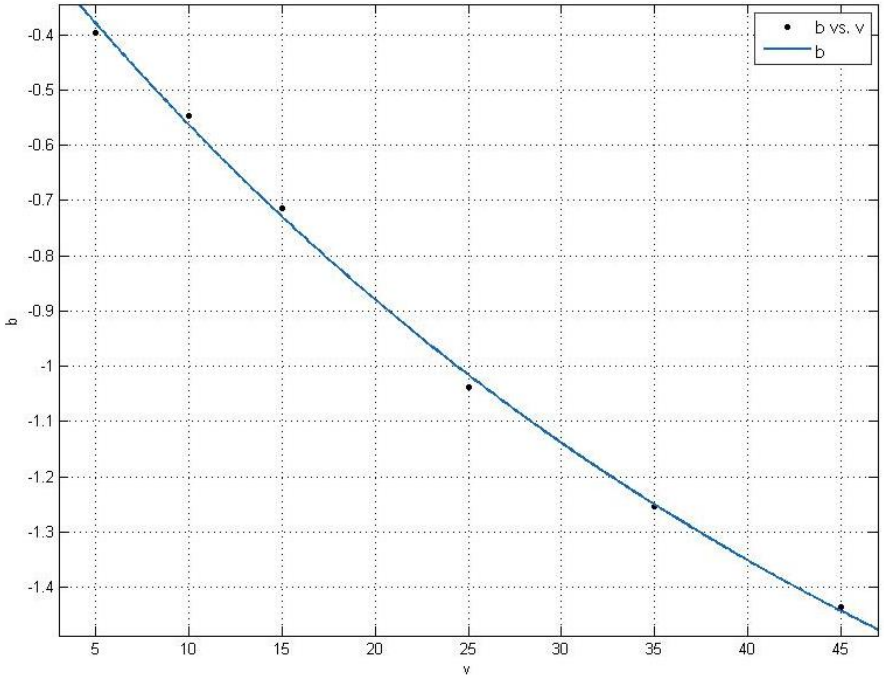

Figure 3.8-3 - β=10 Coefficient 'b' against Velocity

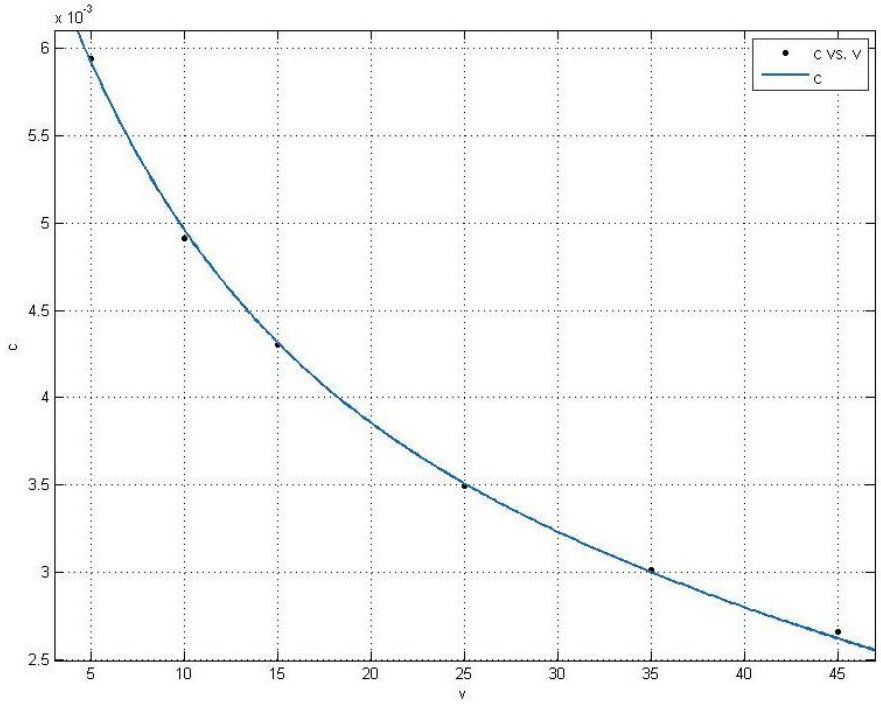

Figure 3.8-4 - β=10 Coefficient 'c' against Velocity

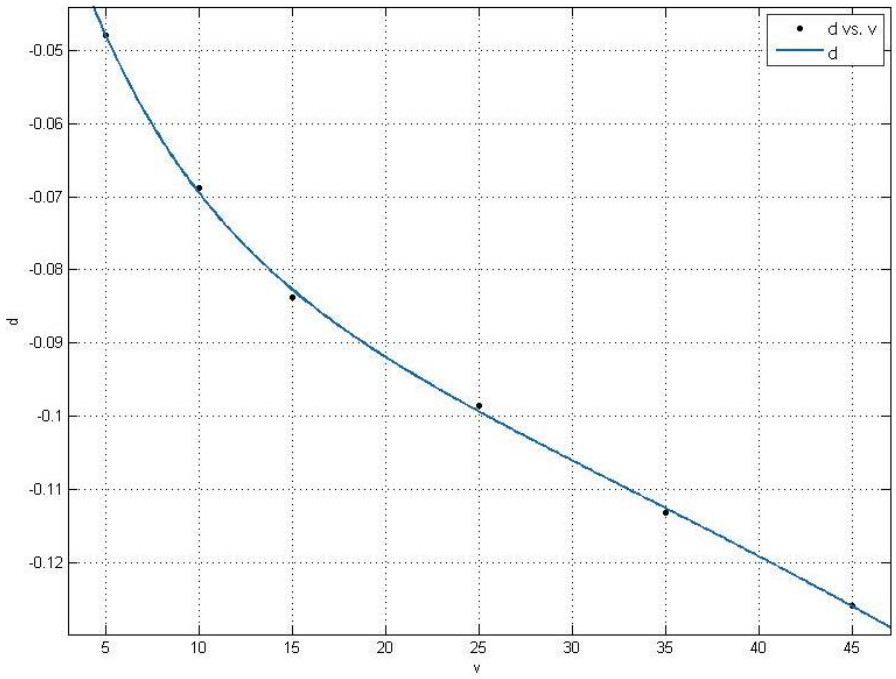

Figure 3.8-5 - β=10 Coefficient 'd' against Velocity

The equations for these coefficients also come with their own set of constants (a_1, b_1, c_1 and d_1) which are shown numerically in the following equations:

$$a = a_1 e^{b_1 v} + c_1 e^{d_1 v}$$

$$a = 0.006521 e^{0.002391 v} - 0.003191 e^{-0.04916 v}$$

$$b = 2.136e^{0.01993v} - 2.134$$

$$c = 0.001048e^{-0.1096v} + 0.004509e^{-0.01224v}$$

$$d = -0.0771e^{0.01094v} + 0.06831e^{-0.1419v} \quad (3.8\text{-}2)$$

Equation 3.8-2 - Coefficients for β=10

These equations can now be returned to the original equation for turbulence intensity, Equation 3.8-1. Where '**v**' is the mean velocity and 'x' is the position at which the user wishes to determine the intensity. Equation 3.8-2 works only for the stated case where turbulence is specified by 'β' and 'I' (where 'I' is determined by Equation 2.3-1). Where β=10 and I=0.01 and the velocity is within the range of values specified in Figure 3.8-1.

This process was repeated for:

- Constant values of 'β' with changing velocities
- Constant values of velocity with changing 'β'
- Constant values of 'k' with changing velocities
- Constant values of 'ε' with changing velocities

It was found in the β investigation, that for β values of 5, 10 and 20 the agreement was good with differences between the CFD and the equation values of no more than 10%. For values below 5 the equations performed poorly, this is true for all velocities. Also when the velocity remained constant only a trend for the largest and the smallest value of **v** could be found (5 and 45ms^{-1}), this is likely down to a poor fit with the coefficients.

When investigating 'k' it was found the best agreement between CFD and the proposed equation was found when 'k' was equal to 0.1 and 0.075 (while at 0.1 prediction was poor for velocities of 5 and 10ms^{-1}). For all other values of 'k' the difference between the CFD values of turbulence intensity and calculated values differed by 30-90%.

It was not possible to propose any equations when looking into 'ε' due to the instantaneous decay in intensity. This resulted in no trend between the coefficients and thus no overall equation could be used.

The graphs for all other investigations are presented in the Appendix. Where an equation was found to accurately predict the level of turbulence it has been presented.

4. Corrections

The wind tunnel set-up will determine which method of correction that should be used. Either the nozzle-method or the plenum-method must be used and each of these has prerequisites. The deciding factor on which method is used is predominantly the position in which the pressure is measured. Another factor is the size of the tunnel, for a small tunnel Mercker et al (1997) recommends that the nozzle method is used. The method that will be used within this study will be the nozzle-method.

This image has been removed

Figure 3.8-1 – Nozzle (left) and Plenum-method (right) (Mercker et al, 1997)

The corrections themselves can be summarised as 'summation of the perturbation velocities' (the correction factors) to determine the value for q_{cor}/q_{∞}. Then a summation of the measured drag and horizontal buoyancy is divided by this value. However, there are more components to each perturbation velocity each varying in complexity. As this paper is only concerned with the nozzle method only the components needed for this will be presented.

$$C_{Dcor} = \frac{(C_{Dm}+\Delta C_{DHB})}{\left(\frac{q_{cor}}{q_{\infty}}\right)} \quad (4\text{-}1)$$

Equation 3.8-1 - Drag Coefficient Correction (Mercker et al, 1997)

$$\frac{q_{cor}}{q_{\infty}} = (1 + \varepsilon_S + \varepsilon_C + \varepsilon_N)^2 \quad (4\text{-}2)$$

Equation 3.8-2 - Nozzle Method (Mercker et al, 1997)

4.1. Horizontal Buoyancy

The first correction that needs to be to be quantified is the horizontal buoyancy. This can be defined as:

$$\Delta C_{DHB} = \frac{1.75}{A_M}(0.5 \cdot V_M \cdot G) \quad (4.1\text{-}1)$$

Equation 4.1-1 - Horizontal Buoyancy (Mercker et al, 1997)

Where ‘G’, is the empty tunnel static pressure coefficient gradient and can be defined as:

$$G = \left(\left(\frac{dC_p}{dx}\right)_N + \left(\frac{dC_p}{dx}\right)_C\right) \quad (4.1\text{-}2)$$

Equation 4.1-2 - Empty Tunnel Gradient (Mercker et al, 1997)

The empty tunnel gradient is a measure in static pressure gradient from the nozzle (‘N’ notation) and from the collector (‘C’ notation), in an empty test section, over half the length of the model volume. As the numerical data is not readily available, the values for both components were extrapolated from the graph in Figure 4.1-1. The box highlights the area of interest with respect to the Wong Model, these values were extrapolated too. This was done by extrapolating the two values at the extremes of the graph and calculating the difference between these points and the points around the model. This gives a value of G, as 0.025.

Thgis image has been remobved

Figure 4.1-1 - Static Pressure Gradient Graph (Mallock and Finnis, 2012)

Once a value for the C_{DHB} has been established, which will be different for each model set-up in this case (due to the after bodies), then the remaining correction factors need quantifying.

4.2. Jet Expansion and the Nozzle Blockage Factor for the Nozzle-method

In Equation 3.8-2 the first perturbation velocity is ε_S. This represents the jet expansion correction factor. Jet expansion is present in open jet tunnels due to the drastic pressure difference between the nozzle and the ambient air surround the test section. With the jet displacing laterally (expanding) the air stream becomes concavely curved (Figure 3.6-9), this means that the area between the model and the jet increases. Continuity dictates that this increasing area must reduce the velocity, which then results in a reduced C_D being measured (Mercker and Wiedemann, 1996). This is why the correction must be applied.

$$\varepsilon_S = \tau \sqrt{\left(\frac{V_M}{L_M}\right)} \left(\frac{A_M}{(A^*)^{\frac{3}{2}}}\right) \tag{4.2-1}$$

Equation 4.2-1 - Jet Expansion Correction (Mercker et al, 1997)

It can be seen that there are two variables that are yet to be defined and these are the tunnel shape factor τ and the reduced nozzle cross sectional area, A^*. The tunnel shape factor is independent to each tunnel and is different for open and closed jets.

$$\tau = -0.03 \left(\frac{B}{H} + \frac{H}{B}\right)^3 \tag{4.2-2}$$

Equation 4.2-2 - Open Jet Tunnel Shape Factor (Wickern, 2001)

For the tunnel used in this report the shape factor is -0.266.

To determine A^* the blockage factor for the nozzle method must be calculated first, as can be seen in Equation 4.2-3 and Equation 4.2-4:

$$A^* = \frac{A_N}{(1+\varepsilon_{QN})} \tag{4.2-3}$$

Equation 4.2-3 - Reduced Nozzle Cross Section (Mercker et al, 1997)

$$\varepsilon_{QN} = \left(\frac{A_M}{2A_N}\right) \left(\frac{1-x_s}{\sqrt{({x_s}^2+{R_N}^2)}}\right) \tag{4.2-4}$$

Equation 4.2-4 - Blockage Factor for Nozzle Method (Mercker et al, 1997)

The complex nature of the equations is now evident with many equations being interlinked. To determine ε_{QN}, another two variables x_s (distance from the model

to the source point) and R_N (equivalent duplex nozzle radius) need to be equated.

$$x_S = \frac{x_M + L_M}{2 + \sqrt{\left(\frac{A_M}{2\pi}\right)}} \tag{4.2-5}$$

Equation 4.2-5 - Distance from Model to Source Point (Mercker et al, 1997)

$$R_N = \sqrt{\left(\frac{2A_N}{\pi}\right)} \tag{4.2-6}$$

Equation 4.2-6 - Equivalent Duplex Nozzle Radius (Mercker et al, 1997)

The above equations have allowed the jet expansion factor (Equation 4.2-1) to be calculated. Meaning that to complete Equation 3.8-2, the collector ε_C and nozzle blockage ε_N factors must be determined.

4.3. Collector Blockage

As in the previous case, to determine the collector blockage other factors must be calculated. In the case of the collector there are some factors that will affect the flow through the collector. The main flow feature that will affect this flow is the wake of the model in the test section. This is known as the wake blockage factor ε_W and can be defined as:

$$\varepsilon_W = \left(\frac{A_M}{A_C}\right)\left(\frac{C_{Dm}}{4 + 0.41}\right) \tag{4.3-1}$$

Equation 4.3-1 - Wake Blockage Factor (Mercker et al, 1997)

Also as was the case with the nozzle, the collector has an equivalent duplex radius.

$$R_C = \sqrt{\frac{2A_C}{\pi}} \tag{4.3-2}$$

Equation 4.3-2 - Equivalent Duplex Collector Radius (Mercker et al, 1997)

With these two factors now defined the collector blockage factor can be determined.

$$\varepsilon_C = \frac{\varepsilon_W + {R_C}^3}{\left((L_{TS} - x_M)^2 + {R_C}^2\right)^{\frac{3}{2}}} \tag{4.3-3}$$

Equation 4.3-3 - Collector Blockage Factor (Mercker et al, 1997)

4.4. Nozzle Blockage Factor

The Nozzle Blockage Factor can also be known as the induced velocity at the model position due to the nozzle effect (Mercker and Wiedemann, 1996) and is affected by the model proximity to the nozzle. The closer the model is to the nozzle the larger the influence the model has on the velocity distribution in the nozzle. If the positive pressure at the front of the model extends into the nozzle this effect is further amplified. As this results in the nozzle experiencing solid blockage which essentially reduces the nozzle exit area, thus increasing the velocity exiting the nozzle relative to the free air (Mercker and Wiedemann, 1996).

$$\varepsilon_N = \frac{\varepsilon_{QN} \cdot {R_N}^3}{({R_N}^2 + {x_M}^2)^{\frac{3}{2}}} \tag{4.4-1}$$

Equation 4.4-1 - Nozzle Blockage Factor (Mercker et al, 1997)

5. Results

5.1. Shroud

The investigation that was carried out once the standard wind tunnel model had been validated was on a version of the Wong Model that will be referred to as the Old Wong Model from now on. This model was already available and in use at the University. There are a number of differences between this model and the new model. The first of which is the Old Wong Model was constructed in such a manner that meant that some sides of the model were curved and they did not line up with the underside; the after bodies were also larger than the rear of the model, the same is also true for the nose. This resulted in some peculiar readings that could not realistically be replicated in CFD. As was previously noted, these minor discrepancies would demand a lot of computing power to simulate and would likely prove to be of little benefit. The Old Wong Model was constructed completely sealed, meaning that all fixings put on the model had to be placed on the exterior, in the path of the flow. This meant that only one sting/strut could be used and this will be referred to as the Shroud (Figure 5.1-2). As the entirety of the shroud is outside the model, when the tare was taken the whole of the shroud could be subtracted from the total measured C_D. The Shroud was purpose built for the testing of a scale F1 model. The collection of all these features resulted in

the Old Wong Model producing results that did not compare well with the findings of Wong and Mair. For example, the noted trend in drag reduction with the addition of the after bodies was 120 counts.

This image has been removed

Figure 5.1-1 – Wong Model ΔC_D Results with increasing Number of After Bodies (Wong and Mair, 1983)

It was found that this model only produced a drag reduction of 70 counts. Comparing the results with Wong and Mair for one after body, there are two measurements taken and presented for this after body, suggesting that this configuration has highly transient features (Wong and Mair, 1983). However, the difference found by Wong and Mair are far smaller than the ones found in Figure 5.1-3. Another point to note would be that even the CFD simulations generated unexpected results when one after body was used. This could also suggest that it could be the Shroud that is interacting with the flow at the rear of the model. Due to the number of inconsistences that were generated with both the wind tunnel and the CFD results further CFD investigations were abandoned. Enough evidence was provided that justified all further tests on the Old Wong Model being abandoned as this was a poor set. It was clear that a new model was needed.

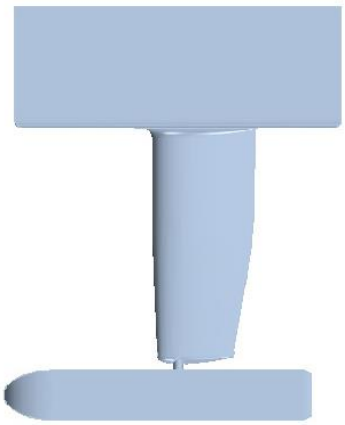

Figure 5.1-2 - Shroud Set-up

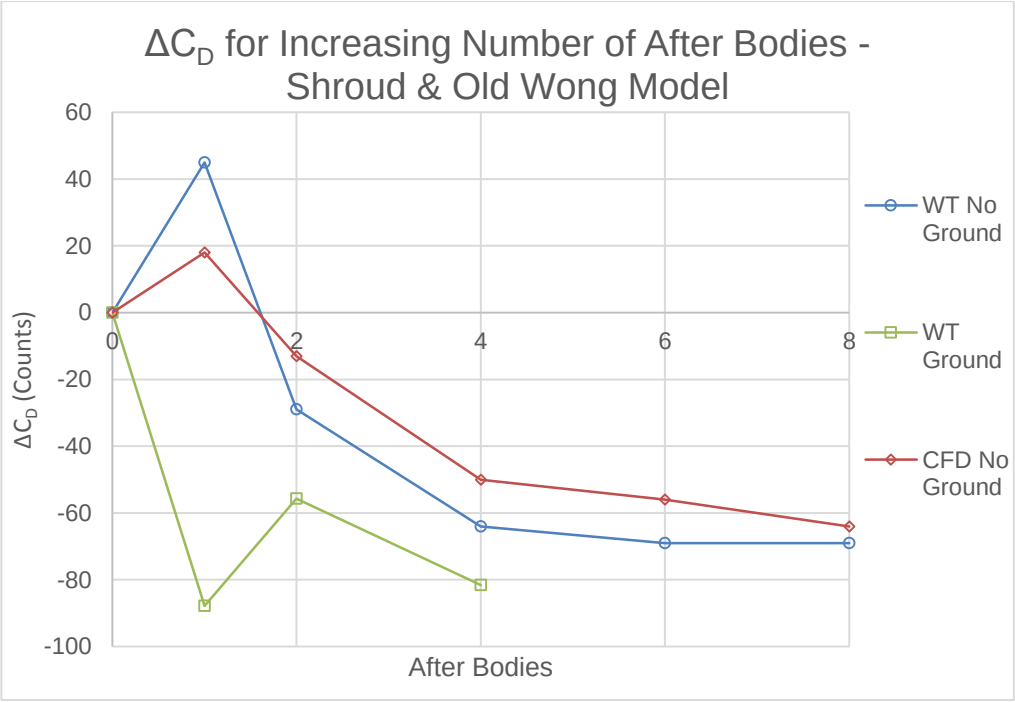

Figure 5.1-3 - Shroud Results

Even with the obvious problem that this Old Model produced the corrections were still applied for comparison with the Carbon Sting.

Shroud Corrected Data – No Ground			
AB	C_{Dm}	Nozzle $C_{D\ Corrected}$	ΔC_D Counts
0	0.242	0.249	7
1	0.287	0.294	7
2	0.213	0.220	7
4	0.178	0.185	7
6	0.173	0.179	6
8	0.173	0.179	6

Table 5.1-1 - Shroud Corrected Data with No Ground

Shroud Corrected Data – Ground			
AB	C_{Dm}	Nozzle $C_{D\ Corrected}$	ΔC_D Counts
0	0.266	0.273	7
1	0.284	0.291	7
2	0.253	0.260	7
4	0.216	0.223	7
6	0.210	0.216	6
8	0.202	0.208	6

Table 5.1-2 - Shroud Corrected Data with Ground

5.2. Carbon Sting

As the Old Wong Model proved problematic, the New Wong Model was used for the remainder of the tests. This did mean, however, that the model set-up was different. The model was moved closer to the balance, meaning that shroud could no longer be used; therefore, the carbon sting was used instead. This sting does not have an aerodynamic profile; its shape resembles more of a truncated cone. This difference in shape was suspected to have an increased influence on the model. Unlike the shroud where all the components are external and in the air flow, the lower part of the Carbon sting is inserted into the new Wong Model (See Figure 5.2-1 inside the red square). This results in the tare value being larger. The way in which the tare was determined was by testing the strut by itself within the wind tunnel. The drag force reading acquired from this would then be subtracted from the test of both the strut and the Wong model, to provide the effective drag generated by the Wong model alone. From this drag force the coefficient could then be determined (see Table 5.2-1, not that the Tare Drag is different for all stings and when the ground board is inserted).

Carbon Sting No Ground 0ab Tare			
Total Drag (N)	Tare Drag (N)	Resultant Drag (N)	Resultant Cd
42.465	35.378	7.087	0.249

Table 5.2-1 - Carbon Tare Values

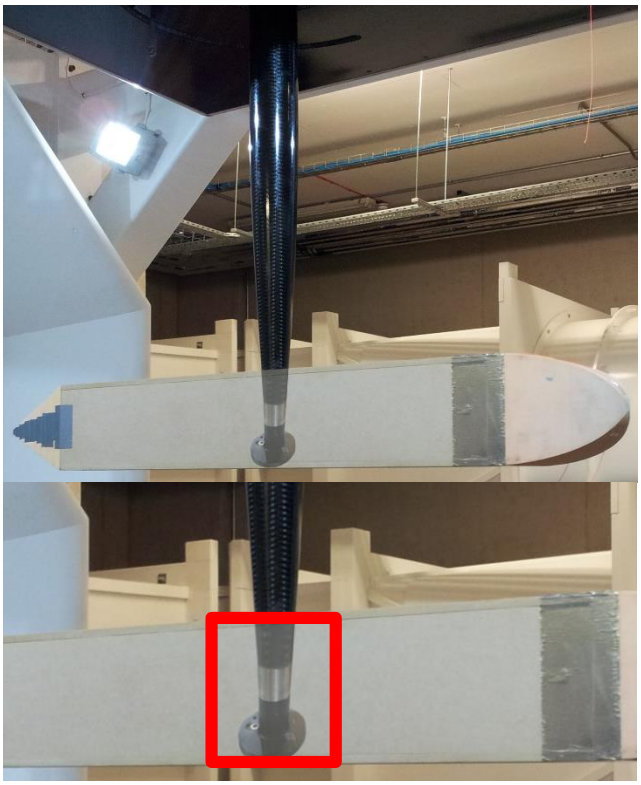

Figure 5.2-1 - Carbon Sting Inside Wong Model

However, a benefit of this set-up was the reduced set-up time and that the previously used Shroud came in many separate pieces, all of which were time consuming to put together. Using the carbon sting also reduced the complexity of the CAD that had to be imported and repaired in CFD.

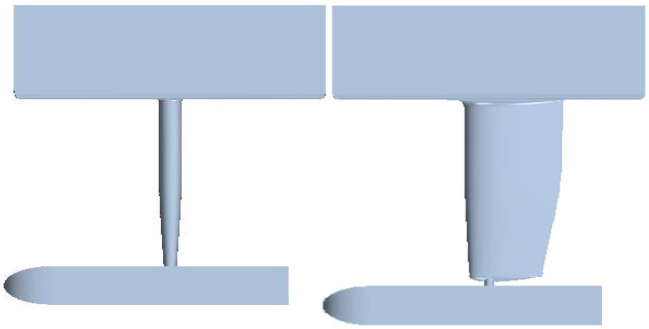

Figure 5.2-2 – Carbon (left) and Shroud (right) Set-up

From the initial wind tunnel tests, it was clear to see that this model was performing much better than the previous one with consistent drops in drag that were expected. Wong and Mair find a drop in C_D of around 120 counts, Figure 5.2-4 shows that the new Wong Model is performing well; this is true for having

the ground in and out. It is again interesting to note the differences in the first after body that Wong and Mair also found (Wong and Mair, 1983). This is likely an issue of scale, with the not having enough time to reattach to the model. Another thing to note is that the CFD model assumes that all the surfaces are completely smooth, where in reality the wood of the Wong Model is not completely smooth. It is therefore expected that the wind tunnel values will be greater due to the greater skin friction generated by the imperfections in the wood surface.

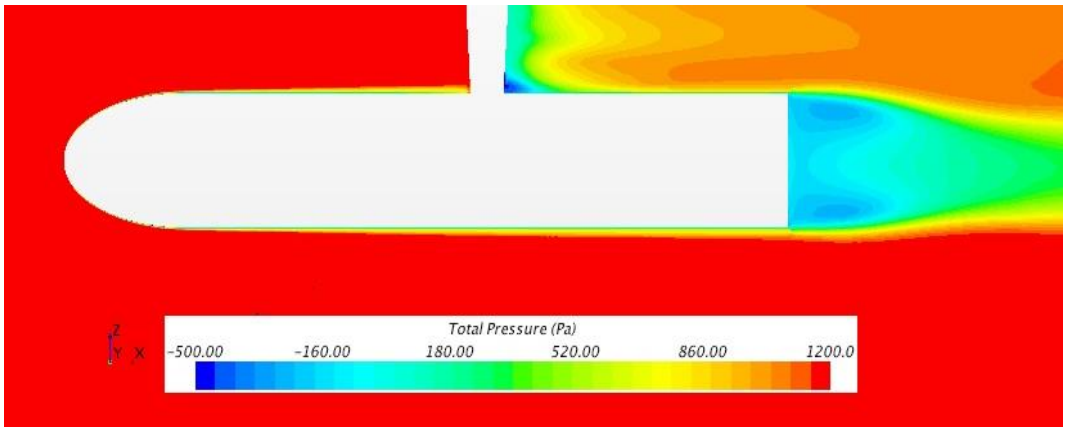

Figure 5.2-3 - Total Pressure Over the Wong Model 0ab

In Figure 5.2-3 the area of separation is exactly where it would be expected to be, which is at the sharp 90° rear of the model. Cross referencing this with Figure 5.2-6 and it can be concluded that this simulation is accurately replicating the wind tunnel.

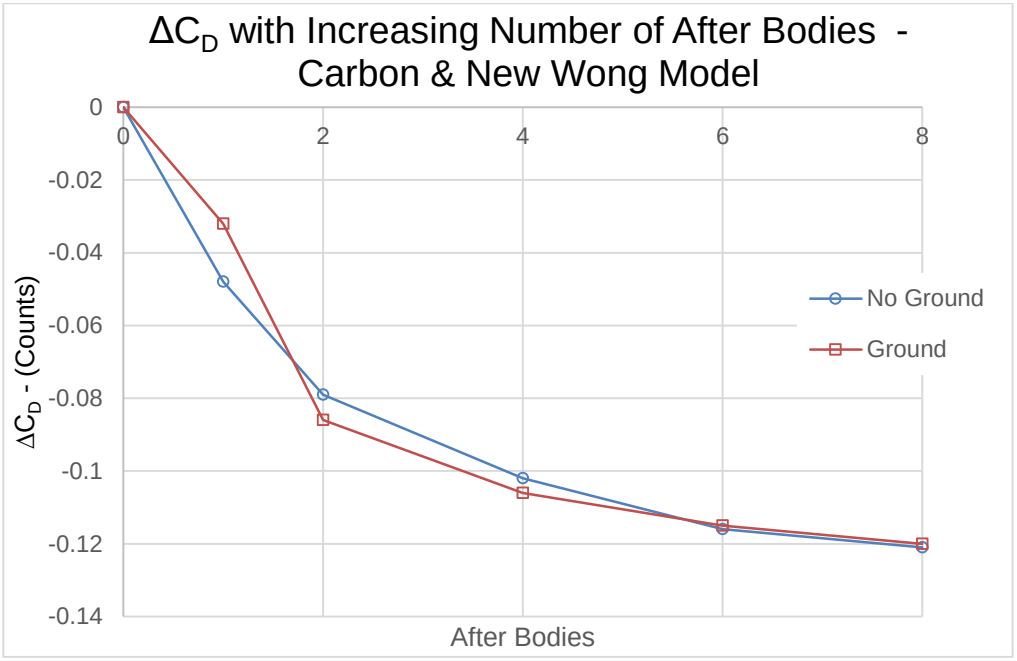

Figure 5.2-4 - Carbon Sting Wind Tunnel Results

Once it was found that this model was performing like that of Wong and Mair, both the CFD and the corrections could then be applied, using the methods presented by Mercker et al (1997) (see Section 4).

As was shown with the Shroud data, the CFD did not generate good agreement with the wind tunnel values. With the Carbon Sting the preparation for CFD was made simpler as there were fewer surfaces to repair. Considering that Fischer et al (2007) found a difference of 10 counts, with a mesh of 200 million voxels, it would be reasonable to expect some differences with the density of the mesh in this study being just over 60 million cells. On average this level of density took around 3 hours to mesh and 72 hours to run to convergence. The level of convergence was determined by monitoring the residuals to ensure that they had stabilised as well as monitoring the drag coefficient. The drag coefficient was more prone to changes over time due to the undulating nature of the wind tunnel flow. Figure 5.2-5 shows that picking a predetermined length of time, is not necessarily good practice; with the C_D clearly changing by a couple of counts.

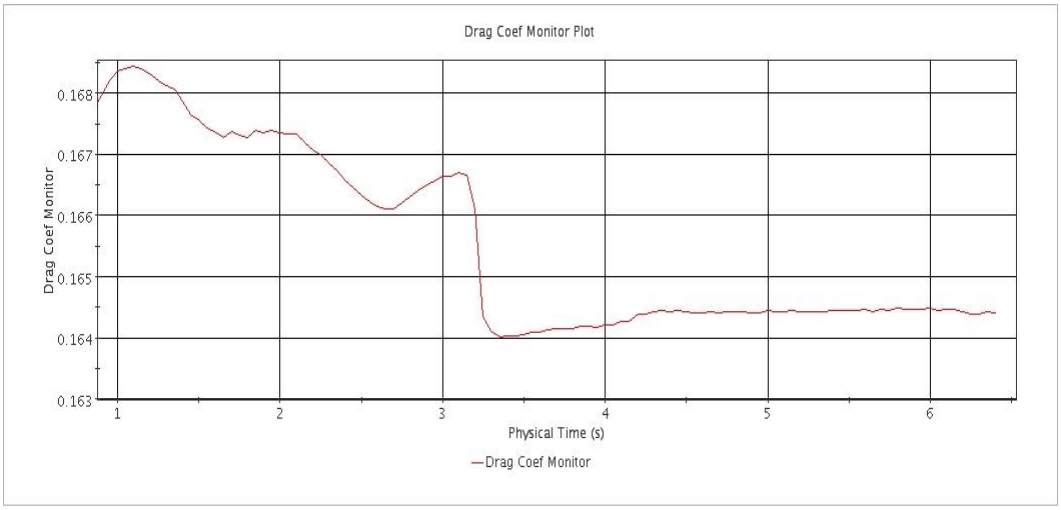

Figure 5.2-5 - C_D Monitor (y) against Time (x)

Once convergence was achieved in the C_D monitor the results were extracted from the simulation. The CFD results for the carbon sting are presented in Figure 5.2-6.

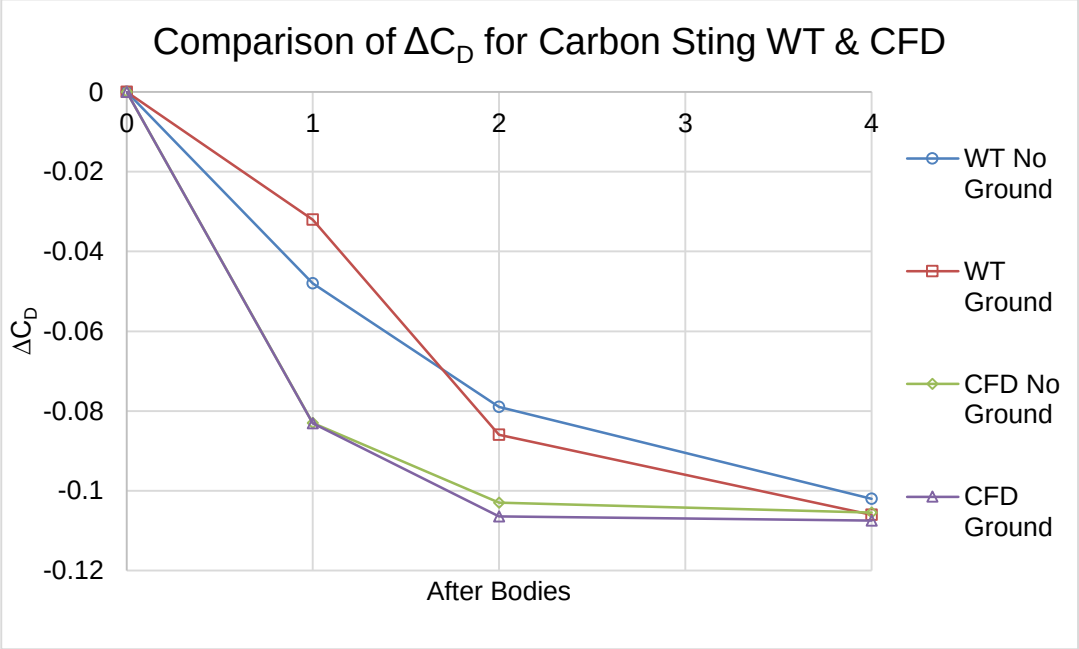

Figure 5.2-6 - Carbon Sting WT & CFD Comparison

It is first interesting to note that the CFD results with and without the ground are essentially the same, while the WT results show greater differences between the two configurations. The trend generated was expected, with the previously stated problems of scale with 1 and 2 after bodies. This is also due to the delayed separation that is present in the k-ε turbulence model due to the shear stress levels which are over predicted (Menter, 1992). This can be seen clearly in Figure 5.2-7 and Figure 5.2-8, where the flow remains attached at the rear of the

model. In the wind tunnel the angle at the rear of the body is much too sharp for the airflow to attach and thus the drag measurements are higher than that of the values generated within CFD.

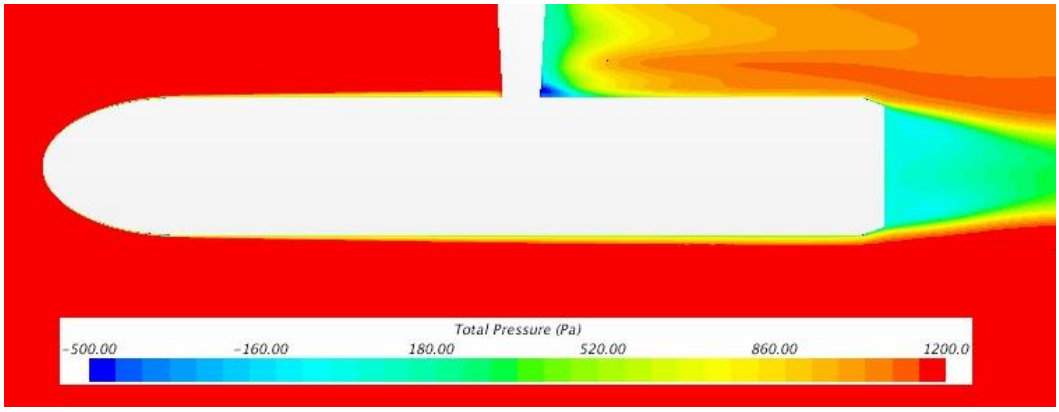

Figure 5.2-7 - Total Pressure Over the Wong Model 1ab

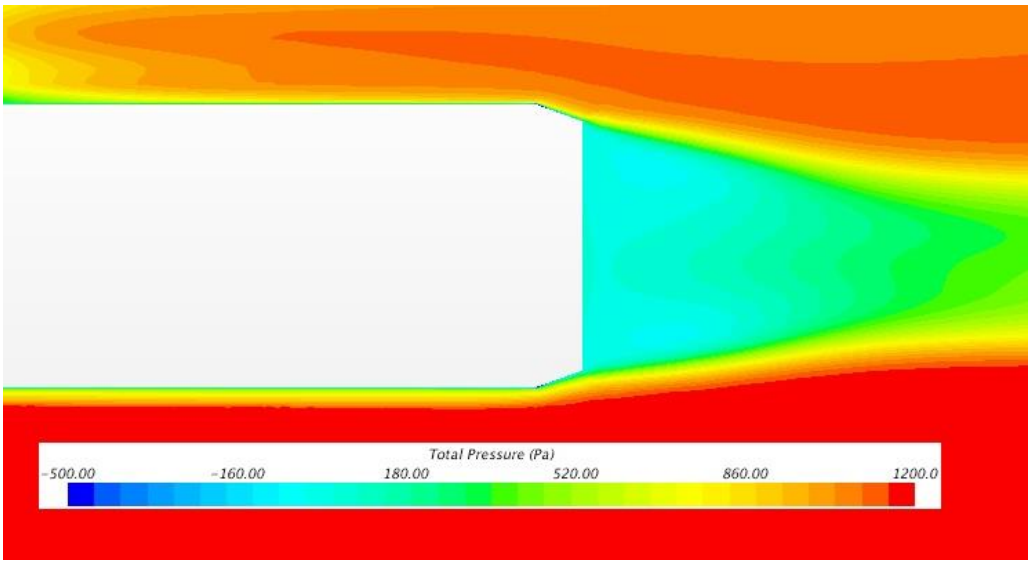

Figure 5.2-8 - Total Pressure at the Rear of the Wong Model 1ab

While under predicted drag in these two areas is likely down to the physics model, the agreement with both 0 and 4 after bodies is encouraging, differing only by a couple of counts. Shih et al (1995) stated that for areas with large amounts of separation, the Realizable model worked very well and it is clear that this is the case with the '0' after body set-up presenting the smallest difference between WT and CFD results, with a maximum difference of 3 counts.

When applying the corrections put forward by Mercker and Wiedemann there are a number of important parameters to consider such as, the length of the model L_m, the model volume V_m and the distance from the centre of the model to the nozzle X_m. All these parameters will change with the addition of after bodies. The

model volume has a large influence on the corrections, with it being present in the correction for horizontal buoyancy. This is then present in the final correction equation, Equation 3.8-1. While this is true for A_M also, its value is constant for the tests. Applying all the corrections to the Carbon Sting WT data there is a maximum difference of 7 counts. Also note that as the model increases in length and thus volume, the amount of error associated with the wind tunnel data increases as was suggested previously.

Comparing both the Ground and No Ground corrected data shows that the difference in counts is relatively constant with a few deviations.

Carbon Sting Corrected Data – No Ground			
AB	C_{Dm}	Nozzle $C_{D\ Corrected}$	ΔC_D Counts
0	0.249	0.256	7
1	0.201	0.208	7
2	0.170	0.177	7
4	0.147	0.154	7
6	0.133	0.140	7
8	0.128	0.134	6

Table 5.2-2 - Carbon Sting Corrected Data without Ground

Carbon Sting Corrected Data – Ground			
AB	C_{Dm}	Nozzle $C_{D\ Corrected}$	ΔC_D Counts
0	0.252	0.259	7
1	0.220	0.227	7
2	0.166	0.173	7
4	0.146	0.153	7
6	0.137	0.144	7
8	0.132	0.138	6

Table 5.2-3 - Carbon Sting Corrected Data with Ground

5.3. Short Sting

The final sting variation that was tested was called the Short Sting or the University made sting. This sting varies from the previous two in a variety of ways. First of all, this sting is particularly heavy and the outer surface is not ideal for use in the wind tunnel with welding joints being in the path of the flow. Second is the restricted way in which the Short Sting can be used. Due to the length of the sting; the model is lifted away from the centre of the jet. The increased height prolongs the model set-up time during the after body changes. For this reason, this configuration was only tested with the ground board in.

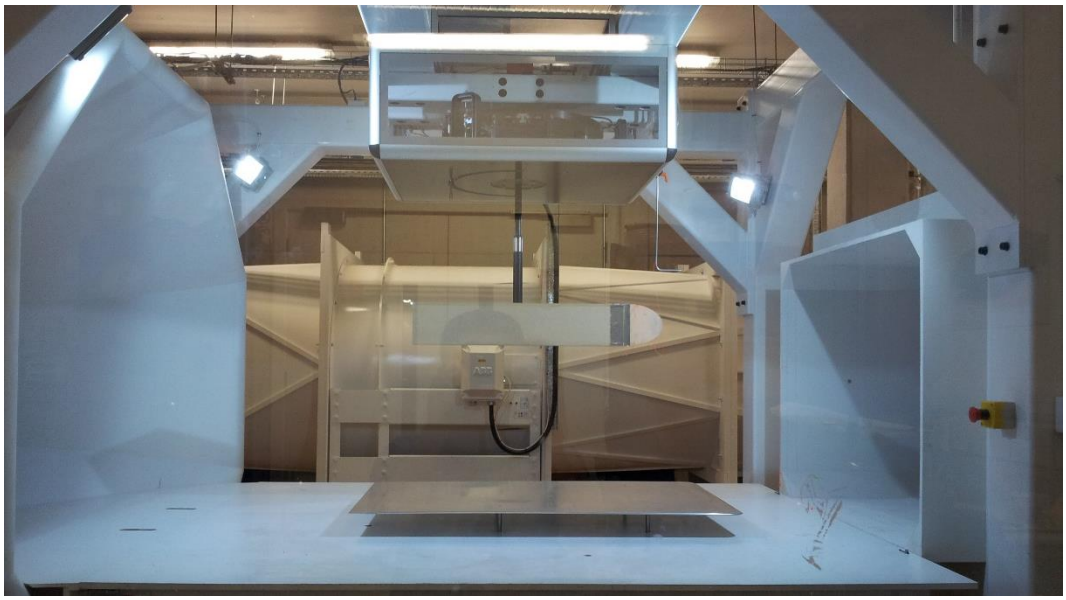

Figure 5.3-1 - Short Sting

Figure 5.3-2 - Short Sting Weld

Due to the basic structure of this sting it was suspected to have the largest influence on the flow. Looking at Figure 5.3-3, the previously noted trend by Wong and Mair and the previously found trend in the Carbon Sting can be seen. In this case however there is a further reduction in C_D, resulting in an overall reduction of 127 counts. This could be due to either the model position or the sting. An increase in the proximity to the shear layer, resulting in a reduced velocity over the model will reduce the drag measurement.

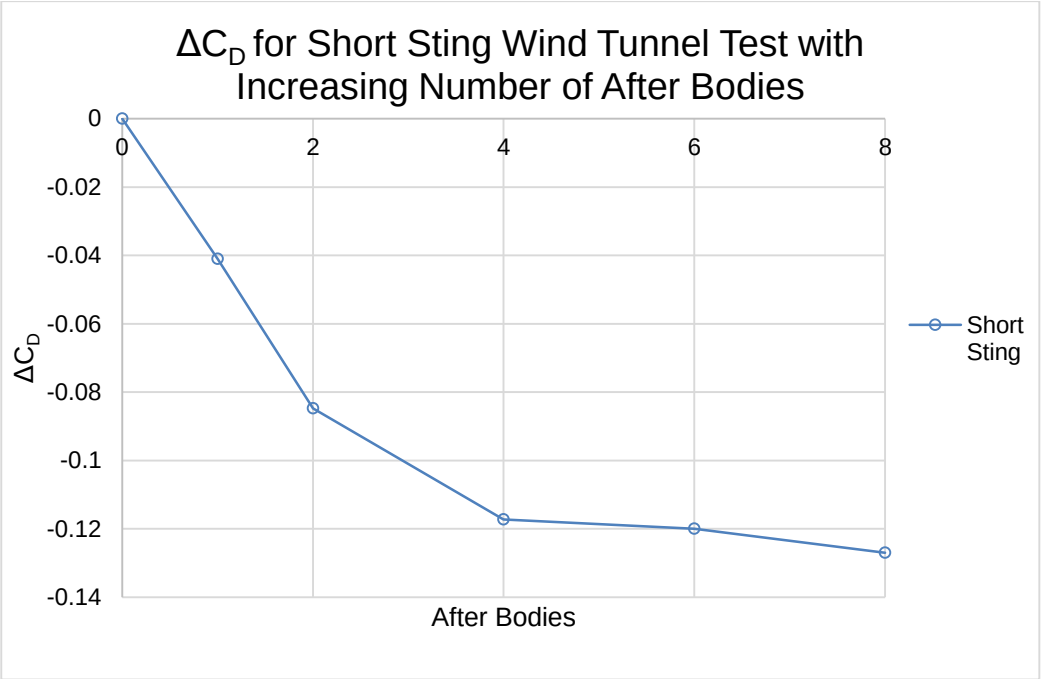

Figure 5.3-3 - Short Sting Wind Tunnel Results

Observing the drag reduction alone would suggest that this is a reasonable set-up for testing this model yet, when looking at the actual measured C_D, a clear problem becomes apparent. The prediction in drag is extremely high considering the experimental and numerical data that has been collected in Section 5.2. The two possible factors that could affect this are model position or the choice of sting; since the model position should reduce the drag the implications are that the Short Sting has a disruptive influence on the coefficient measurements within the tunnel. With this in mind the final project objective (Section 3.2) will be focused on this sting.

Short Sting Corrected Data – Ground			
AB	C_{Dm}	Nozzle $C_{D\ Corrected}$	ΔC_D Counts
0	0.490	0.495	5
1	0.449	0.455	6
2	0.405	0.411	6
4	0.373	0.379	6
6	0.370	0.375	5
8	0.363	0.368	5

Table 5.3-1 - Short Sting Corrected Data

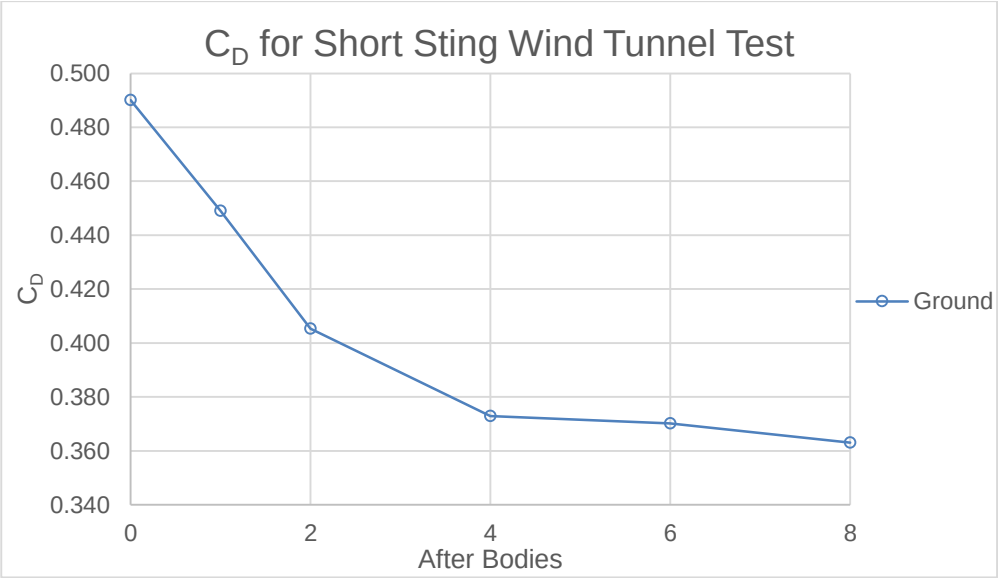

Figure 5.3-4 – C_D for Short Sting Wind Tunnel Test Results

From the correction data for this sting it can be deduced that the increase in measured drag has resulted in an increase in the overall correction difference. This also highlights an aspect of the corrections that is not currently included and this is the model position in z.

5.4. Summary of Different Stings

As was previously mentioned the Shroud presented a number of problems both in the wind tunnel and with CFD thus further simulations were not run. However, for completeness and for the purposes of comparison the corrections were applied to the Shroud data. Considering the number of flaws that the Old Wong Model had it was not expected that there would be many similarities within the corrected data, yet the ΔC_D suggests otherwise.

This similarity between the two data sets further emphasises the previously stated about the importance of the model dimensions. As the C_D for 1 after body differs by at least 60 counts between the Carbon Sting and the Shroud, it would be expected that the C_{DCor} would echo this. However, the C_{Dm} seems to have a lesser effect than the model dimensions. Comparing the two sets of correction data shows that the ΔC_D for both supports are the same. This, therefore, means that the corrections should not be misunderstood or misused as a way of filtering out poor data; the data must either be discarded or repeated with the necessary improvements made, like a new model.

In the case of the Short Sting, the wind tunnel data was largely influenced by the sting itself, hence the reason for the final project objective being implemented on this sting.

5.5. Individual Correction Factors

The ΔC_D with and without the ground inserted show no differences overall. This would suggest that the addition of the ground has no effect on the corrected C_D. Yet this is not the case, the individual correction factors that are shown in Section 4 do in fact change. Other than the previously discussed variables (V_m, L_m and X_m) the area of the collector A_C must also be taken into account, especially as the ground board in this case goes into the collector and reduces the overall area (Figure 3.4-2 shows the collector has a reduced cross sectional area). This removes the shear layer in the negative z direction and replaces it with a boundary layer. All the figures that follow in this section are for all the correction factors, for the Carbon Sting case, with and without the ground, they show in counts the effect they have on the overall corrected C_D.

The Nozzle Blockage factor for the Nozzle method, for both wind tunnel set-ups shows that the results are the same for each case. Equation 4.2-4 shows that this correction factor is dependent on the nozzle dimensions.

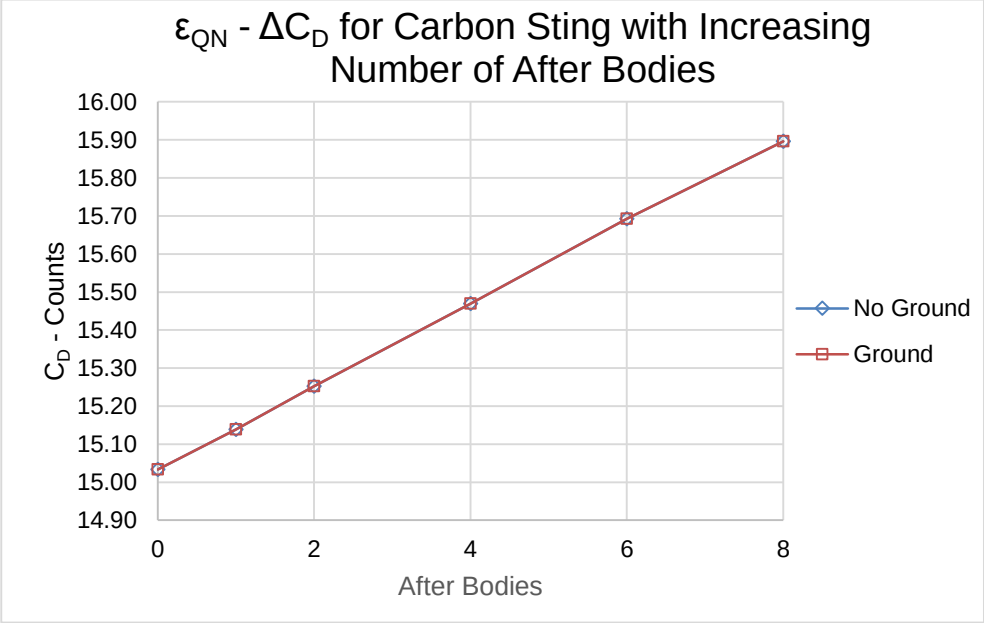

Figure 5.5-1 - ε_{QN} Carbon Sting

Equation 4.3-1 shows that the wake blockage is determined with the C_{Dm} and A_C, it is, therefore, of little surprise to note that this correction factor varies by less

than one count. The trend lines echo that of the full wind tunnel data, except this case shows the effect of the reduced collector area.

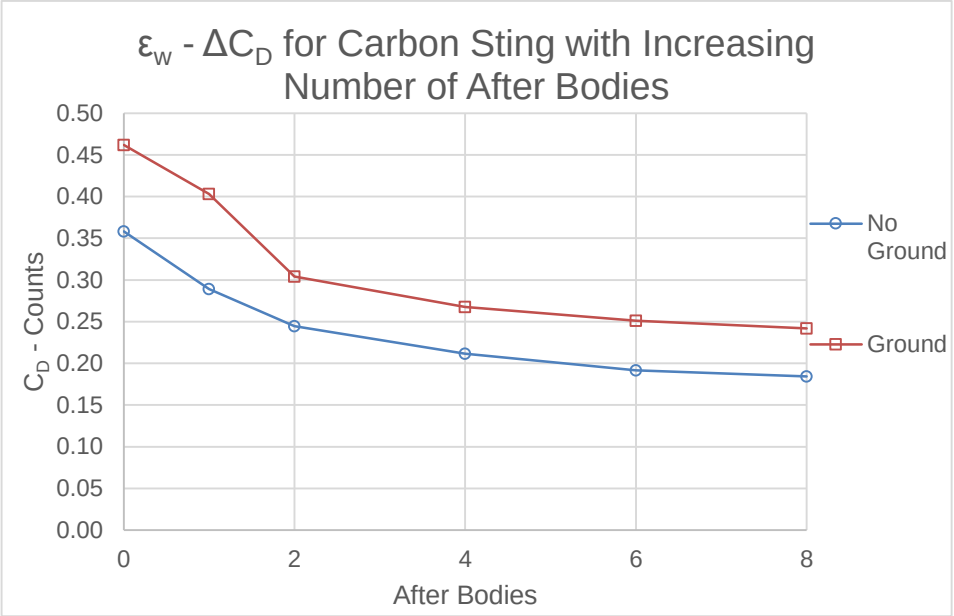

Figure 5.5-2 - ε_w Carbon Sting

Reducing the collector area reduces its effective radius and thus increases its blockage effect as can be seen in Figure 5.5-3.

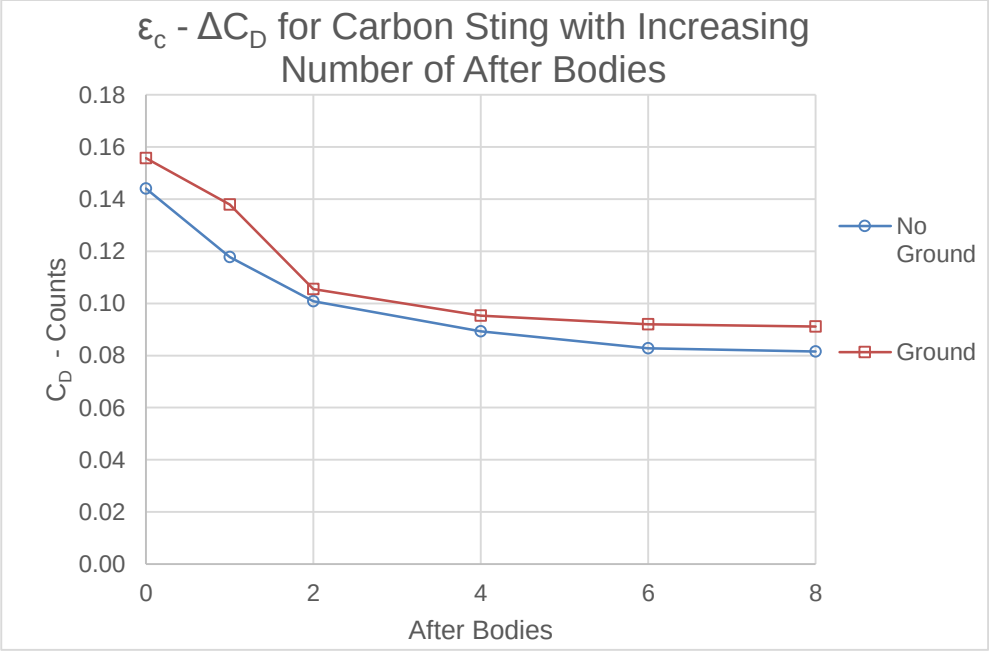

Figure 5.5-3 - ε_c Carbon Sting

As with ε_{QN}, the following correction factors are the same for both with and without the ground board inserted into the tunnel; ε_S, ε_N and ΔC_{DHB}. This is due to

their relationship to the nozzle and model dimensions as well as the measured $C_{D.}$

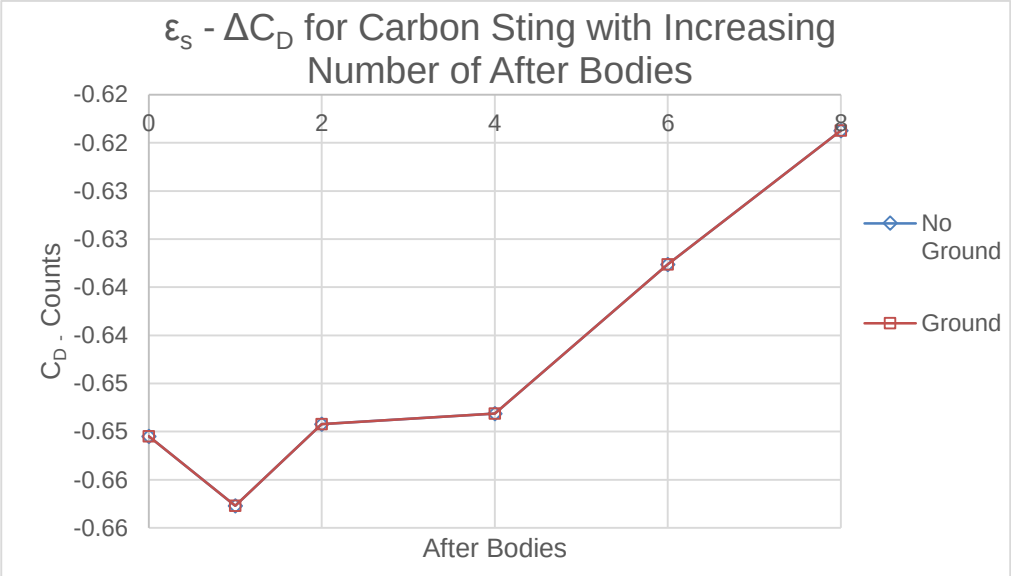

Figure 5.5-4 – ε_s Carbon Sting

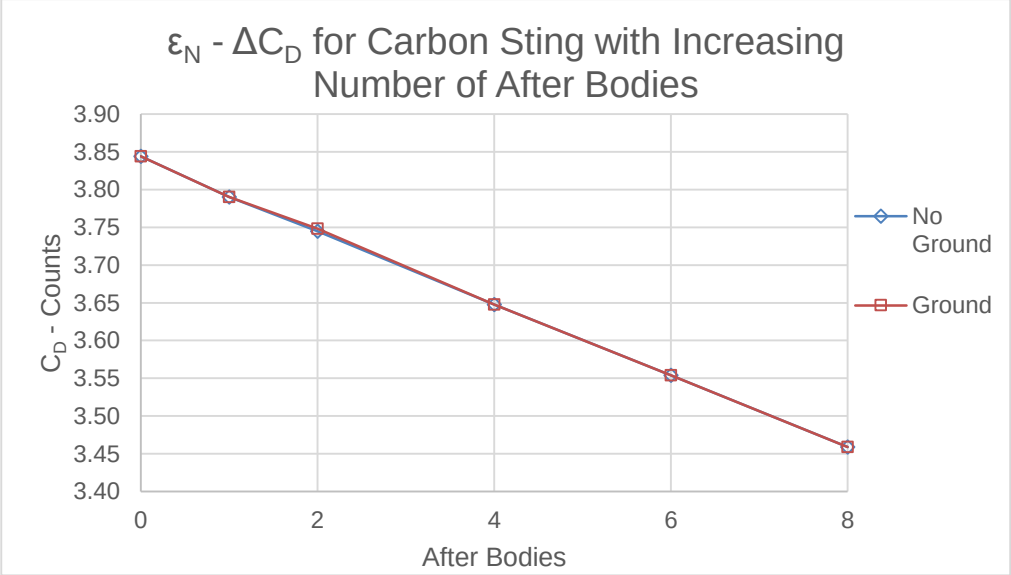

Figure 5.5-5 – ε_N Carbon Sting

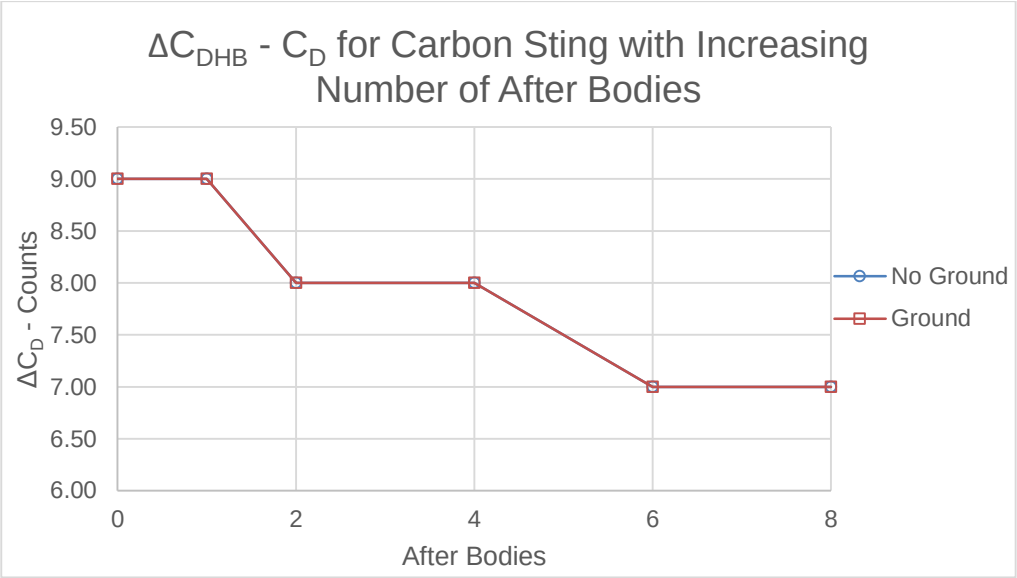

Figure 5.5-6 - ΔC_{DHB} Carbon Sting

Presenting the individual correction factors in this manner allows for greater clarity when determining which factor has the largest influence on the corrected C_D and in this case it is clearly the horizontal buoyancy. While it can be said that the ε_{QN} shows a notable amount of counts, its minimal presence in the overall correction equations results in this factor having a smaller effect than the horizontal buoyancy.

6. Sting Improvements

The results from the Short sting showed that the overall model C_D was being over predicted. It was deduced that the main factor in this rise was the Short Sting; therefore, the focus upon improving a support apparatus will be on this particular sting.

The main problem with this sting was the profile; this coupled with the weld that is in the path of the air flow is clearly not an ideal aerodynamic shape. From this it was decided that another Shroud (Aerofoil Cover) would be designed and manufactured. In this case it would be made in sections so that it can be applied to other supports where this cylindrical strut is in the airflow. This method is also much more cost effective than producing a complete new Sting from aluminium for example. The material chosen for this was Foam as it is light and any changes in design that are necessary can be implemented quickly as well as being light and thus not increasing the difficulty of the model set-up.

The design of the Aerofoil Cover was taken from that of the already available Shroud. The aerofoil profile (blue) at the base of the shroud was extruded outwards; removing the rounded edges and allowing the profile to extend to the model face (Figure 5.5-1). This allowed for rapid integration of the design as the diameter of the Short Sting already fits within the dimensions of the Shroud opening.

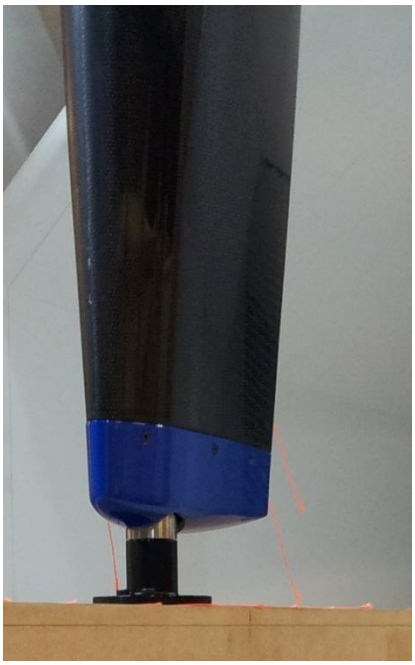

Figure 5.5-1 - Sting Fixing within Shroud

Once the Aerofoil Cover's had been designed they were manufactured through the use of a CNC capable of cutting foam. A number of copies of the Aerofoil were made to allow the sections to be different thicknesses.

Figure 5.5-2 - Aerofoil Covers during Manufacture

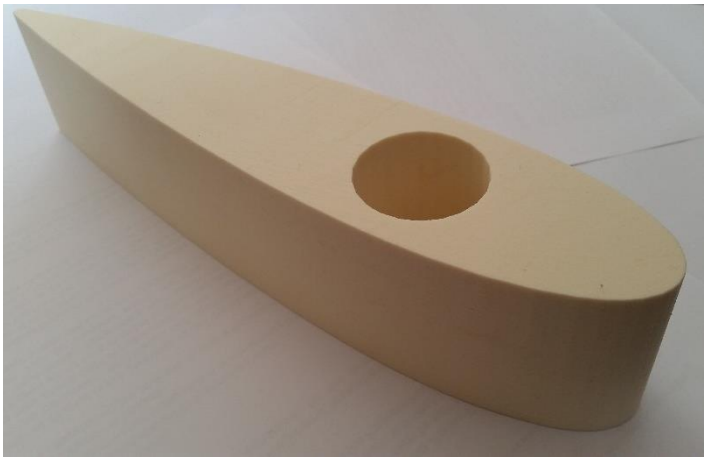

Figure 5.5-3 - One Completed Aerofoil Section

Figure 5.5-4 - Proposed Set-up for Improved Sting with Foam Shroud

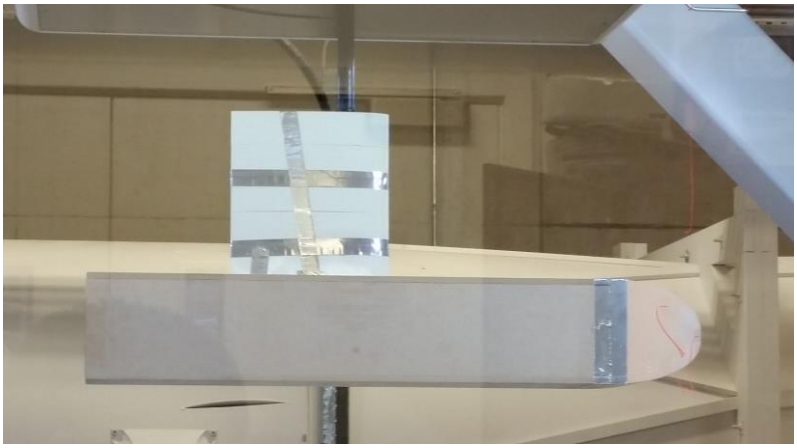

Figure 5.5-5 –Wind Tunnel Set-up of Foam Shroud

Looking at Figure 5.5-6 the data shows that the modifications seem to further enhance the overall drag reduction. This would suggest that the modified sting is reducing the drag of the original sting. However, as with the previously presented data on the Short Sting, Table 5.3-1, the actual C_D values where almost double that which were expected.

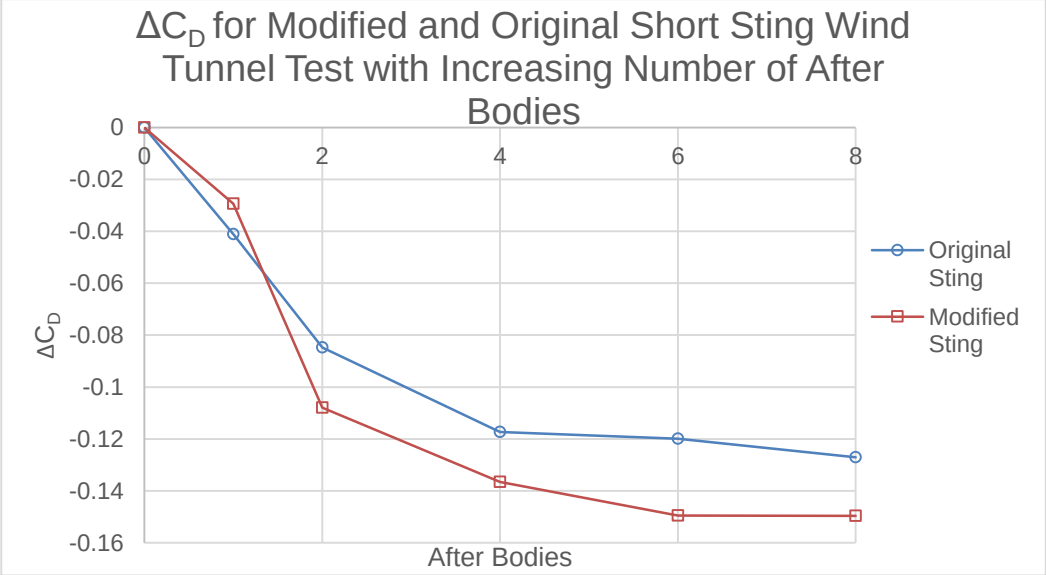

Figure 5.5-6 – Wind Tunnel Results of Modified and Original Short Sting

Modified Short Sting Corrected Data – Ground			
AB	C_{Dm}	Nozzle $C_{D\ Corrected}$	ΔC_D Counts
0	0.378	0.402	24
1	0.348	0.374	26
2	0.270	0.294	24
4	0.242	0.267	25
6	0.229	0.255	26
8	0.229	0.256	26

Table 6-1 - Modified Short Sting Data

Table 6-1 shows that the overall drag has been reduced by the addition of the shroud when comparing the results to the previous in Table 5.3-1. Table 6-1 also echoes the larger drag measurement at 1 after body (ab) for the modified sting. It is possible that this is created by the shroud as the drop in drag is not as great as would be expected with the addition of 1ab. The results from the modified sting are still promising, showing that the C_{Dm} is closer to that of is expected, reducing the original by almost 90 counts. As the foam shroud comes in sections it can be applied to other models with different dimension (where more or less sections are needed), making the foam shroud more versatile than the original shroud shown in Figure 5.5-1. The sections can also be easily modified because they are made of foam, if a thinner section is needed then the sections can be cut to size quickly and with ease.

7. Conclusion & Recommendations

Using the methods that were originally put forward by Mercker and Wiedemann (1996), the individual correction factors for the Universities 'Mercedes AMG PETRONAS Formula One Team Open Jet Wind Tunnel' have been investigated and quantified. These corrections highlighted the main factor that influences the corrected data from this wind tunnel which was the horizontal buoyancy, with the rest of the corrections (excluding ε_{QN} and ε_{N}) being less than one count. Maeda et al (2005) looked at three different open jet wind tunnels and found that each showed varying levels of horizontal buoyancy influence. The values ranged from -2 to -15 counts. The reason for these values being negative is due to the value of G in these tunnels being negative. This would suggest that the value for the University tunnel are very large when compared to that of these tunnels presented by Maeda et al (2005). From the derivation of the horizontal buoyancy (Mercker and Wiedemann, 1996):

$$F_H = \int p \, dA \int \frac{\partial p}{\partial x} \, dV \tag{7-1}$$

Equation 5.5-1 - Horizontal Buoyancy Force

It can be seen that the pressure across the tunnel and the effective volume are the main components. This equation then becomes Equation 4.1-1, where the role of the difference in pressure becomes greater (G). The pressure within the test section is greatly affected by the turbulent shear layer that surrounds the test section. In this case the shear layer expands and thus the pressure coefficient

across the test section length increases which in turn effects the value of G. It should be noted that tunnels investigated by Maeda et al (2005) are of ¾ scale while the University tunnel is 1/5 scale. The overall correction value (ΔC_D) was found by Maeda et al (2005) to effect the C_{Dm} by as much as 22 counts in one of the wind tunnels that was investigated, with the spread across the tunnels being between 3 and 22 counts. Suggesting that the difference found within the University tunnel being a reasonable amount. It has also been shown that the addition of the ground board has less of an effect on the overall corrected C_D than was expected, only effecting ε_W and ε_C.

Through the use of CFD, it has been shown that it is possible to recreate a wind tunnel test using an actual wind tunnel model. This also appeared possible with the relatively coarser meshes, as was shown in the Shear Layer Investigation (Section 3.5.1). Both turbulence models used in this scenario also produced similar results. However, when investigating the Wong Model within CFD it was found that this was more sensitive to mesh densities and with this in mind it is recommended that any future user of the CFD Wind Tunnel model that a base size no larger than 0.2m is used. Considering that Fischer et al (2010) found a difference in C_D of 10 counts with a much denser mesh than was used in this study, using a larger base size would generate too greater difference between wind tunnel and CFD results. It should be noted however that additional VC's maybe needed in the test section (alongside the shear layer VC) to increase the accuracy of the results.

Mapping both the turbulence intensity and the velocity profile through the test section has shown that the flow within the test section is behaving like that of a free square jet. It is recommended that these features are investigated experimentally in the future to show how accurately they are represented with the simulation. Also through the use of MATLAB a sensitivity study was conducted showing that for this case the best way to monitor turbulence intensity so that clear trend can be found is through the use of β. The study also highlighted the very sensitive nature of ε, which showed an instantaneous drop in intensity.

Improvements to a poorly made sting have been proposed and it has been found that the use of foam sections as a shroud does improve the measured drag considerably. The sections increase the versatility of this shroud when it is compared to the original.

When considering conducting a wind tunnel test it is important to understand what influence the support apparatus will have on the results. Where possible, it is recommended that the Shroud is not used in conjunction with a model that is of poor quality. Furthermore a model of poor quality should not be used at all. When resources are available that allow the user to create a more accurate, better quality model that represents the 3D CAD model or the full scale model it is imperative that one is made. While the drag around all the stings used can be removed through the process of a tare, an accurate value is difficult to obtain in the cases of the short and carbon sting. This is due to the sting being inserted into the model, this results in the tare value being larger and thus the overall drag value being reduced. It would be very difficult to determine the amount of drag that the concealed part of the sting contributes to the overall tare. It is very difficult to determine the influence on the stings on the aerodynamic behaviour of the model in an experimental manner. Having the sting inserted or on top of the model influences the flow along the model surface. Considering the difference in C_D values of the Wong Model between the carbon sting and the short sting, a future study looking into the characteristics of the short sting.

It is recommended that a future study looks into a selection of stings all with the same profile but of different length, where a minimal amount of the sting is inside the model. This will provide some more clarity on the stings influence on the models drag as well as the influence on model position. Mounting the model as far forward as possible on the stings will reduce the effect of horizontal buoyancy, as the pressure gradient in front of the sting is more desirable than at the rear. This will also reduce the under prediction of drag at the rear of the model, which occurs as the model length increase, due to the increase in static pressure coefficient on the rear surfaces of the after bodies. A further recommendation is that a shorter shroud could be manufactured to cover the length of the carbon sting from the balance to the model.

8. Bibliography

Barnard, R. (2009) 'Wind Tunnel and Road Testing'. in *Road Vehicle Aerodynamic Design*. ed. by Anon St Albans: MechAero, 230

Blazek, J. (2005) *Computational Fluid Dynamics: Principles and Applications*. 2nd edn: Elsevier

CD-adapco (2014) *STAR-CCM+ User Guide* [online] available from <http://www.cd-adapco.com/products/star-ccm%C2%AE> [16/4/2014]

CD-adapco (2013) *Dynamics - Simulating System*. 35th edn. London: CD-adapco

ERCOFTAC (2000) *Special Interest Group on "Quality and Trust in Industrial CFD" - Best Practice Guidelines*. 1st edn: ERCOFTAC

Fischer, O., Kuthada, T., Mercker, E., and Wiedemann, J. (2010) *CFD Approach to Evaluate Wind-Tunnel and Model Set-up Effects on Aerodynamic Drag and Lift for Detailed Vehicles*. Stuttgart: International Society of Automotive Engineers

Fischer, O., Kuthada, T., Widdecke, N., and Wiedemann, J. (eds.) (2007) . 'CFD Investigation of Wind Tunnel Interference Effects'. held 16/4/07 at Detroit, Michigan: International Society of Automotive Engineers

Hoffman, J., Martindale, B., Arnette, S., Williams, J., and Wallis, S. (eds.) (2003) . 'Development of Lift and Drag Corrections for Open Jet Wind Tunnel Tests for an Extended Range of Vehicle Shapes'. held 3/3/2003 at Detroit, Michigan. Detroit, Michigan: International Society of Automotive Engineers

Katz, J. (1995) 'Tools of the Trade'. in *Race Car Aerodynamics*. ed. by AnonCambridge, Massachusetts: Bentley Publishers, 61

Kulkarni, V., Sahoo, N., and Chavan, S. (2010) 'Simulation of Honeycomb-Screen Combinations for Turbulence Management in a Subsonic Wind Tunnel'. *Journal of Wind Engineering and Industrial Aerodynamics* 99, 37

Lasher, W. and Sonnenmeier, J. (2008) 'An Analysis of Practical RANS Simulations for Spinnaker Aerodynamics'. *Journal of Wind Engineering and Industrial Aerodynamics* 96 (1), 143

Lateb, M., Masson, C., Stathopoulos, T., and Bedard, C. (2013) 'Comparison of Various Types of k-Epsilon Models for Pollutant Emissions around a Two-

Building Configuration'. *Journal of Wind Engineering and Industrial Aerodynamics* 115, 9

Little, B. and Wilbur, S. (1951) *Turbulence-Intensity Measurements in a Jet of Air Issuing from a Long Tube*. Langley Field, Virginia: National Advisory Committee for Aeronautics

Luca, di Marco. "The "nightmare" of aerodynamic correlation in F1" *Bernoulli* November 2013: 22-29. Print.

Mallock, B. and Finnis, M. (2012) *Coventry University Wind Tunnel Commissioning Report*: Mercedes AMG PETRONAS Formula One Team

Maeda, K., Kitoh, K., Nozaki, H., Nambo, K., Nakamura, T., Ido, A. (2005) *Correlation Tests Between Japanese Full-Scale Automotive Wind Tunnels Using the Correction Methods for Drag Coefficient.* Detroit: International Society of Automotive Engineers

Menter, F. (1992) *Improved Two Equation k-ω Turbulence Models for Aerodynamic Flows*. California: National Aeronautics and Space Administration

Mercker, E., Wicker, G., and Wiedemann, J. (eds.) (1997) . 'Contemplation of Nozzle Blockage in Open Jet Wind-Tunnels in View of Different 'Q' Determination Techniques'. held 24/2/1997 at Detroit, Michigan. Detroit, Michigan: International Society of Automotive Engineers

Mercker, E. and Wiedemann, J. (eds.) (1996) . 'On the Correction of Interference Effects in Open Jet Wind Tunnels'. held 26/2/1996 at Detroit, Michigan. Detroit, Michigan: International Society of Automotive Engineers

Miller, P., Madina, C., and Givi, P. (1995) 'Numerical Simulation of Non-Circular Jets'. *Computers & Fluids*24 (1), 1

Mohammadi, B. and Pironneau, O. (1994) *Analysis of the K-Epsilon Turbulence Model*. 1st edn. Chichester: Wiley

Quinn, W. and Militzer, j. (1988) 'Experimental and Numerical Study of Turbulent Free Square Jet'. *Physics of Fluids* 31 (1017), 1

Rae, W. and Pope, A. (1984) *Low-Speed Wind Tunnel Testing*. 2nd edn. New York: John Wiley & Sons

Shih, T., Liou, W., Shabbir, A., Yang, Z., and Zhu, J. (1995) 'A New k-Epsilon Eddy Viscosity Model for High Reynolds Number Turbulent Flows'*. Computers Fluids* 24 (3), 227

Sims-Williams, D. and Dominy, R. (eds.) (2002) . 'The Design of an Open-Jet Wind Tunnel for Model Testing'. held 2/12/02 at Indianapolis, Indiana: International Society of Automotive Engineers

The SAE Standards Committee (1994) *Surface Vehicle Information Report: Aerodynamics Testing of Road Vehicles - Open Throat Wind Tunnel Adjustment*. Warrendale, Pennsylvania: International Society of Automotive Engineers

White, F. (2009) *Fluid Mechanics*. 7th edn. New York: McGraw Hill

Wickern, G. and Schwartekopp, B. (eds.) (2004) . 'Correction of Nozzle Gradient Effects in Open Jet Wind Tunnels'. held 8/3/2004 at Detroit, Michigan: International Society of Automotive Engineers

Wickern, G. (ed.) (2001) . 'On the Application of Classical Wind Tunnel Corrections for Automotive Bodies'. held 3/5/2001 at Detroit, Michigan: International Society of Automotive Engineers

Wong, D. and Mair, W. (1983) 'Boat-Tailed After bodies of Square Section as Drag-Reduction Devices'*. Journal of Wind Engineering and Industrial Aerodynamics* 12 (1), 229

Xu, M., Pollard, J., Mi, J., Secretain, F., and Sadeghi, H. (1994) 'Effects of Reynolds Number on some Properties of a Turbulent Jet from a Long Square Pipe'*. Physics of Fluids* 25 (035102), 1

9. Appendix

9.1. Sensitivity Study for Constant β with Changes in v

For all graphs where the intensity value appears to drop to zero, the intensity is in fact 1×10^{-10}.

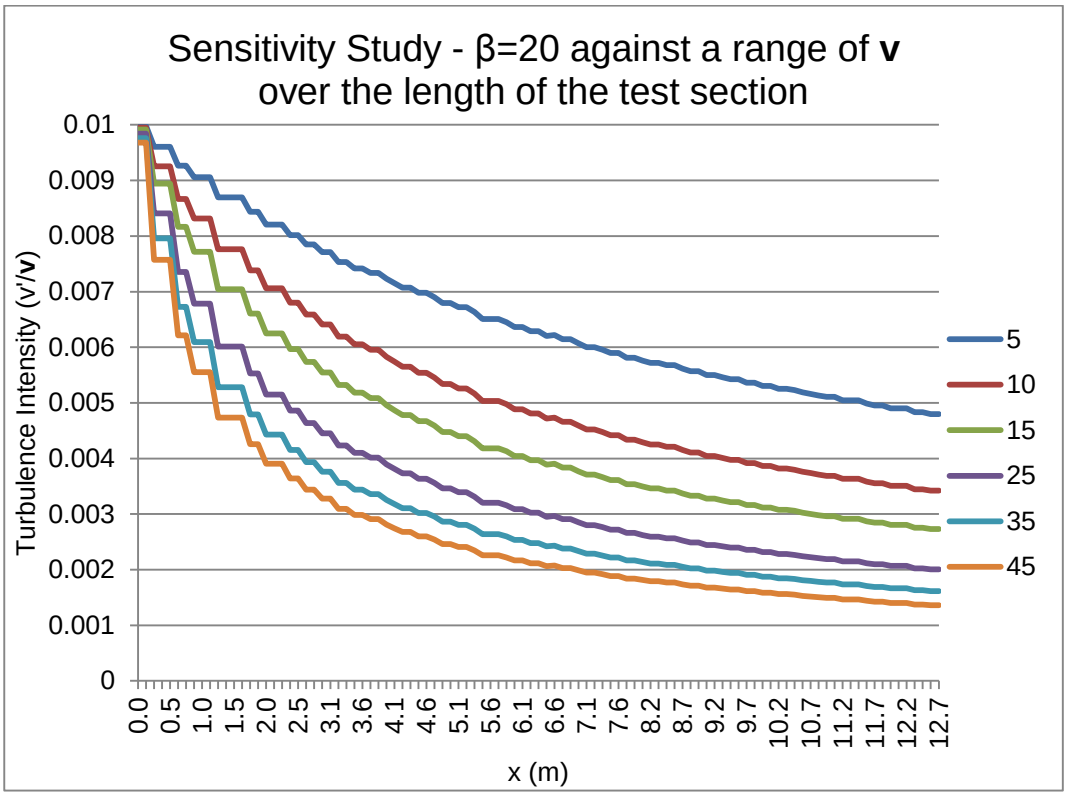

Figure 9.1-1 - Constant value of β=20 across a range of v

$$I = ae^{-bx} + ce^{-dx}$$

$$a = 0.007019e^{-0.005652\boldsymbol{v}} - 0.004252e^{-0.09734\boldsymbol{v}}$$

$$b = 2.13e^{-0.0007535\boldsymbol{v}} - 1.515$$

$$c = 0.002174e^{-0.1476\boldsymbol{v}} + 0.004949e^{-0.01662\boldsymbol{v}}$$

$$d = -0.06922e^{0.004716\boldsymbol{v}} + 0.02867e^{0.01488\boldsymbol{v}} \quad (9.1\text{-}1)$$

Equation 9.1-1 - Coefficients for β=20

It was found that when using this equation the prediction works best for values of **v** above 15ms^{-1}. Below this value and the equation generates around a 40% error, while above generates errors 1-15%.

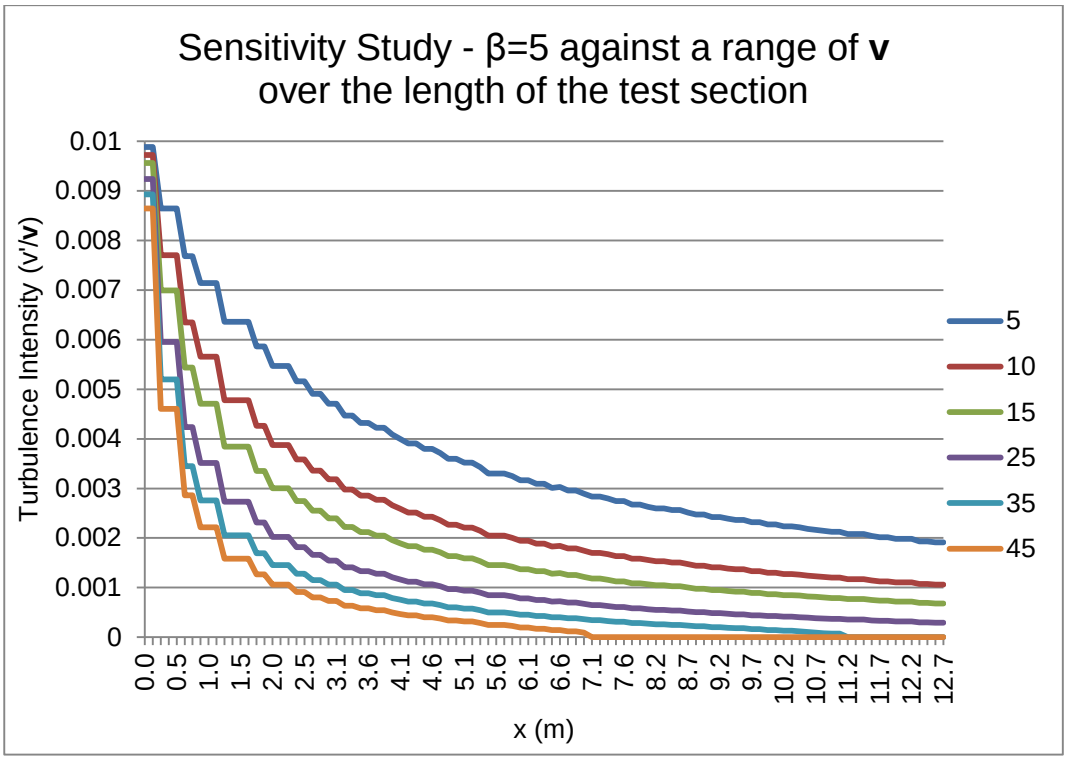

Figure 9.1-2 - Constant value of β=5 across a range of v

$$I = ae^{-bx} + ce^{-dx}$$

$$a = 0.008037e^{-0.004453\boldsymbol{v}} - 0.004627e^{-0.09268\boldsymbol{v}}$$

$$b = (-0.04923 \times \boldsymbol{v}) - 0.4056$$

$$c = 0.004494e^{-0.1028\boldsymbol{v}} + 0.002097e^{0.005174\boldsymbol{v}}$$

$$d = -0.07293e^{0.0399\boldsymbol{v}} + 0.07255e^{-0.3658\boldsymbol{v}} \quad (9.1\text{-}2)$$

Equation 9.1-2 - Coefficients for β=5

Equation 9.1-2 works well for all values of **v** with a maximum error of 4%.

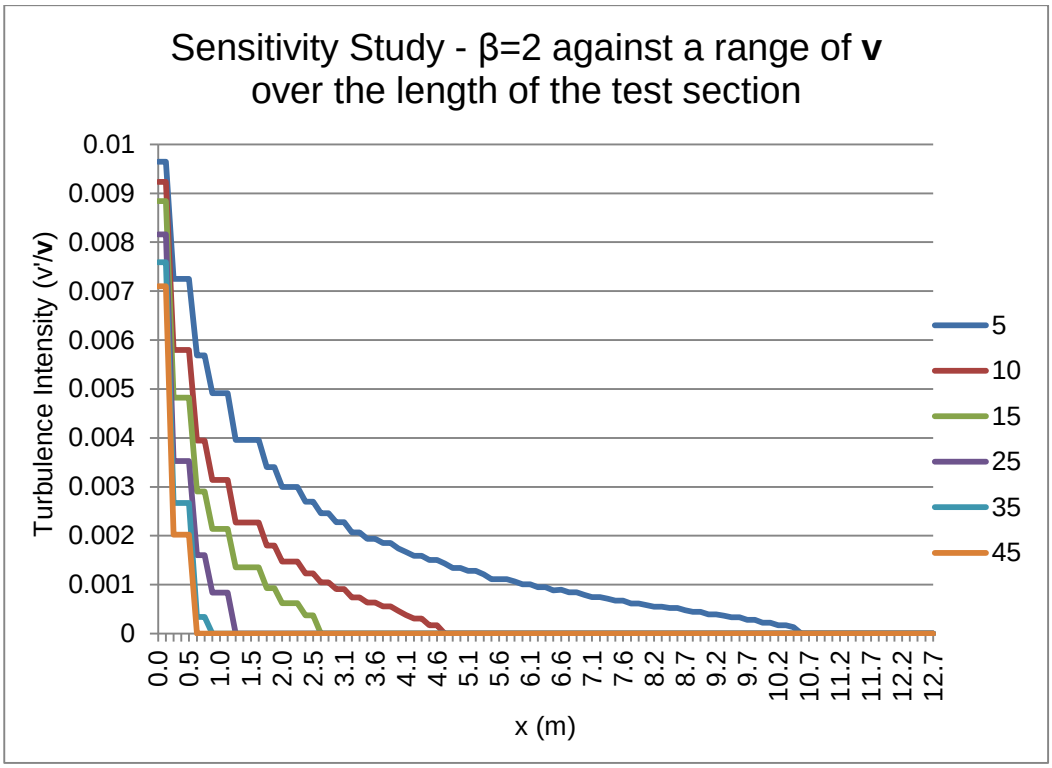

Figure 9.1-3 - Constant value of β=2 across a range of v

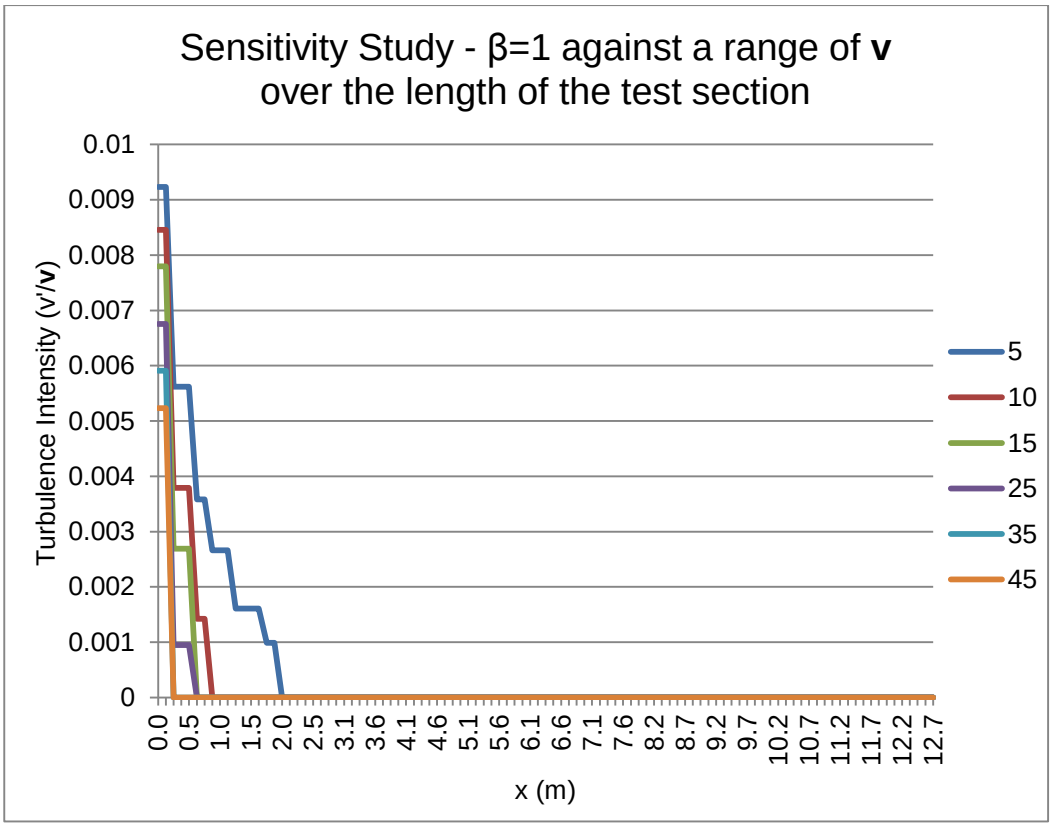

Figure 9.1-4 - Constant value of β=1 across a range of v

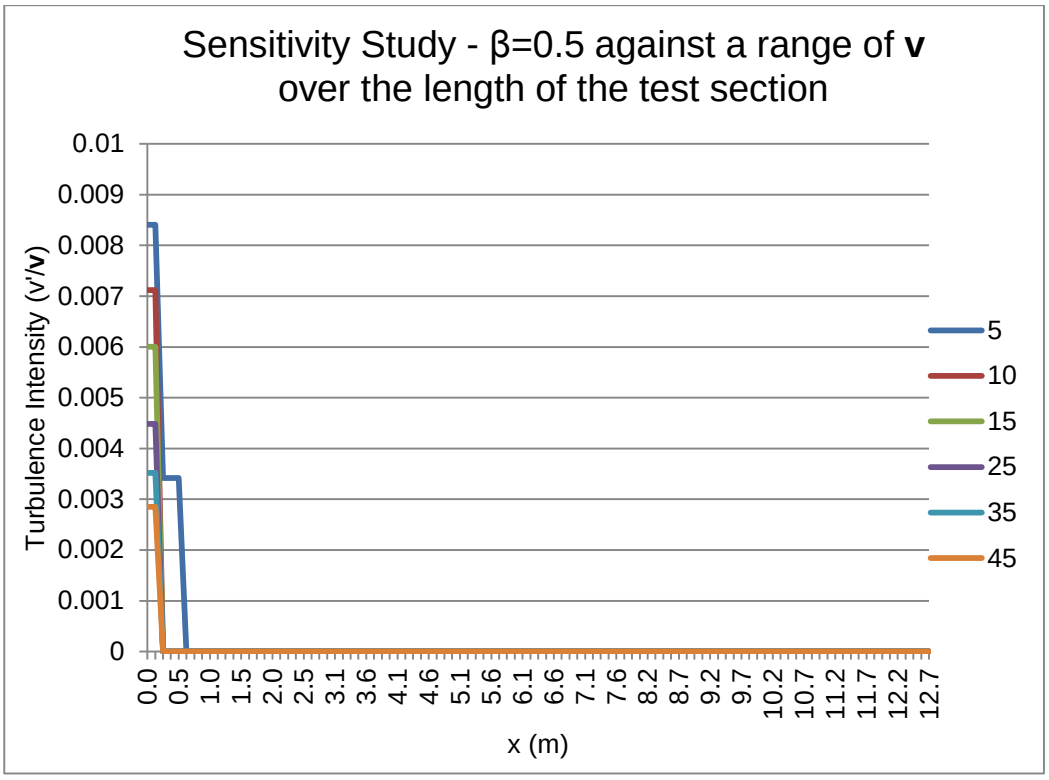

Figure 9.1-5 - Constant value of β=0.5 across a range of v

9.2. Sensitivity Study for Constant v with Changes in β

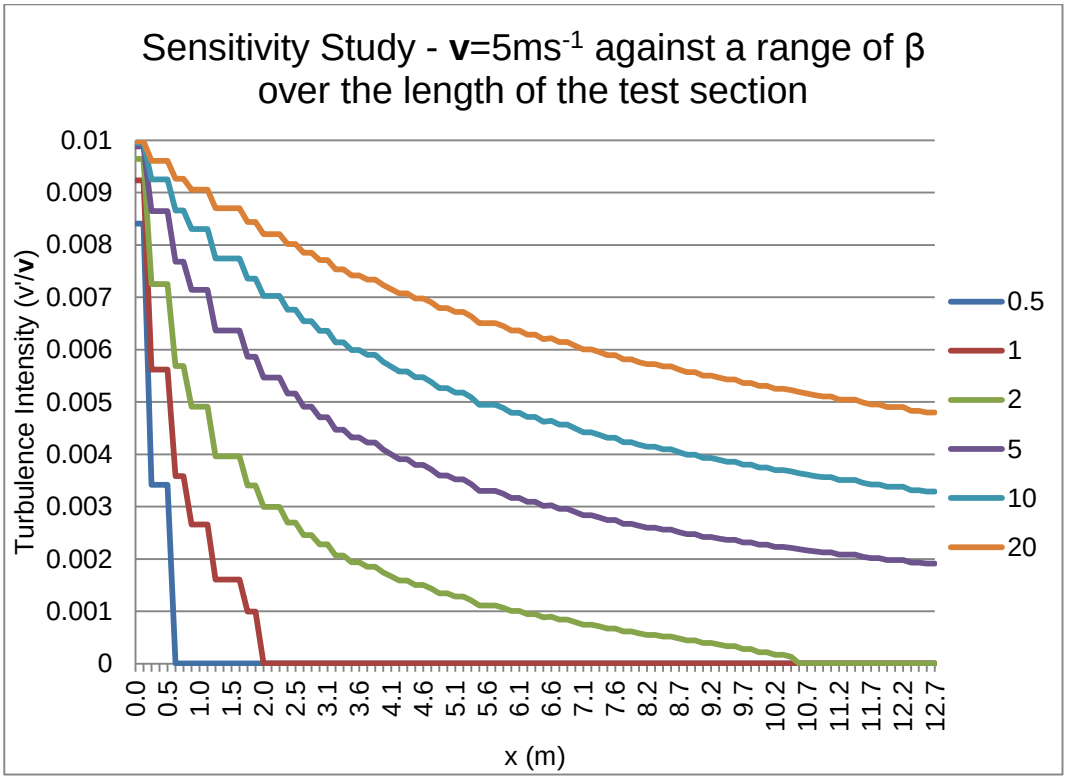

Figure 9.2-1 - Constant value of v=5ms^{-1} across a range of β

Considering Figure 9.2-1, the overall equation and the coefficients is slightly different:

$$I = ae^{-bx} + c$$

$$a = 0.002417e^{-0.3871\beta} + 0.007464e^{-0.0119\beta}$$

$$b = 6.658e^{-1.96\beta} + 0.4037e^{-0.05148\beta}$$

$$c = 0.004938 \times \left(\frac{1}{e^{0.1316\beta}} - 0.8871\right) \quad (9.2\text{-}3)$$

Equation 9.2-1 - Coefficients for v=5ms^{-1}

Equation 9.2-1 predicts well for values of β above and including 5, generating a maximum 10% error, with the equation becoming more accurate, with a larger values of β. When β is less than 5 the prediction is very poor.

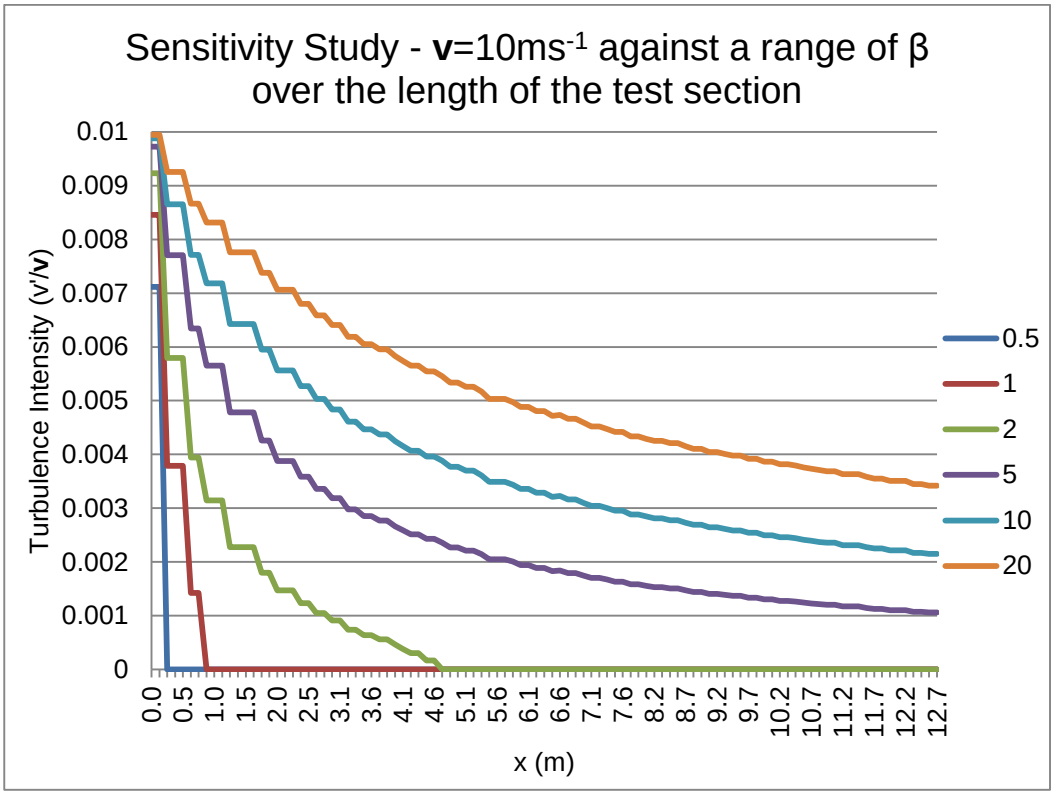

Figure 9.2-2 - Constant value of v=10ms^{-1} across a range of β

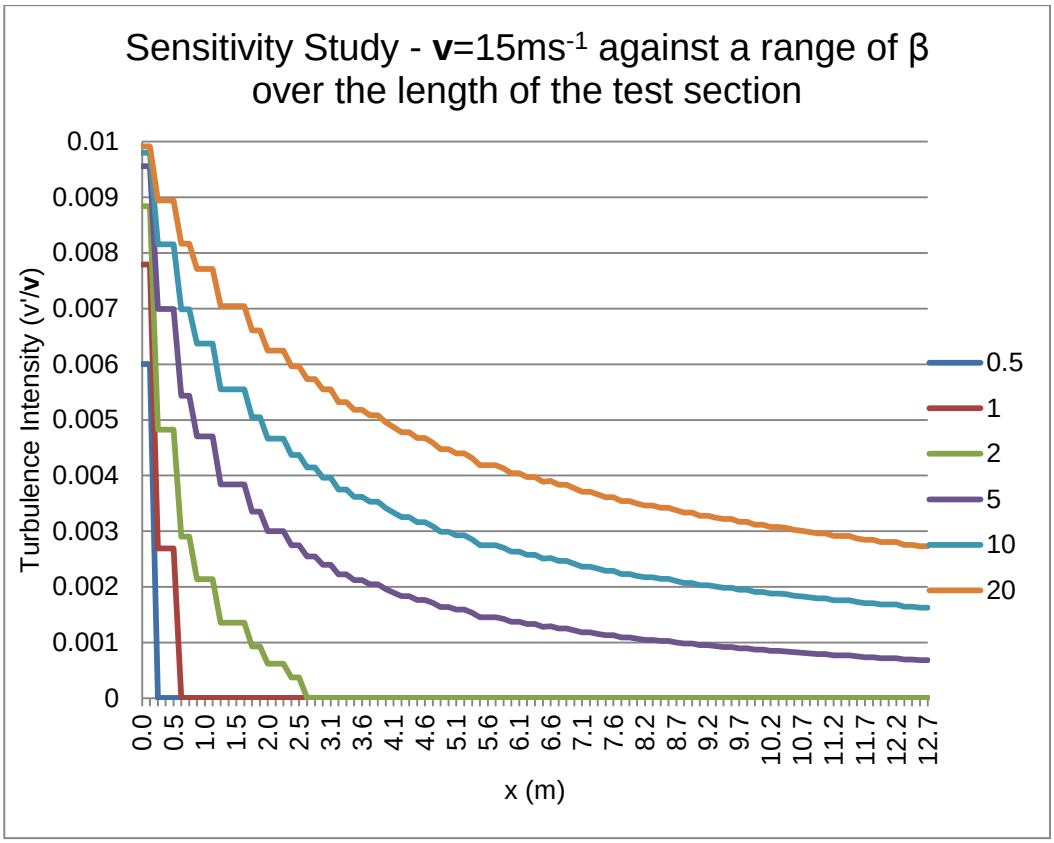

Figure 9.2-3 - Constant value of v=15ms^{-1} across a range of β

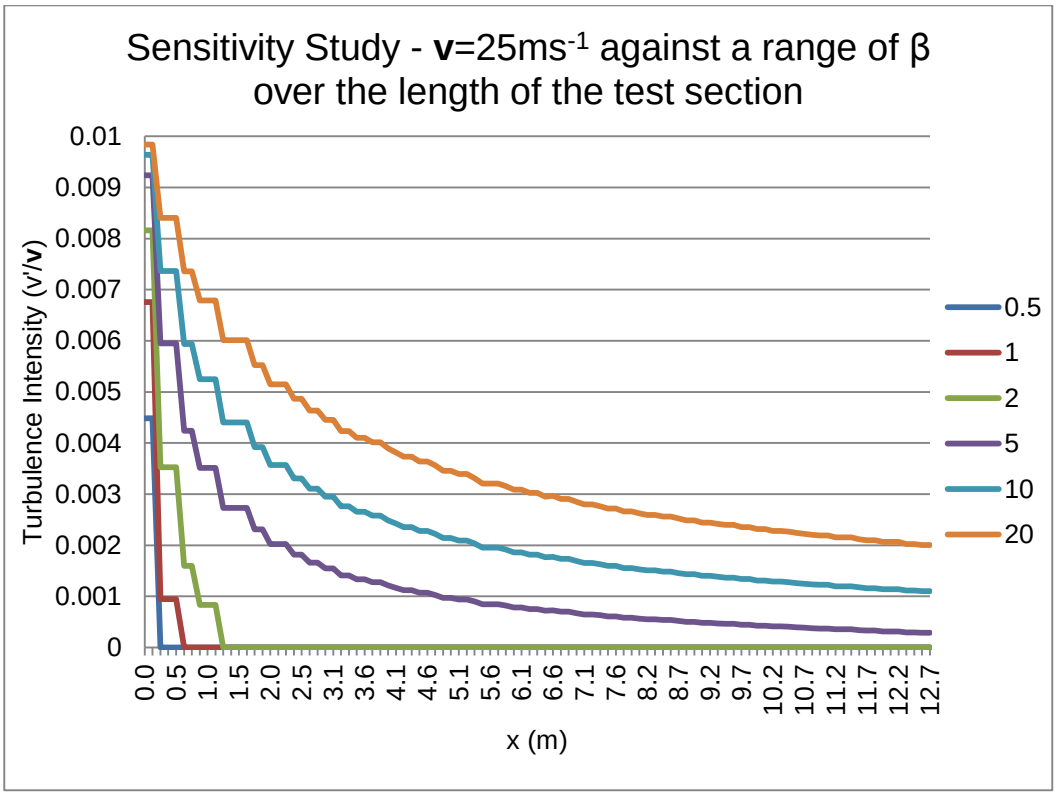

Figure 9.2-4 - Constant value of v=25ms^{-1} across a range of β

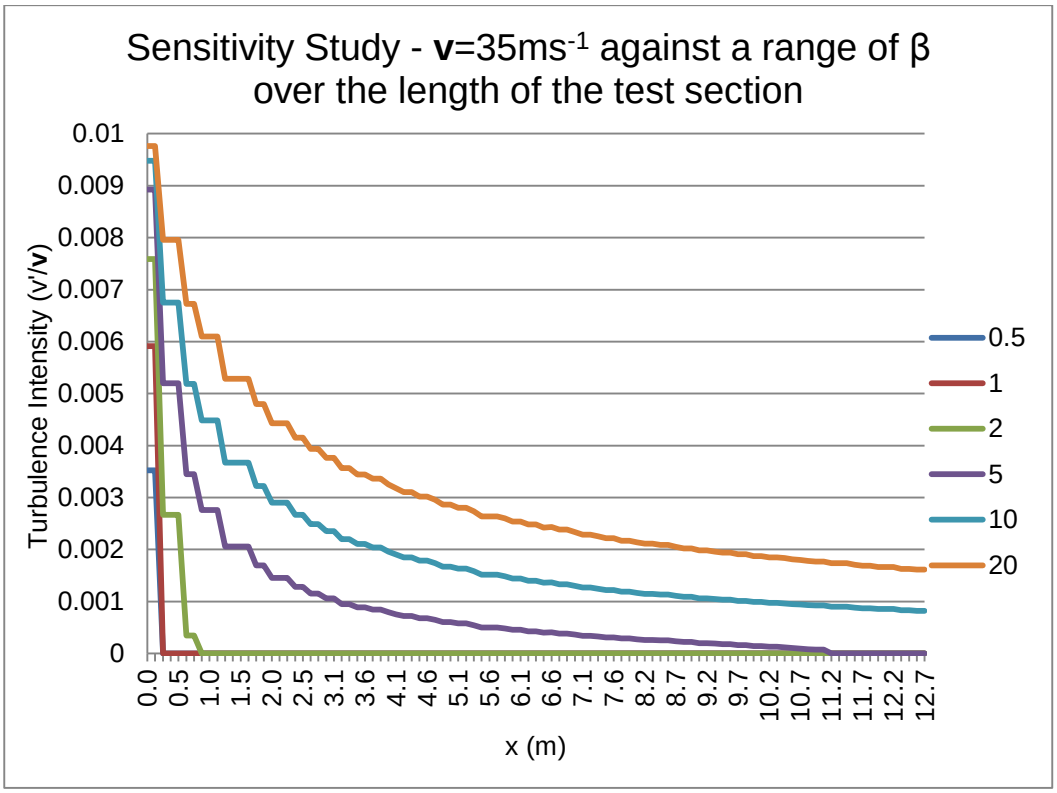

Figure 9.2-5 - Constant value of v=35ms^{-1} across a range of β

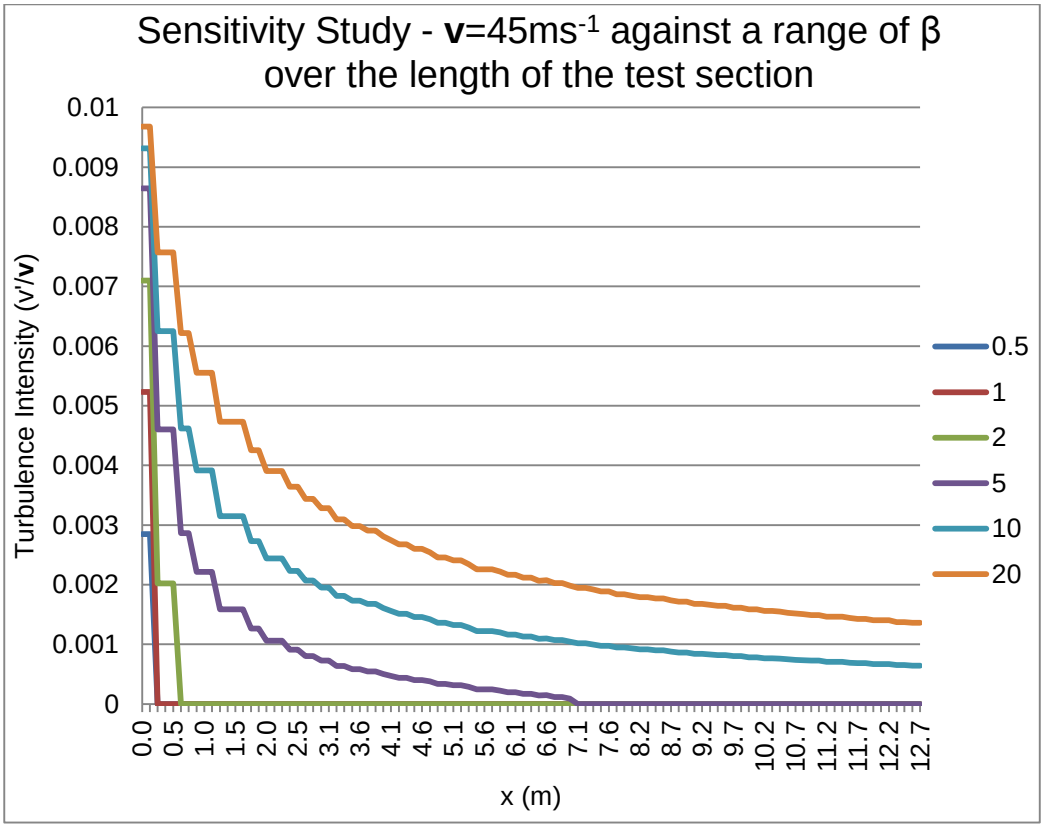

Figure 9.2-6 - Constant value of v=45ms^{-1} across a range of β

When examining Figure 9.2-6 it is clear to see that only the values of β show a definite exponential curve, while all other values drop close to zero showing no mathematical trend. This is reflected in the efficiency of Equation 9.2-2 as prediction is best at β=10 and 20. This being said the prediction at β=10 generates an error of 18%, while β=20 generates an error of 2%.

$$I = ae^{-bx} + c$$

$$a = 0.008268e^{-0.006612\beta} - 0.01121e^{-1.588\beta}$$

$$b = 6.025e^{-0.3507\beta} + 0.4772$$

$$c = (9.054 \times 10^{-5} \times \beta) - 1.321 \times 10^{-4} \quad (9.2\text{-}4)$$

Equation 9.2-2 - Coefficients for v=45ms^{-1}

9.3. Sensitivity Study for Constant k with Changes in v

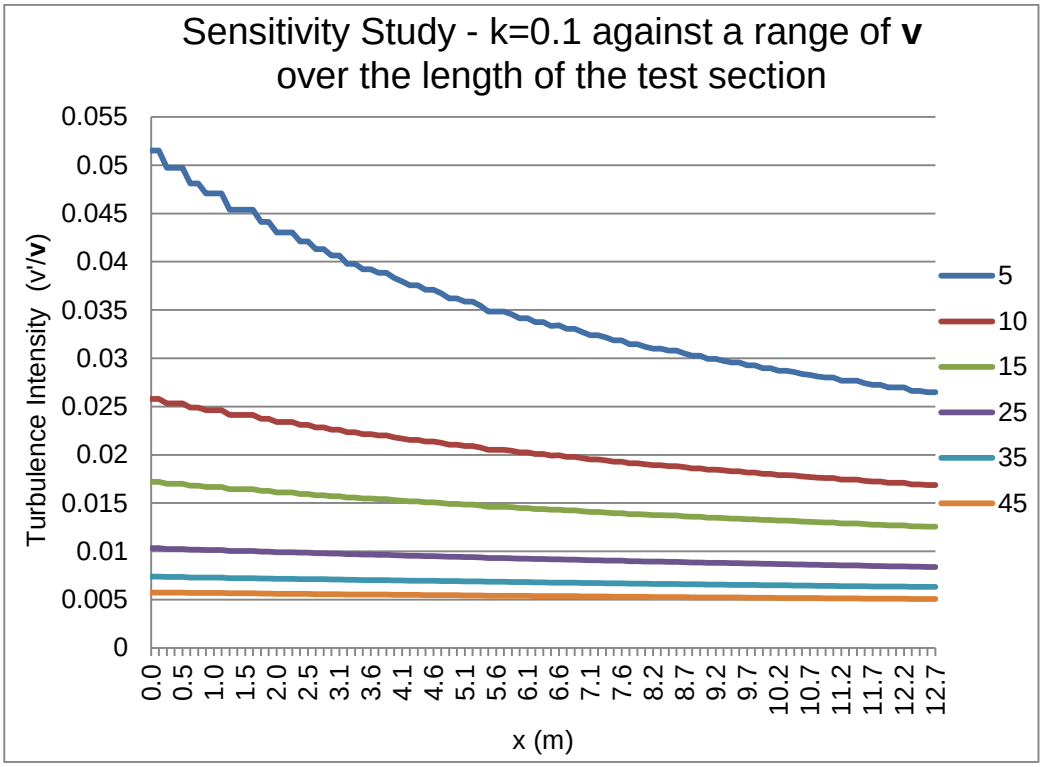

Figure 9.3-1 - Constant value of k=0.1 across a range of v

It is interesting to note that again for low values of **v** the calculated value (when using Equation 9.3-1) generates a large amount of error when comparing it to that of the CFD results in Figure 9.3-1. Equation 9.3-1 shows the relationship that was found between all the results for k=0.1.

$$I = ae^{-bx} + c$$

$$a = 0.003909e^{-0.01561v} + 0.07138e^{-0.264\beta}$$

$$b = 0.03569e^{-0.0226v} + 0.1923e^{-0.1725\beta}$$

$$c = 0.001152e^{-0.02713v} + 0.03524e^{-0.2099\beta}$$

Equation 9.3-1 - Coefficients for k=0.1

When using Equation 9.3-1 results were accurate to within 2% when using a value of **v** 15-45ms^{-1}. The equation over predicts the intensity for 5 and 10ms^{-1} by 96% and 25% respectively.

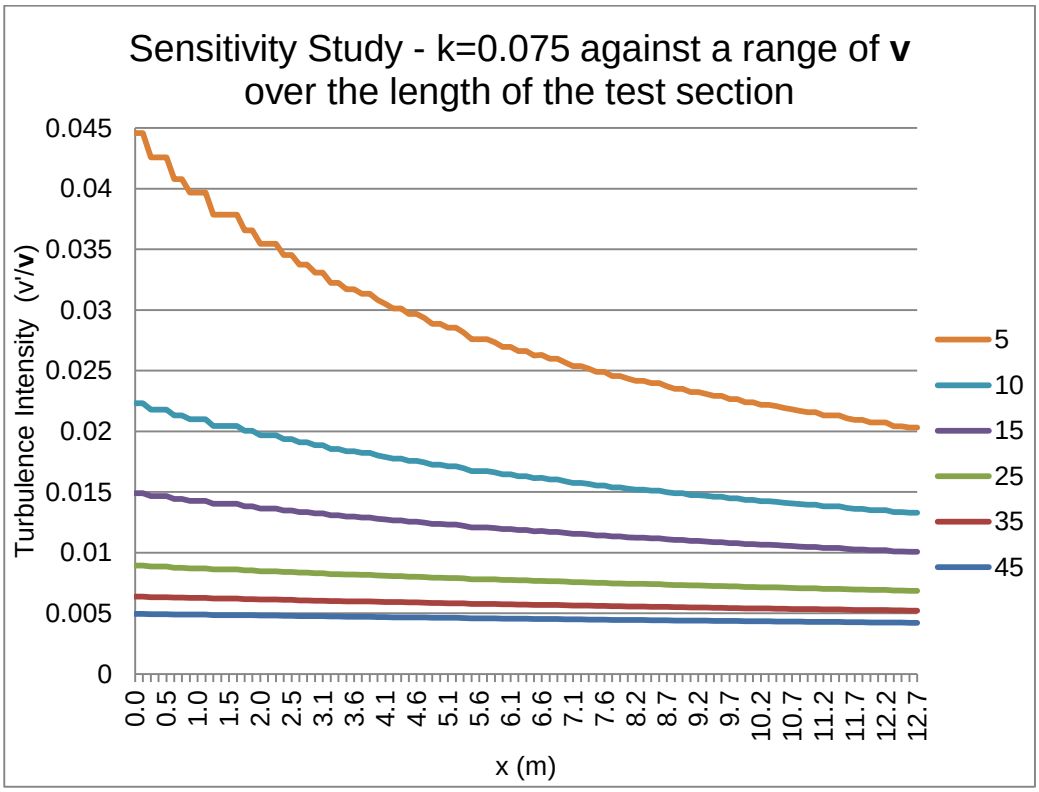

Figure 9.3-2 - Constant value of k=0.075 across a range of v

For values of k that are below 0.075 a reasonable trend could be found that could be expressed mathematically. This is due to the drastic difference between the low and high velocities. The high velocity values seem to present a trend that is linear, while the low velocities show clear exponential features. The equation for k=0.075, creates a maximum error of 6% (at 5ms^{-1}).

$$I = ae^{-bx} + ce^{-dx}$$

$$a = 3.364 \times 10^{-10} e^{0.3641v} + 0.003704 e^{0.04305v} b$$
$$= 0.01572 e^{-0.14785v} + 0.004244 e^{0.04513v}$$

$$c = 1.383 \times 10^{-4} e^{0.1003v} + 0.001473$$

$$d = 2.22 e^{-0.2821v} + 0.03457 e^{0.04859v} \quad (9.3\text{-}2)$$

Equation 9.3-2 - Coefficients for k=0.075

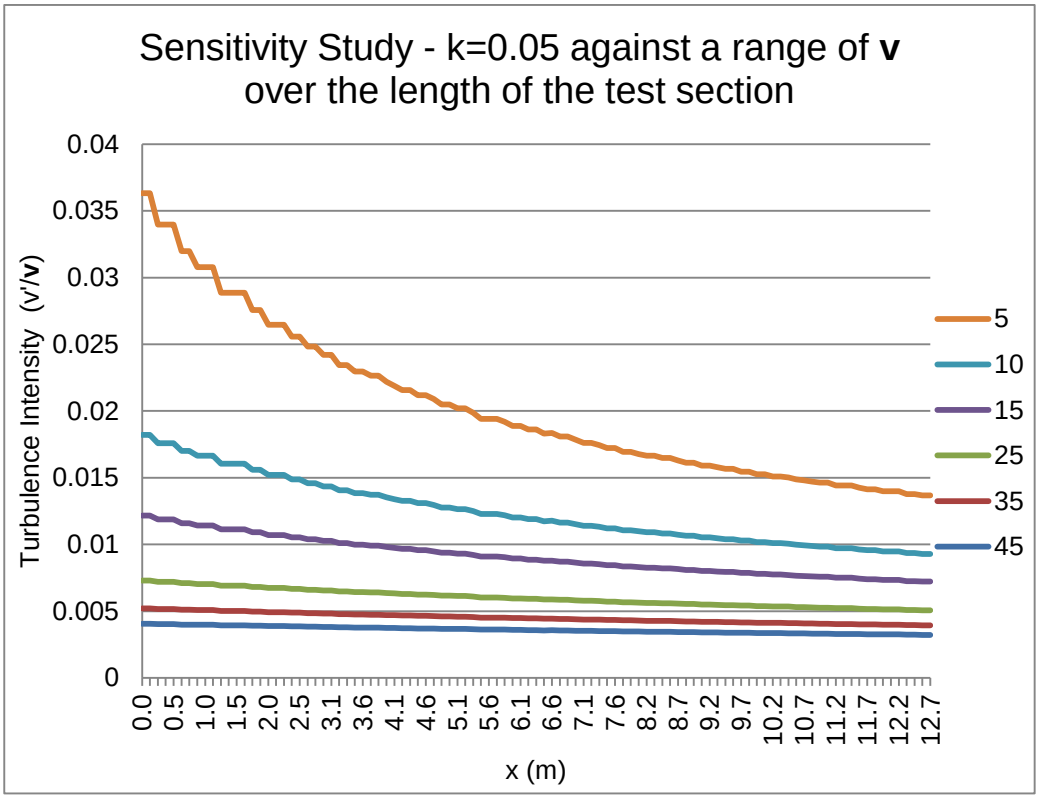

Figure 9.3-3 - Constant value of k=0.05 across a range of v

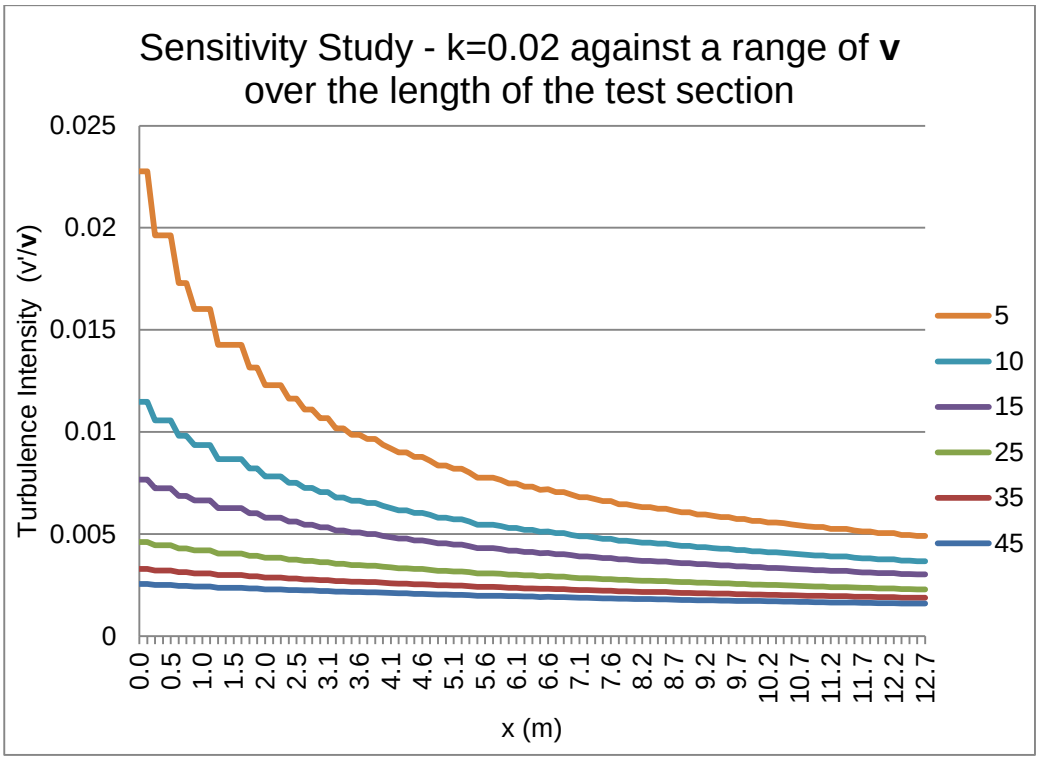

Figure 9.3-4 - Constant value of k=0.02 across a range of v

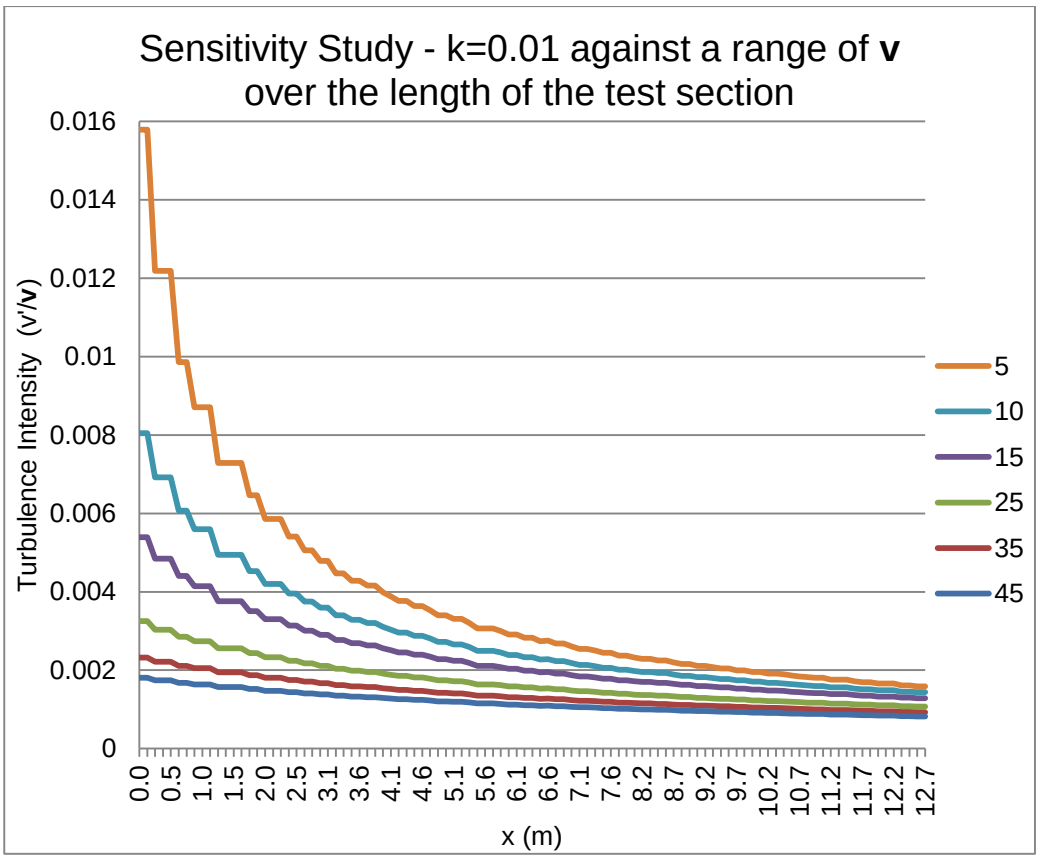

Figure 9.3-5 - Constant value of k=0.01 across a range of v

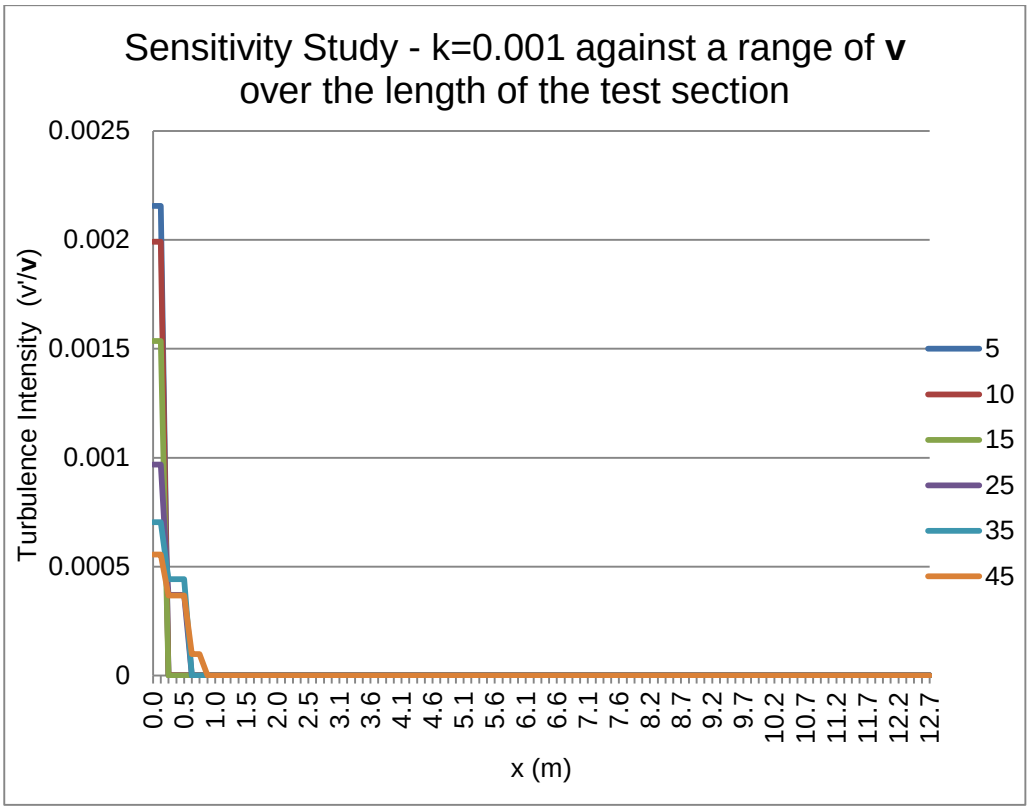

Figure 9.3-6 - Constant value of k=0.001 across a range of v

9.4. Sensitivity Study for Constant ε with Changes in v

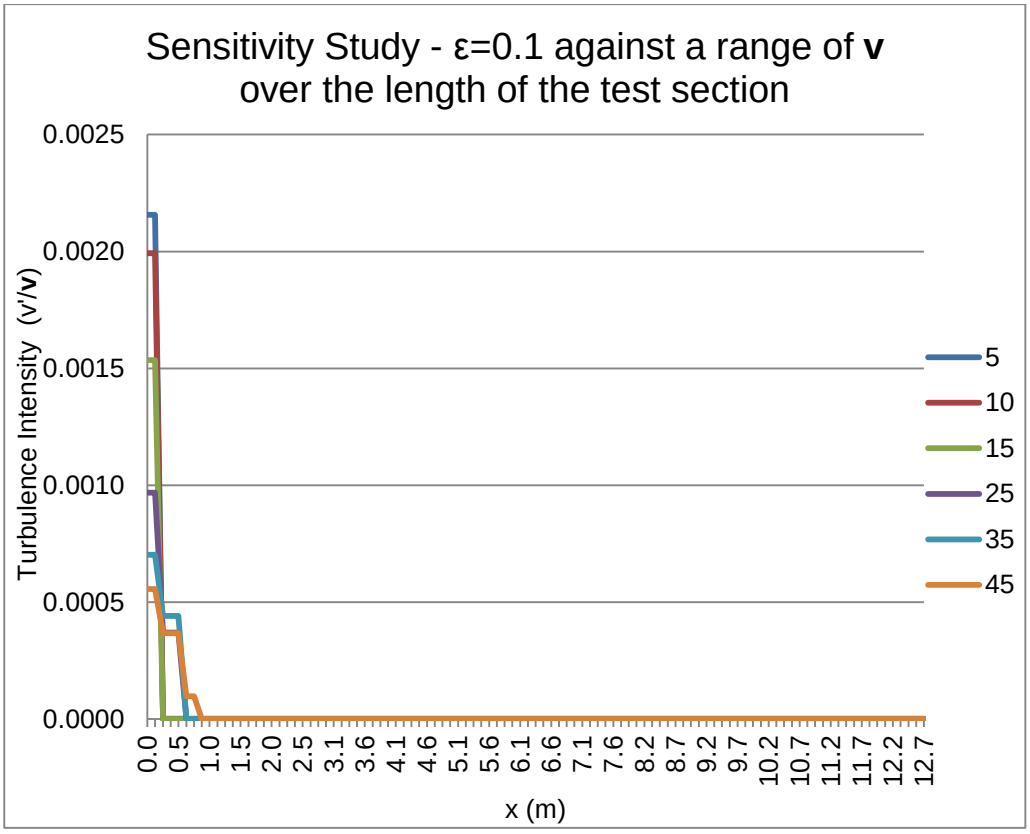

Figure 9.4-1 - Constant value of ε=0.1 across a range of v

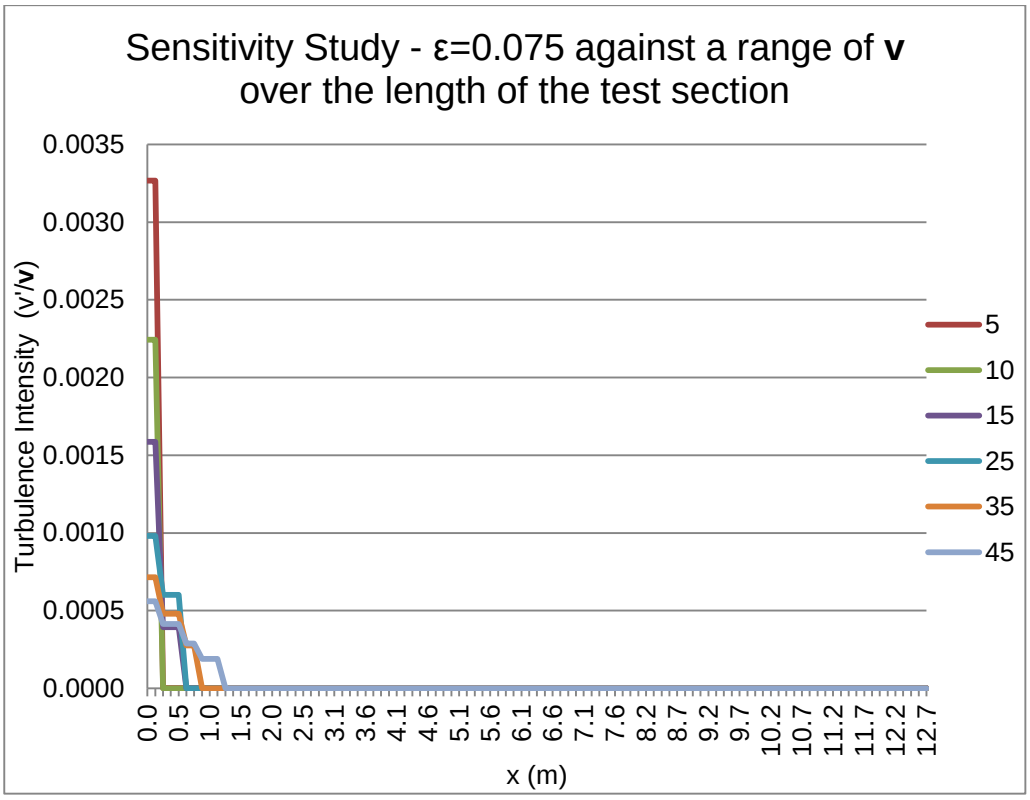

Figure 9.4-2 - Constant value of ε=0.075 across a range of v

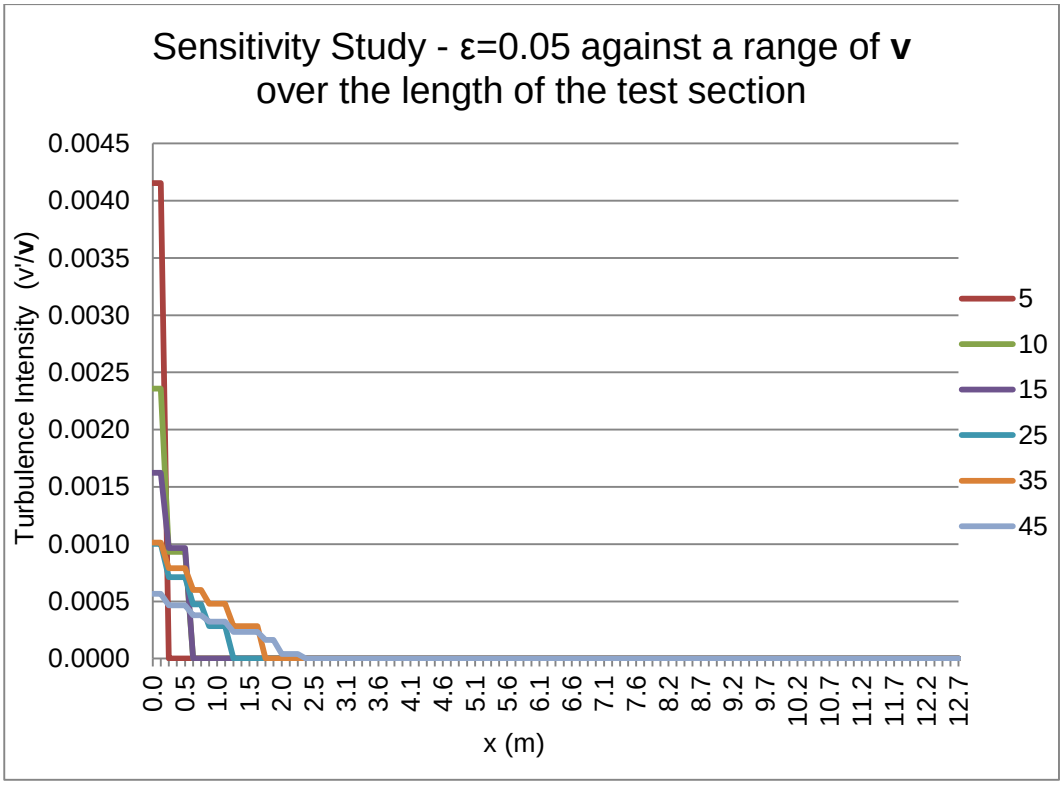

Figure 9.4-3 - Constant value of ε=0.05 across a range of v

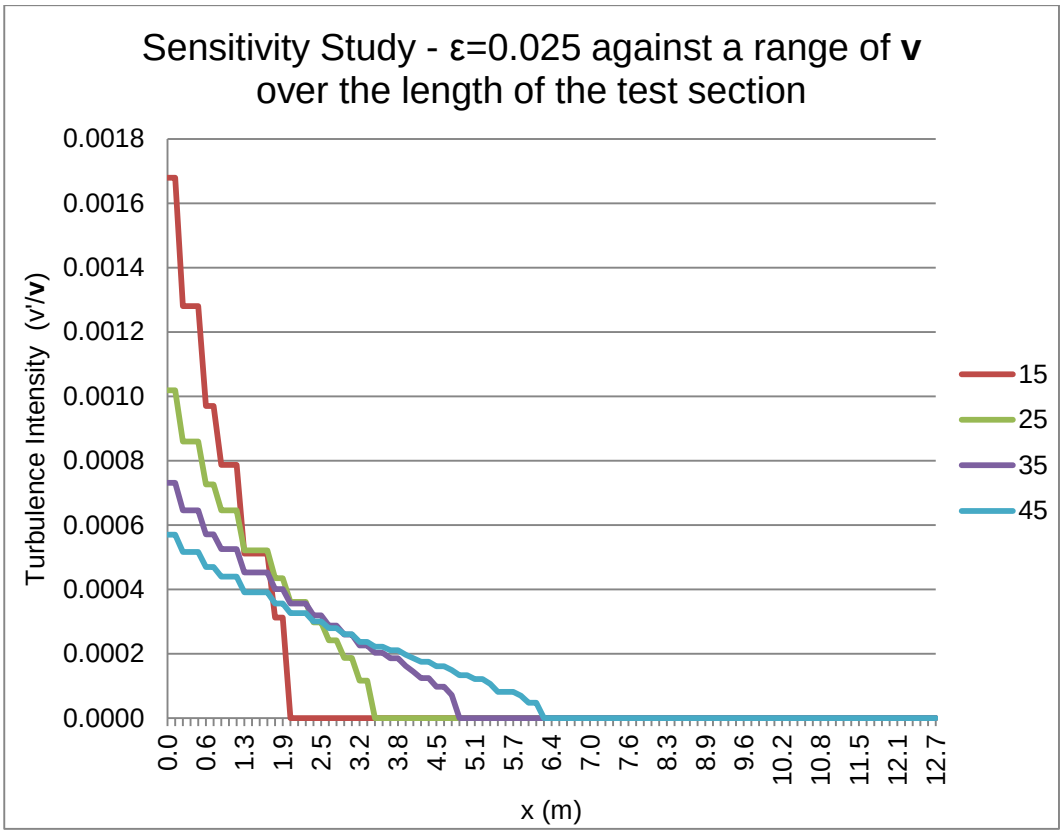

Figure 9.4-4 - Constant value of ε=0.025 across a range of v

Figure 9.4-4 only shows velocities of 15 and above. This is because it emphasises the non-similar nature of the profiles.